



SAPIENZA
UNIVERSITÀ DI ROMA

Constellation Design for a Lunar Global Navigation Satellite System

Facoltà di Ingegneria Civile e Industriale
Laurea Magistrale in Ingegneria Spaziale ed Astronautica

Alessandro Di Muzio
ID number 1743619

Advisor
Prof. Christian Circi

Co-Advisors
Prof. Emiliano Ortore
Dr. Marco Cinelli

Academic Year 2024/2025

Constellation Design for a Lunar Global Navigation Satellite System
Master thesis. Sapienza University of Rome

© 2025 Alessandro Di Muzio. All rights reserved

This thesis has been typeset by L^AT_EX and the Sapthesis class.

Author's email: alez.dimuzio97@gmail.com

*Dedicated to my parents,
Domenico and Esther*

Abstract

In the coming decades, the Moon is poised to be the common thread of countless missions, requiring both human and robotic presence on its surface and in orbit. To support these mission and their operations a proper infrastructure must be established.

This thesis' goal is to propose a set of possible configurations for a lunar GNSS constellation, capable of providing robust, reliable positioning and timing services. The constellation patterns considered are only a subset of all possible configurations. Two sets of classes are investigated to find the most efficient circular constellation with common altitude and inclination: the Walker-Delta class and the Street-of-Coverage class.

All studied configurations need to guarantee a 4-fold, global and continuous coverage over the lunar surface, at minimum.

The most efficient constellations are those able to guarantee the coverage requirements with the smallest number of satellites at the lowest altitude possible. These constellations are also called minimal constellations.

A total of 26 configuration, chosen an optimization-based approach, have been further analyzed on the basis of selecting the most appropriate configuration. Among these, the best constellation in terms of coverage efficiency, *DOP* values and the required ΔV for orbital stability was chosen as a lunar GNSS candidate.

In conclusion, a coverage analysis was run for a detailed topography of the Moon, in proximity to Shackleton crater, and gray areas for coverage were determined.

Acknowledgments

*You can't direct the wind,
but you can adjust your sails*

Unknown

From a young age, I have always been fascinated with space and all that entails. I dreamt of spaceships and space elevators for as long as I can remember. With an innate curiosity, choosing this career path was a natural and easy decision for me.

First and foremost, I would like to thank my entire family for standing by me and supporting me through all the challenges I faced during my studies.

To my parents and my sisters, with whom I have shared so much of my life, I am forever grateful for the memories we have created together. Your unwavering support gave me the strength to see this journey through to the end.

I would like to express my gratitude to the professors who guided me in defining the argument for this thesis and supported me through the challenges and uncertainties of its development.

Thank you, Professors Circi, Ortore, and Cinelli, for your invaluable support and for the many pieces of advice regarding my future endeavors and career opportunities.

A heartfelt thank you to Professor Laneve, who helped me develop the algorithm used in the final part of this thesis.

A mention to my friends, that I had the pleasure of getting to know despite the many different paths in life we took.

From the childhood friends, to those I made through the high school and university years, I would like to offer my thanks for the support and having made me the person that I am today.

In conclusion, I offer my thanks to the support team of Ansys STK, who provided me with the license needed to run the simulations, and the Dipartimento di Scienze Statistiche Sapienza for giving me access to the university supercomputer Terastat2, without which I would not have been able to complete this thesis in time.

Contents

Abstract	iii
Acknowledgments	iv
List of figures	viii
List of tables	x
1 Introduction	1
1.1 Background	1
1.2 Scope of the thesis	2
1.3 State of the art	4
1.4 Thesis outline	7
2 Constellation geometry	10
2.1 Coverage problem	10
2.2 Spherical geometry	14
2.3 Circular constellations	15
2.3.1 Symmetric vs non-symmetric	16
2.3.2 Walker-Delta	17
2.3.3 Streets-of-Coverage	18
2.3.4 Hybrid constellations	19
2.4 Examples	19
2.4.1 GPS	19
2.4.2 GLONASS	20
2.4.3 Galileo	20
2.4.4 Iridium	20
2.4.5 BeiDou	21
3 Orbital mechanics	27
3.1 Keplerian motion	27

3.2	Earth-Moon system	30
3.3	Perturbations	33
3.3.1	Selenopotential	34
3.3.2	Third bodies	36
3.4	Secular effects of J2	38
3.5	Repeating ground-track orbits	39
3.6	Software used	44
3.6.1	MATLAB	44
3.6.2	SaVi	44
3.6.3	STK	45
4	Constellation design methods	46
4.1	Analytical vs numerical methods	46
4.2	Methods for SoC constellations	46
4.2.1	Beste coverage method	47
4.2.2	Ulybyshev coverage method	49
4.2.3	General coverage method	53
4.3	Methods for Walker-Delta constellations	54
4.3.1	Walker circumcircle coverage method	56
4.3.2	Lang coverage method	65
4.3.3	RGTO coverage method	67
5	Global Navigation Satellite System	69
5.1	Overview	69
5.2	Requirements	71
5.3	Navigation equations	72
5.3.1	Timekeeping	72
5.3.2	Pseudorange	73
5.3.3	Non-linear model	74
5.4	Dilution of Precision	75
6	Results	80
6.1	Streets-of-Coverage	80
6.1.1	More SoC solutions	83
6.2	Walker-Delta	84
6.3	Moon Walker tables	87
6.4	Comparison and selection	92
6.5	Coverage performance	95
6.6	Orbital stability	97

6.7	Proposed constellation	100
7	Determination of gray areas for coverage	103
7.1	DEM	103
7.2	LOS algorithm	105
7.3	Gray areas	108
7.4	Application: Shackleton crater	109
8	Conclusions	114
8.1	Key results	114
8.2	Final remarks	115
8.3	Future work	116
A	SoC tables for the Moon	117
B	Walker tables for the Moon	120
	Bibliography	128

List of Figures

1.1	GNSS architecture example [1]	2
1.2	Initial LCRNS lunar service volume [2]	5
1.3	LNSS architecture [3]	6
2.1	Coverage geometry for an orbiting satellite	10
2.2	Coverage angle as a function of altitude and elevation angle	13
2.3	Spherical distance between two points on the surface of a sphere . .	15
2.4	Street-of-Coverage geometry [4]	18
2.5	GPS constellation (Walker-Delta 24/6/2)	22
2.6	GLONASS constellation (Walker-Delta 24/3/1)	23
2.7	Galileo constellation (Walker-Delta 24/3/1)	24
2.8	Iridium constellation (SoC 66/6)	25
2.9	BeiDou S1-S3 constellation (Hybrid)	26
3.1	Classical orbital parameters	27
3.2	Earth-Moon system [5]	31
3.3	Lunar coordinate systems	32
3.4	Main and perturbation accelerations	33
3.5	Spherical harmonics	35
3.6	Geometry for a satellite orbiting the Moon with a third body present	37
3.7	Secular effects of J_2 on the orbital elements	38
3.8	Altitude as a function of the repeat factor and inclination	41
3.9	Coverage angle as a function of the repeat factor and inclination . .	42
3.10	RGTO examples	43
3.11	Coverage map made with SaVi	45
4.1	Beste's method geometry	47
4.2	Multiple coverage streets	49
4.3	Geometry for an inclined SoC [6]	50
4.4	Spherical triangles defined by 3 points [7]	57

4.5	Circumcenter inside the spherical triangle	58
4.6	Circumcenter outside the spherical triangle	60
4.7	Search for optimal configuration	63
4.8	2-fold coverage	64
4.9	Multiple coverage	64
4.10	Lang coverage test grid (for a Walker-Delta 12/4/3 constellation) . .	66
4.11	RGTO coverage test grid	68
5.1	3D trilateration geometry [8]	69
5.2	Terrestrial service volume [9]	70
5.3	Pseudorange measurement [10]	74
5.4	DOP geometry [11]	78
5.5	Galileo DOPs	79
6.1	Streets-of-Coverage for different inclinations	81
6.2	Minimum number of satellites for SoC constellations	82
6.3	Search for a lower bound SoC 27/3 solution	84
6.4	Walker-Delta optimal configurations	85
6.5	Minimum number of satellites for Walker-Delta constellations . . .	87
6.6	Moon Walker-Delta tables	88
6.7	Moon Walker-Delta optimum ($\varepsilon = 0$ deg)	89
6.8	Poly55 fit	92
6.9	Streets-of-Coverage vs Walker-Delta comparison	93
6.10	Configuration ID 16 - orbital stability	100
6.11	Lunar GNSS constellation (Walker-Delta 18/6/2)	101
6.12	Lunar GNSS ground-track grid ($m = 1, R = 67$)	101
6.13	Lunar GNSS constellation properties	102
7.1	Moon DEM (450 arcsec)	103
7.2	LOS algorithm	105
7.3	Bilinear interpolation for the DEM	107
7.4	LOS algorithm employed by the mission SPOT	108
7.5	Shackleton crater DEM (20 m)	110
7.6	LOS and DEM intersections around Shackleton crater	111
7.7	Gray areas, Shackleton crater	112
7.8	Average number of visible satellites, Shackleton crater	112
8.1	Distribution of surface ice at the Moon's south pole [12]	116

List of Tables

1.1	Moonlight 4-sat constellation [13]	6
2.1	GNSS transmitter beamwidths [14]	14
2.2	Coverage options for SoC constellation	19
3.1	Normalized zonal harmonic coefficients for the Moon [15]	35
3.2	Normalized sectorial and tesseral harmonic coefficients for the Moon [15]	36
3.3	Repetition coefficients for the most known constellations [16]	43
5.1	Interpretation of <i>DOP</i> values [17]	78
6.1	Coefficients value for poly55 fit	91
6.2	List of GNSS constellation candidates	94
6.3	List of GNSS constellation candidates - coverage efficiency	96
6.4	Configuration ID12 - orbital stability	98
6.5	Configuration ID16 - orbital stability	98
6.6	Configuration ID17 - orbital stability	99
6.7	Configuration ID26 - orbital stability	99
6.8	Failure of a satellite for the lunar GNSS constellation	102
7.1	Longitudinal distance by latitude and precision (in arcsec)	104
A.1	Street-of-Coverage constellations for $n = 1, \varepsilon = 0$	117
A.2	Street-of-Coverage constellations for $n = 2, \varepsilon = 0$	118
A.3	Street-of-Coverage constellations for $n = 3, \varepsilon = 0$	118
A.4	Street-of-Coverage constellations for $n = 4, \varepsilon = 0$	119
B.1	Walker-Delta constellations for $n = 1, \varepsilon = 0$	120
B.2	Walker-Delta constellations for $n = 2, \varepsilon = 0$	122
B.3	Walker-Delta constellations for $n = 3, \varepsilon = 0$	124
B.4	Walker-Delta constellations for $n = 4, \varepsilon = 0$	126

Chapter 1

Introduction

1.1 Background

The Moon has remained through the ages an enduring object of fascination, but despite this longstanding enchantment, the Moon has seen little human activity since the Apollo missions of the 1960s and 1970s. After the last human left the lunar soil in 1972, lunar exploration ceased completely.

Renewed interest in the space sector has recently reinvigorated the push for new ventures: both space agencies, and private companies are preparing for an increasing number of lunar missions that aim to push the boundaries of human presence beyond Earth.

Moreover, the Moon presents a unique testing ground for new technologies that will be essential for broader space exploration. Establishing a sustained human presence on the lunar surface will require innovations in various fields, including habitat construction, life support systems, and resource utilization.

Indeed, one of the most promising aspects of lunar exploration is the potential use of in-situ resources. The discovery of water ice at the Moon's poles has sparked interest in its potential to support human settlements. Water can be used for life support, as well as converted into hydrogen and oxygen for rocket fuel, significantly reducing the cost and complexity of space travel.

Crewed lunar missions provide a perfect opportunity to address challenges related to radiation exposure, psychological effects of isolation and the sustainability of life support systems.

A sustained presence on the Moon can also act as a gateway for deeper space exploration. Establishing a lunar base of operations would create a launchpad for more ambitious missions to destinations beyond the Moon, such as asteroids and Mars. Both the low-gravity environment and the absence of an atmosphere around

the Moon mean that a rocket could lift-off from the lunar surface with a fraction of the fuel were it to be launched from Earth.

Lastly, given its proximity to Earth and the increasing number of future missions traveling to and from deeper space, it is not unrealistic to envision a lunar base evolving into a hub for industrial and commercial activities.

1.2 Scope of the thesis

One of the key enablers of successful lunar exploration is the development of a robust space communication and navigation system. Reliable communication between Earth and the Moon is essential, enabling real-time data transmission, remote operations, and safety monitoring. Similarly, precise navigation systems are crucial for ensuring the accuracy and safety of lunar surface and low-orbit operations.

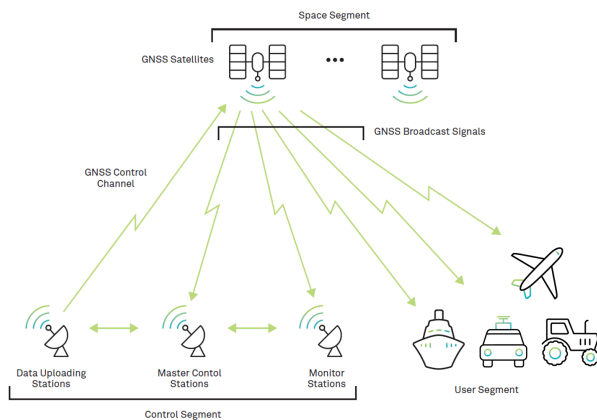


Figure 1.1. GNSS architecture example [1]

In this context, the development of a lunar constellation for Global Navigation Satellite System (GNSS) applications represents a critical step toward supporting future lunar exploration efforts. Today, GNSS constellations on Earth support essential services like navigation, banking, power grid synchronization, cellular networks, and telecommunications. It is apparent how a dedicated GNSS constellation around the Moon could support, through continuous and precise positioning services, future human activities on the lunar soil.

This dissertation explores the design and implementation of such a constellation, addressing the unique challenges of the lunar environment, guaranteeing the coverage requirements needed for nominal operation.

Among all possible configurations that a lunar GNSS can take form, it has been decided to restrict the search to circular orbits with common altitude and inclination, since literature is extensive and many practical applications to which we can compare already exist.

Therefore, two classes of constellation have been investigated: the Street-of-Coverage (SoC) and the Walker-Delta constellations.

Both classes have been used extensively in the past, and they still represent the starting blocks for every mission requiring the use of a satellite constellation. There are many examples of constellation based on these classes, starting from the terrestrial GNSS versions (GPS, GLONASS and Galileo) and other communication services (i.e. Iridium). The two classes are analyzed and their design methodologies explained.

An original part of this work consists in the generation of Walker tables for the Moon, taking into consideration the rotation period of the Moon, capable of providing the minimum number of satellites for a complete and continuous four-degree coverage of the lunar surface at different angles of elevation.

From said table a list of possible configurations for the lunar GNSS was made up comprising the optimum (in terms of number of total satellites) for a four-degree coverage and minimum elevation angle of 5 degrees. Other configurations, with a more varied number of orbital planes, were considered to populate the table data. Each configuration was simulated over approximately a lunar day to evaluate its coverage indexes, first and foremost the geometric dilution of precision (GDOP). The minimum number of satellites at any given point in time was also recorded as well as the coverage spread (and therefore efficiency) of the few satellites in orbit. Due to third bodies perturbations all these configurations are unable to stay in place for longer than 3 or 4 lunar days (meaning 80-95 days), as they would inexorably drift towards Earth, if left to their own devices. To have them in place, there would need to be active station-keeping, acting at the end of each cycle to keep the orbital parameters in check. A brief strategy was deployed to estimate how much would be the ΔV , and the constellation requiring the least was chosen as the best candidate for a lunar GNSS.

In conclusion, the best configuration found was the Walker-Delta constellation 18/6/2, at an inclination of 51.65 deg and with a semi-major axis of 6040.34 kilometers.

1.3 State of the art

As of January 2025, there is currently no lunar GNSS in existence, however there is a handful of plans and studies being developed and brought forward by the major space agencies. This section provides the reader with a summary of current projects, that are envisioned to take form in the next 10-20 years.

NASA (National Aeronautics and Space Administration) Artemis program is already in its eighth year, and envisages the return of humans on the lunar surface. It will lay foundation for a future permanent human outpost on the Moon and will also provide funds to both private and public companies to research and develop missions capable to support NASA Moon endeavors through its CLPS (Commercial Lunar Payload Services) initiative. Many missions have been greenlighted, and among these is interesting the case of LuGRE (Lunar GNSS Receiver Experiment), a demonstration mission jointly developed with ASI (Italian Space Agency), launched recently that aims to demonstrate GNSS-based PNT services on the Moon [18] [19]. Its payload comprise of a weak-signal GNSS receiver, a high-gain L-band patch antenna, a low-noise amplifier and a radio frequency filter, all mounted on a lander. The receiver will track GPS and Galileo signals during the transfer to the Moon, in-orbit around the Moon, and later on from the lunar surface. It will return pseudorange, carrier phase and Doppler measurements. Other parts of the Artemis program include the build-up of the Gateway space station, an outpost in cis-lunar space, placed in a NRHO (near-rectilinear halo orbit) orbit and the development of the LunaNet, an Internet analogue based on the Moon [20]. LunaNet is meant to be the Moon-based analogue to terrestrial Internet, a data network capable to store-and-forward data to provide a Delay/Disruption Tolerant Network (DTN), granting it a certain grade of autonomy from Earth-based solutions. More importantly, LunaNet will also offer PNT (Position, Navigation and Timing) services to its user, necessary for orbit determination or navigation on the lunar surface, such as a lunar rover or an EVA (extra-vehicular activity). It is a NASA and ESA (European Space Agency) project intended to be fully operational in the mid-30s, and a standard has been proposed to allow interoperability between different providers [21][2]. Consequently, LuGRE will also serve as foundation for NASA's proper instantiation of LunaNet, called LCRNS (Lunar Communication Relay and Navigation System). Initial operating capabilities are expected to be met around September 2026, with at least an AFS (Augmented Forward Signal) satellite. Plans for expansion foresee at least 4 AFS for the year 2030. Initial Service will be limited to the South Polar region, as depicted in Figure 1.2, with requirements stating the coverage to be guaranteed between the -90 and -75 degrees latitudes, up

to the 200 km in altitude.



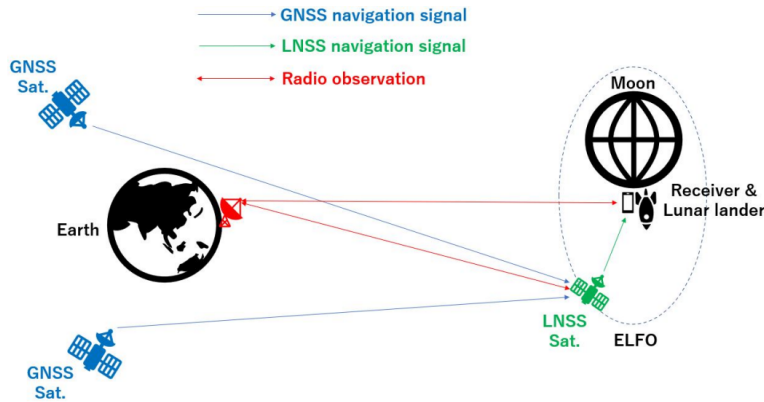
Figure 1.2. Initial LCRNS lunar service volume [2]

ESA's Moonlight program aims to be Europe's first dedicated satellite constellation for telecommunications and navigation services for our natural satellite. It will be compatible with the LunaNet standard. Current plans envision a constellation of 4 satellites orbiting the Moon in ELFO (elliptical lunar frozen orbit). The details of the considered orbits are reported below in Table 1.1. It will primarily focus on covering the area of the lunar South Pole, since it contains a few possible locations regarded as primary targets for future lunar landings, like Shackleton crater, but it will also assure coverage over the entire lunar surface when fully deployed . The Keplerian orbital elements of the ELFO orbits have been selected to minimize orbit-keeping maneuvers. Due to its small size, it will not be able to guarantee 4 satellites in simultaneous visibility from all points on the surface, so in the first phases it will take into consideration signals from Earth GNSS like GPS and Galileo satellites. The system should be able, according to numerical simulations, to maintain a mean GDOP of about 20 with the aforementioned satellites, and a mean GDOP of around 4 with the inclusion of a surface beacon to be deployed later. A demonstration mission, Lunar Pathfinder is expected to launch in 2026 [13]. The proposed road map conceives that Moonlight services will be gradually deployed, with initial operations starting from the end of 2028 and full operational capabilities by 2030.

Table 1.1. Moonlight 4-sat constellation [13]

Orbital elements	SAT 1	SAT 2	SAT 3	SAT 4
Semi-major axis a [km]	9750.73	9750.73	9750.73	9750.73
Eccentricity e	0.6383	0.6383	0.6383	0.6383
Inclination i [deg]	54.33	54.33	61.96	61.96
Argument of perigee ω [deg]	55.18	55.18	121.7	121.7
RAAN Ω [deg]	277.53	277.53	59.27	59.27
True anomaly ν [deg]	123.42	0	180	0

JAXA (Japanese Aerospace Exploration Agency) is also a close collaborator to the LunaNet project, and is proposing its own constellation of satellites in ELFO orbits, called Lunar Navigation Satellite System (LNSS) [22], capable to service users on the lunar surface by providing them with communication, positioning, navigation and timing services. The plan, as can be seen in Figure 1.3, is to have 2 satellites orbiting the Earth in GEO or MEO, working as relay satellites, and a set of 8 satellites orbiting around the Moon, in two ELFO planes. The two relay satellites mostly help with communication, while PNT services rely on communication with the lunar satellites and existing terrestrial GNSS. A lunar demonstration mission is set to launch in 2028, consisting of a LNSS satellite and a LNSS receiver to be deployed at the South Pole region [3].

**Figure 1.3.** LNSS architecture [3]

CNSA (China National Space Administration) has plans of its own to answer to the LunaNet project. Its main lunar program, Chang'e, will certainly need supporting missions, to provide critical services like communication and PNT. Plans are not currently known in deep-detail, but a mixed near-Moon constellation seems the more plausible idea [23]. Such a constellation will consist of 18 satellites in four different types of orbits: ELFO, NHRO, distant retrograde orbits (DRO), and

libration point halo orbits, and will be aided, in due time, by surface infrastructure, specifically in the lunar South Pole. [24] Queqiao-1 was a mission launched in 2018, with the scope of serving as communication link between the Earth and the far-side of the Moon and was placed in a halo orbit around the Earth-Moon system L2 point. More recently, Queqiao-2 was inserted into an ELFO orbit, and carried two smaller satellites, Tiandu-1 and Tiandu-2 which will verify the feasibility of lunar communication and navigation.

All these solutions hereinbefore discussed involve small initial constellations, usually arranged in ELFO orbits, and are heavily dependent, in the initial phases, on existing Earth-based GNSS systems. The key advantage of this solution is that infrastructure is already set up. On the other hand, in order to use Earth GNSS signals, satellites must carry a high gain antenna to compensate for the low power signals due to long distances. The cost for these spacecraft is certainly greater, and could limit the number of lunar orbiters. Only in successive iterations, these proposed constellations forecast increasing independence from Earth-bases GNSS systems. The study here proposed has the scope to lay out a feasible Moon-based GNSS constellation, independent of the terrestrial GNSS system, but capable nonetheless to provide PNT services on the lunar surface. Nevertheless, it is not the aim of this work to discuss the build up of such a constellation.

1.4 Thesis outline

This thesis is organized as follows:

Chapter 1 is the introduction chapter, where both the background that led to develop this work and the scope of the thesis are discussed. The state of the art on constellation design is thoroughly examined, and relevant comments are made with respect to the envisioned application of a GNSS.

Chapter 2 deals with the problem of coverage of a planet surface, as it is both related to the altitude to the satellite which performs the observing, and independent of it, due to the definition of spherical distance between two points on the planetary surface. It is indeed this concept that allows for the search of the lower-bound solutions for both SoC and Walker-Delta classes. In the same chapter, the definition of multiple, global and continuous coverage is explained, as well as a first definition of constellation classes: symmetric and non-symmetric constellations. Examples from each class are provided.

In chapter 3 the model used for orbital analysis is explained, starting from the simple keplerian model, to a more complex model that takes into consideration

secular effects of the zonal harmonic coefficient J_2 , and to a complete model with perturbations due to both the non-spherical gravity model of the Moon and to third bodies, such as the Earth and the Sun. In this chapter, the concept of a repeating ground-track orbit is introduced to be used in numerical simulations later.

Chapter 4 deals with the methodologies for designing satellite constellations. The methods to develop a SoC constellation have been described in detail, from the very first to the successive iterations in time. All of these are regarded as analytical approaches, and are well defined. An original aspect of this work is the reformulation of the problem by generalizing its domain. This extension increases the solution space, enabling more diverse and effective solutions to be considered. On the other hand, methodologies for designing a Walker-Delta constellation are varied, although they are all numerical methods, and vary from simple spherical trigonometry to using a gridded set to compare results. An alternative version of the gridded method, also known as Lang's coverage method, is proposed with the scope of limiting the search to a smaller time frame.

Chapter 5 focuses on the Global Navigation Satellite System (GNSS). Its basic principles, meaning trilateration and the use of pseudoranges are explained. A form of the navigation equations is examined, and linearized for an estimated position of the receiver. The corresponding linearized model is used to explain the dilution of precision (DOP), a figure of merit of the positioning estimate process that is capable to quantify the error propagation on positional measurement precision.

Chapter 6 addresses the results obtained using the methodologies explained in chapter 4. A comparison between the two classes is made, and it is shown that Walker-Delta are more efficient for multiple global coverage. A list of feasible configurations comprised of Walker-Delta constellation is then analyzed for coverage efficiency, and the best configurations among these are studied in an orbital analysis, to estimate the amount of ΔV needed not to drift from the nominal phasing. Based on these parameters, the Walker-Delta 18/6/2 configuration is chosen to be the proposed lunar GNSS constellation.

In chapter 7, a detailed coverage analysis is conducted for the proposed GNSS constellation over a limited area, with the scope to identify gray areas, regions that experience the intermittent loss of a single satellite, due to obstruction of the line-of-sight. The analysis is based on an algorithm, originally conceptualized for observation missions and later adapted with the implementation of the DEM to convey the location and extent of these areas. The application region is Shackleton crater, an area on the South Pole of significant scientific importance.

Chapter 8 serves as a recap and display of what the proposed GNSS constellation achieves in terms of requirements and performance. It also outlines potential future work that can enhance the search for other minimal constellations.

Lastly, in the appendixes A and B, tables for lower-bound solutions of both classes of constellation are provided for further use.

Chapter 2

Constellation geometry

2.1 Coverage problem

The coverage area is, by definition, the region on the planet surface which is visible from an orbiting satellite.

In general, the coverage area is defined at a point in time, since the location of both the observed area and the position of the satellite keep changing.

The satellite is able to interface only with users on the surface within the coverage circle, while users outside of it cannot receive any signal. The ability to communicate is fundamental for the correct operation of a GNSS constellation.

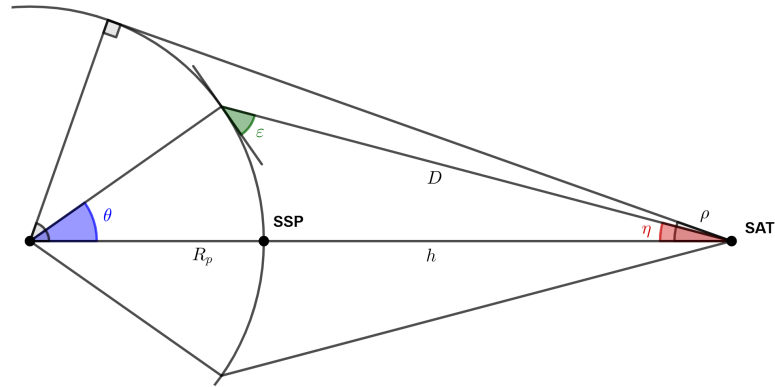


Figure 2.1. Coverage geometry for an orbiting satellite

From this point forward the general target planet is modeled as a perfect sphere, but corrections will be made to account for the topography of the planet in Chapter 7. The two dimensional geometry of the problem is depicted in Figure 2.1, but the relations that will be found are also valid in the three dimensional space.

Consider a satellite orbiting a planet of radius R_p at an altitude h over its surface. The projection of the satellite's position on the planet is known as the sub-satellite

point (SSP).

If the sensor is oriented along the nadir direction, the coverage area is delimited by a spherical circle centered on the SSP, also known as the pole of the circle.

The angle defined at the center of the planet between the SSP and the edge of the coverage disk is known as the planet central angle θ . In this dissertation the angle is called the coverage angle.

The same spherical circle can be described from the point of view of the satellite. In this case the same circular arc from the SSP to the edge of the disk is subtended by the nadir angle η , at the satellite's position.

Lastly, there remains an angle to be defined to describe completely the triangle presented in Fig. 2.1 and it is the elevation angle ε .

Consider a point (relatively close to the SSP) on the surface of the planet and the plane tangent to the surface in that point. The angle between said plane and the segment to the satellite (known as the slant range D) is the elevation angle.

If the point considered lies on the edge of the coverage spherical circle, the elevation angle is equal to a threshold value, the minimum elevation angle ε_{min} . This value defines the size of the coverage circle, as only points on the sphere that have a greater elevation angle belong to the coverage area. At the same time, points on the outside possess an elevation angle that is smaller than the threshold value.

$$\varepsilon \begin{cases} < \varepsilon_{min} & \text{outside the coverage circle} \\ = \varepsilon_{min} & \text{the coverage circle} \\ > \varepsilon_{min} & \text{inside the coverage circle} \end{cases}$$

The coverage problem is, in this simple case, a symmetric one. We can therefore focus on the triangle depicting the situation and the circular arc representing the coverage circle from Fig. 2.1.

The largest triangle represents the ideal coverage, and is a right triangle.

The elevation angle is zero in this case, meaning that an observer stationed at the coverage circle edge would see the satellite on the horizon. The ideal case can be simply considered as the coverage circle obtained by a minimum elevation angle $\varepsilon_{min} = 0$ deg.

The planet from the satellite's perspective appears as occupying a portion of its field of view, known as the angular diameter of the planet. Here we talk about the angular radius of the planet ρ (also found in other texts as the viewing angle) and it depends solely on the satellite altitude.

As a side note, the nadir angle η defined before can generally vary between 0 and ρ , its maximum physical value.

In the real case a satellite on the horizon would not be visible, because of the non-spherical shape of the planet, the presence of obstructions in the line-of-sight direction (like the trees, mountains and buildings) and the atmosphere degrading signals.

For this reason the minimum elevation angle is used: below this value signals from a satellite are ignored. Consequently, the effective coverage area will be generally lower than the theoretical one.

To sum it up, the angles that subtend the coverage area are always dependent on the satellite's altitude and the elevation angle considered. Nonetheless, for the applications considered, a certain threshold value is used, relinquishing the dependency on the elevation angle.

$$\begin{cases} \eta = f(h, \varepsilon) \\ \theta = f(h, \varepsilon) \end{cases} \quad \text{in the general case}$$

$$\begin{cases} \eta = f(h) \\ \theta = f(h) \end{cases} \quad \text{for a fixed } \varepsilon_{min}$$

To find the relation between these three parameters, we can use some basic geometry [6]. Since any triangle has the sum of its interior angles equal to 180 degrees, we can derive the nadir angle η from the other two.

$$\eta = \frac{\pi}{2} - (\theta + \varepsilon) \quad (2.1)$$

Then, using the law of sines for the smaller triangle and substituting the angle η with the value previously obtained in Eq. (2.1), we reach the expression of the coverage angle as a function both of the elevation angle and the altitude.

$$\theta = \arccos \left(\frac{R_p}{R_p + h} \cdot \cos \varepsilon \right) - \varepsilon \quad (2.2)$$

Fig. 2.2 show the dependence of the coverage angle from the two other parameters for the Earth and the Moon.

Simply put, the coverage angle increases with the altitude of the satellite, while it decreases for increasing values of the minimum elevation angle required.

Whereas at high altitudes, the coverage angle is a strong function of the elevation angle, it presents low susceptibility at low altitudes.

The graphs for both celestial bodies are in the same scale, so one can appreciate how the radius of the planet plays a role. A smaller radius, considering fixed all

other parameters results in a larger coverage angle. For reference the radius of the Moon is around 3.5 times smaller than the Earth's.

$$h = R_p \left(\frac{\cos \varepsilon}{\cos(\varepsilon + \theta)} - 1 \right) \quad (2.3)$$

For a fixed value of ε_{min} , this curve shows the maximum coverage angle θ for a satellite at a given altitude, or conversely the minimum altitude for a requested coverage angle, as it can be inferred from Eq. 2.3.

Alternatively, if the satellite altitude is fixed, the coverage angle θ can be limited with the intention of maximizing the operating elevation angle [4].

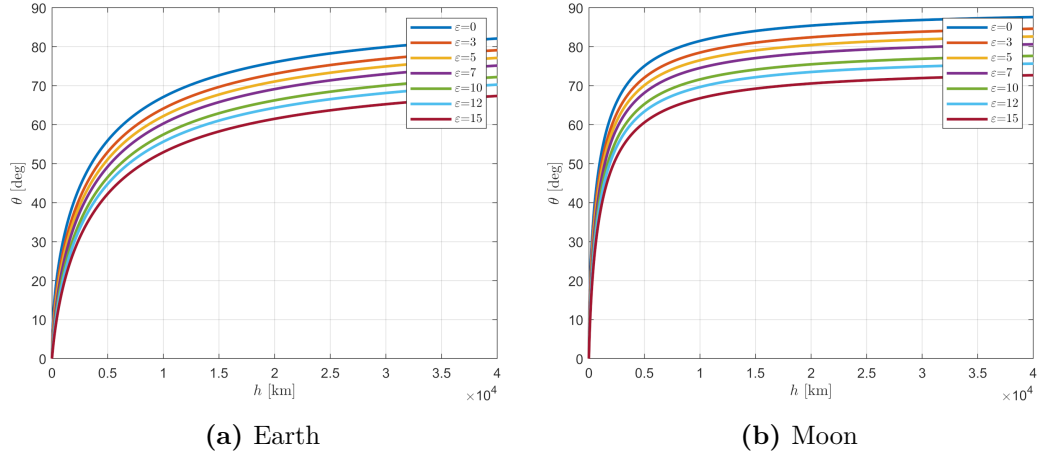


Figure 2.2. Coverage angle as a function of altitude and elevation angle

Other dependencies (optional)

Other parameters that can affect the coverage angle or area shape are the eccentricity of the orbit, and the orientation of the sensor.

An eccentricity different from zero would cause the satellite to vary its altitude over time, consequently altering the size of the coverage circle at intervals.

Conversely, if the sensor is modeled as directional, its sensing region can be represented as a cone and the effective coverage area on the planetary surface is determined by the intersection of the cone with the sphere, forming a spherical cap. As a consequence the coverage area assumes the form of a circle for nadir orientation, as depicted in Fig. 2.1. For different orientation the geometry becomes more complex.

Another restriction on the coverage is the field of view of the instrumentation (either optical or a transmission device) that is onboard the satellite and can limit the angle η .

For GNSS applications, the aspect to consider is the antenna beamwidth, defined as the angular span of the main lobe of the antenna radiation, namely the region where most of the power is radiated. In this case, we talk about an idealized version of the coverage region, where signals are received the best.

Some values used in GNSS constellation are shown in Table 2.1, obtained by the United Nations Office for Outer Space Affairs [14].

Table 2.1. GNSS transmitter beamwidths [14]

GNSS constellation	L1 beamwidth [deg]
GPS	23.5
GLONASS	26
Galileo	20.5
BeiDou-MEO	25
BeiDou-GEO/IGSO	19

2.2 Spherical geometry

The geometry that involves itself with the study of the 2-dimensional surface of a sphere is known as spherical geometry. This branch of mathematics has found large applications in practical fields such as astronomy, navigation and geodesy.

The biggest difference between Euclidean and spherical space is the metric utilized, the latter one having a curvature. Whereas a line is straight in the planar space, it assumes the form of a circle in the spherical space.

Consequently, the distance between any two points on the surface of a sphere is measured along the great circle arc passing through them, and it is the shortest path available.

Circles are the intersection of a plane with a sphere, and depending on where the plane intersect the sphere, they define either a great or small circle.

Great circles are obtained when the center of the sphere belongs to the plane, and small circles are obtained for all other planes that intersect the same sphere. Any two points that are not at the antipodes both lie on a unique great circle, which the points separate in two arcs: minor arc and major arc, the former one being defined as the spherical distance.

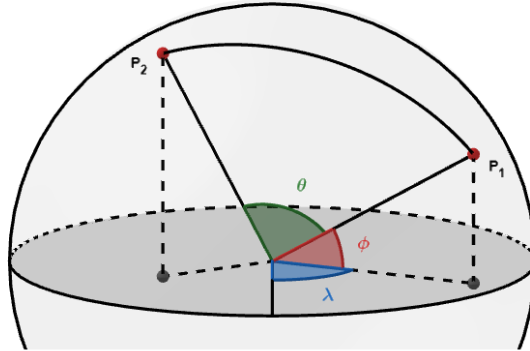


Figure 2.3. Spherical distance between two points on the surface of a sphere

Given the coordinates (longitude λ and latitude ϕ) of two points on a sphere we can use the spherical law of cosines to obtain the central angle that defines the minor arc between them. The result is given in Eq. 2.4, while Fig. 2.3 shows the geometry for any two points on the sphere.

We've already discussed the planet central angle θ in the previous section, but this time it is completely unrelated by coverage geometry concerns, and it defines only the angular distance on the sphere for any two points.

$$\theta = \arccos(\sin \phi_1 \sin \phi_2 + \cos \phi_1 \cos \phi_2 \cos \Delta\lambda) \quad (2.4)$$

If one these point is taken to be the SSP, we have defined once again the coverage circle. And since the SSP's position is independent from the satellite's height h and the elevation angle ε , so is the newfound circle.

Therefore θ can be defined both as the half-angle of the coverage circle and the spherical distance between a point on the surface of the planet and the SSP of the aforementioned satellite.

This new definition will be useful in Chapter 4, as the simulations will consider the distance between gridded points on a sphere to design the minimal constellations.

2.3 Circular constellations

A constellation is a group of satellites designed to fulfill a common mission, in our case coverage [10].

While the maximum area that can be covered for a single satellite is 50% of the planet surface, as it can be seen for the asymptote for $\varepsilon_{min} = 0$ deg in Fig. 2.2, a constellation is able to provide global coverage (100% of the surface).

To have multiple coverage it is required that any point considered to be within range of multiple satellites. The wording "n-fold" is used to indicate the degree of

coverage n requested. Conversely, continuous coverage means that the preceding properties for the coverage are maintained at all times.

The constellations considered are composed of satellites with the same orbital parameters, particularly with the same semi-major axis a and prograde inclination i . Furthermore, only circular orbits ($e = 0$) are considered, since they allow for constant coverage properties.

There are countless configurations of satellites able to meet the requirements of a given coverage problem, hence the main aim is to find the most efficient constellation. This optimization problem can be uncoupled from the satellite altitude h and the elevation angle ε by using the planet central angle/spherical distance θ as the primary independent variable [4].

An efficient constellation, for this thesis' sake, is the one able to guarantee the coverage requirements with the lowest number of satellites T at the lowest altitude h possible. In this regard, both the number of satellites T and the coverage angle θ , (from which depends the altitude for a given ε_{min}) can be considered efficiency values.

A consideration must be made for constellations that strive to achieve global coverage. Regardless of its class, a constellation must satisfy Eq. 2.5 to reach the poles of the planet. This is a necessary equation to guarantee single global coverage, albeit not sufficient.

$$\theta \geq \frac{\pi}{2} - i \quad (2.5)$$

The first constellation of satellites was proposed by Clarke in 1945, and consisted of three GEO satellites that could ensure global coverage. Since then, many authors came up with different ideas for constellations. Among these, the most important contributors were Walker, Mozahev, Lüders, Lang, Rider, Beste, Ulybyshev and Mortari [25, 26].

2.3.1 Symmetric vs non-symmetric

Constellations can be organized based on their symmetrical properties [27].

A symmetric constellation entails an even distribution of orbital planes in space and of satellites on each plane. The ease of completely describing them through just a few parameters is considered to be their main advantage. Generally, the number of satellites, of planes and the phasing suffice to describe the shape of the constellation and are known altogether as the constellation parameters. Furthermore, the symmetric configuration provides predictable properties, that can be surmised

from a limited analysis both in space and time. Conversely, the symmetry of the configuration might lead to inefficient solutions, clustering satellites and coverage over certain portions of the surface. A homogeneous constellation is a special case of symmetric constellation, in which all the satellites share the same orbital parameter, such as altitude, inclination and eccentricity.

A non-symmetric constellation has no discernible pattern that can be used to predict its coverage properties. The constellation is built in accordance to a certain logic that minimizes the number of satellites, while ensuring the requested coverage. The result is an uneven distribution of satellites and planes. For this reason, a plethora of parameters is necessary to completely describe a non-symmetric constellation. The concept of repeating ground-track orbits is paramount to study their behavior in a limited time frame.

2.3.2 Walker-Delta

Walker-Delta constellations are the results of studies made by J.G. Walker with the British Royal Aircraft Establishment in the 60s [28, 29, 30]. Similar constellations were developed independently by Mozhaev, and they're sometimes known as kinematically regular satellite constellations (KRSC).

Walker-Delta constellations are symmetric homogeneous constellations, that involve only circular orbits. Four parameters are enough to describe completely its shape, namely the number of satellites T , the number of orbital planes P , the phasing factor F and the inclination of the reference orbital plane i . The size is instead given by the altitude of the reference satellite h .

$$T, P, F, h, i \quad \Rightarrow \quad \text{to completely define a Walker-Delta constellation}$$

As a remark, the phasing factor F is an integer ranging from 0 to $(P-1)$ and describes the relative positioning of satellites in different orbital planes. We define intraphasing ΔM_{intra} as the phasing between satellites on the same plane, whereas interphasing ΔM_{inter} is the phasing between successive satellites in adjacent orbital planes, where "successive" refers to satellites passing their respective ascending nodes in succession. Lastly, the phasing $\Delta\Omega$ that occurs between orbital planes is entirely defined by its number and the range over which to distribute them, alas 2π .

$$\Delta M_{intra} = \frac{2\pi T}{P} \quad (2.6)$$

$$\Delta M_{inter} = \frac{2\pi F}{T} \quad (2.7)$$

$$\Delta\Omega = \frac{2\pi}{P} \quad (2.8)$$

2.3.3 Streets-of-Coverage

Streets-of-Coverage (or SoC) is a class of non-symmetric constellations that uses the concept of streets to guarantee the requested coverage.

A street is the ensemble of the covered area by all the satellites in a given orbital plane, during an orbital period. It is shown in Fig. 2.4. Stringing a few streets together it is possible to cover the entire planet.

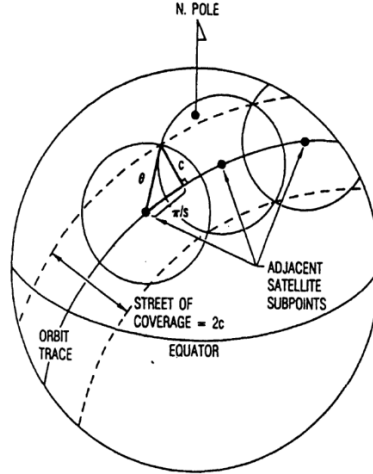


Figure 2.4. Street-of-Coverage geometry [4]

The range over which orbital planes are distributed is therefore limited to π , since a street is defined both in its ascending and descending phases, but the spacing, as well as the phasing of the satellites are optimized to minimize the number of satellites T . Eqs. (2.6)-(2.8) are no longer applicable.

$T, P, h, i, \Delta\Omega, \Delta M_{inter}$ \Rightarrow to completely define a SoC constellation

The coverage requirement assumes a different expression for SoCs. Whereas j is the coverage guaranteed by a single street of coverage along its orbital plane, k is the coverage guaranteed across different streets of coverage adjacent to each other. In this study we only considered constellations with $k = 1$.

Table 2.2. Coverage options for SoC constellation

$n = j \cdot k$	$j = 1$	$j = 2$	$j = 3$	$j = 4$	$j = 5$
$k = 1$	1	2	3	4	5
$k = 2$	2	4	6	8	10
$k = 3$	3	6	9	12	15
$k = 4$	4	8	12	16	20
$k = 5$	5	10	15	20	25

2.3.4 Hybrid constellations

Constellations that cannot be easily categorized are called hybrid. They can either symmetric (only heterogeneous) and non symmetric.

A hybrid constellation can consist of several homogeneous constellations, called shells that differ in altitude, eccentricity and/or inclination.

Two examples are BeiDou and Starlink, as they both employ different shells to provide coverage. Hybrid constellation tend to be larger, and consequently more difficult to analyze and design.

2.4 Examples

2.4.1 GPS

The GPS (acronym for Global Positioning System), depicted in Fig. 2.5 was developed by the United States during the Cold War in the 1970s for military applications.

The GPS constellation is the both the first GNSS and Walker-Delta constellation to be built. The system was originally named Navstar GPS, and the first GPS satellite, Navstar 1, was launched in 1978. The system was made available to the civilian sector in 1983, which eventually stimulated the development of commercial GPS applications.

The GPS was originally a Walker-Delta 24/6/2 constellation (at the present the satellites are somewhat displaced from nominal positions) and consists nominally of 24 satellites in 6 different orbital planes, at an altitude of approximately 20200 kilometers above Earth and at a common inclination of 55 degrees. Together they are capable to guarantee 4-fold global coverage. Each satellite completes a full orbit around the Earth every 12 hours.

2.4.2 GLONASS

GLONASS (russian acronym for Global'naya Navigatsionnaya Sputnikovaya Sistema) is Russia's GNSS answer to the GPS. It was originally conceptualized in 1980 by the Soviet Union, and only became operational in 1996.

Financial challenges constrained its development and functionality, which was restored in the early 2010s. It is intended for both military and civilian use.

The system, shown in Fig. 2.6, includes 24 satellites in MEO orbits with an inclination of 64.8 deg, providing complete Earth coverage, with a bias towards higher latitudes, since that's where most of Russia's land is located. The constellation is a Walker-Delta 24/3/1, the satellites orbit at around 19100 kilometers above Earth and complete an orbit in approximately 11 hours and 15 minutes.

2.4.3 Galileo

The Galileo satellite navigation system is Europe's independent GNSS. It was jointly developed by the EU (European Union) and the ESA to reduce reliance on the American and Russian systems, as it was feared that access could be restricted or degraded during conflicts or geopolitical spats. The system is intended primarily for civilian use.

The EU announced plans for a European GNSS in 1999. Due to difficulty of acquiring the funds, the first two operational satellites were only launched in 2011. The system reached fully operational status in 2018.

The current setup, shown in Fig. 2.7, comprises 24 satellites, with many spares in orbit. The Galileo system is a Walker-Delta 24/3/1 constellation with satellites distributed on 3 different orbital planes at an inclination of 56 degrees. The satellites orbit at an altitude of 23222 kilometers above Earth, ensuring 4-fold global coverage. Each satellite completes an orbit in about 14 hours.

2.4.4 Iridium

The Iridium constellation, shown in Fig. 2.8, is a system of LEO satellites designed to provide satellite phone and data communication from any point on Earth.

The initial concept originated in the 1980s, developed by the American company Motorola. It envisioned 77 satellites, which explains the constellation name as iridium is the element with atomic number 77. The system was later shrunk to 66 satellites, but the name was kept. The first satellites were launched in 1997, and full global coverage was achieved in 2002.

The Iridium constellation is a Street-of-Coverage 66/6 constellation, with 11 satellites on each of the 6 orbital planes. The planes are almost polar, displaying an inclination

of 86.4 degrees. The satellites, being LEO, orbit Earth at an altitude of 781 kilometers and complete 14 orbits per day, and are able to provide 1-fold global coverage of the surface.

2.4.5 BeiDou

The BeiDou Navigation Satellite System is China's GNSS and is operated by the CNSA.

Throughout its development, BeiDou went through three iterations. BeiDou-1 was a regional system that used three GEO satellites and was launched in 2000. It provided 4-fold coverage only to China and nearby regions. Its second iteration, BeiDou-2, came online in 2012, and managed to cover the extended Asia-Pacific region. The last and actual version, BeiDou-3, is able to guarantee a 4-fold global coverage with increased accuracy. The full constellation was completed in 2020.

BeiDou, shown in Fig. 2.9, is a uniquely hybrid constellation, that comprises 30 satellites in three different shells (or mini-constellations). Shell 1 is a simple Walker-Delta 24/3/1 constellation at 55 deg, with the satellites in MEO orbit (at around 21500 kilometers in altitude). The orbital period of a satellite is around 12 hours. Shell 2 is comprised of 3 IGSO (inclined geosynchronous orbits) satellites at 55 deg and therefore could be considered a Walker-Delta 3/3/2 constellation. Lastly, shell 3 is constituted by 3 GEO satellites accurately placed in such a way to enhance user service within China.

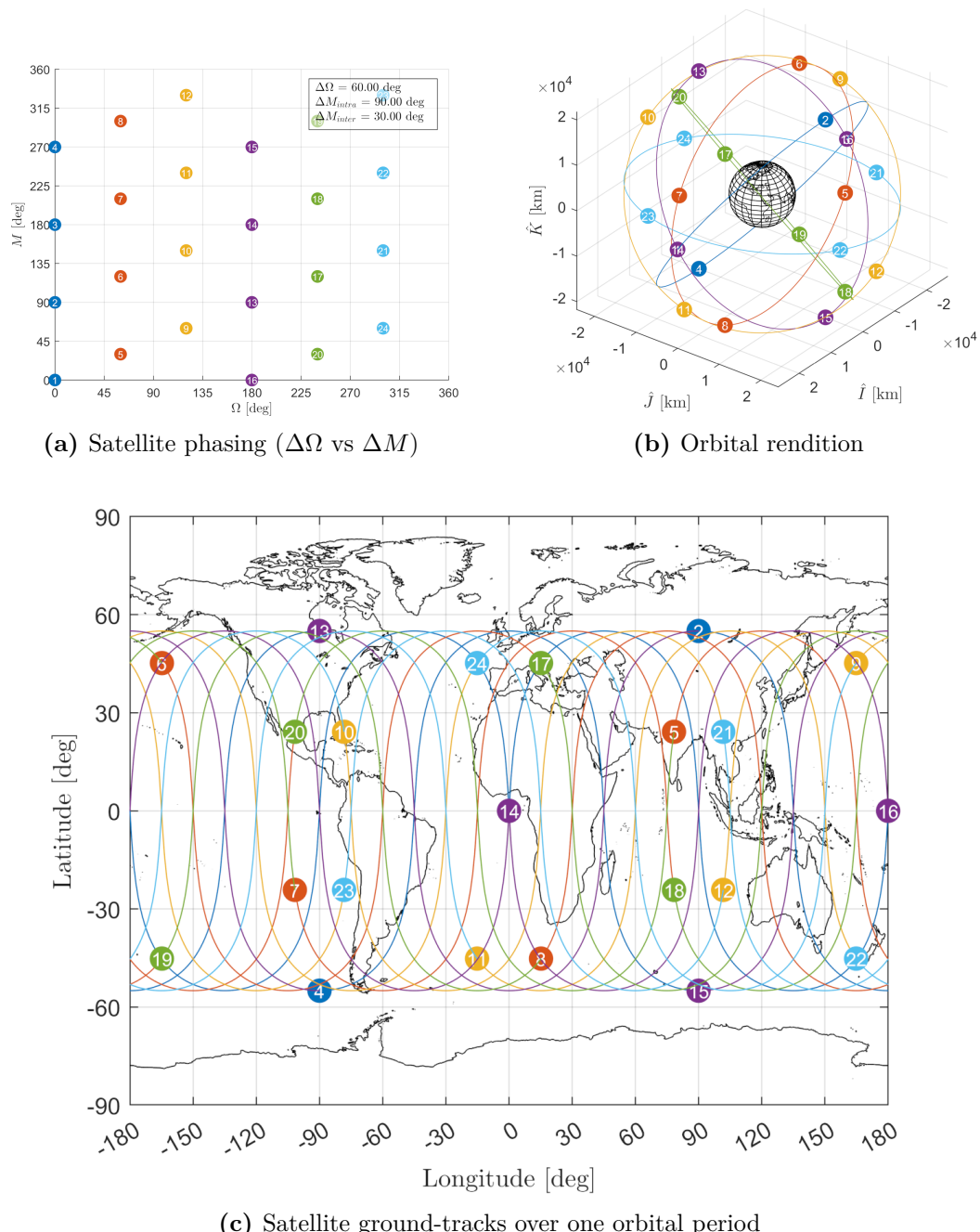


Figure 2.5. GPS constellation (Walker-Delta 24/6/2)

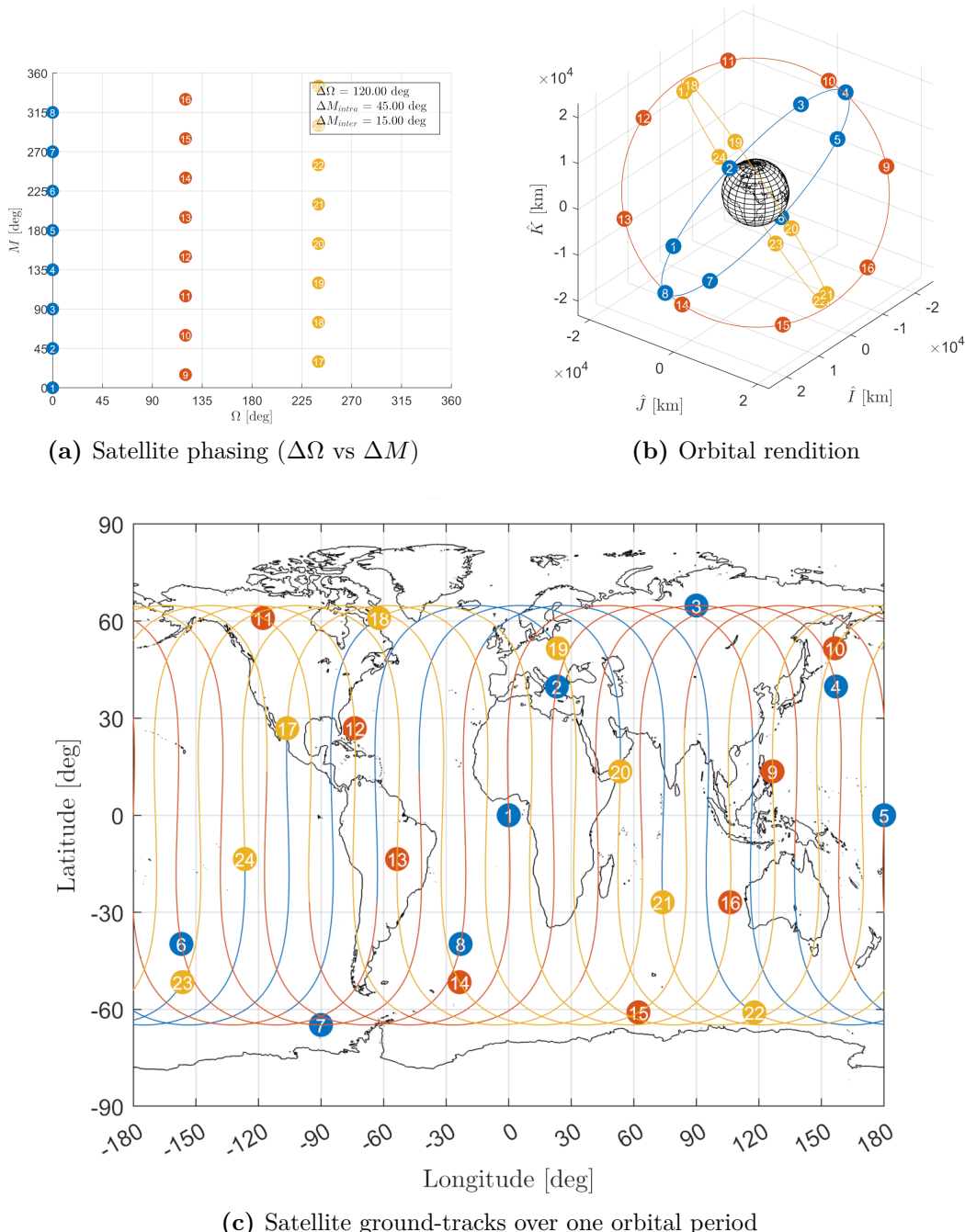


Figure 2.6. GLONASS constellation (Walker-Delta 24/3/1)

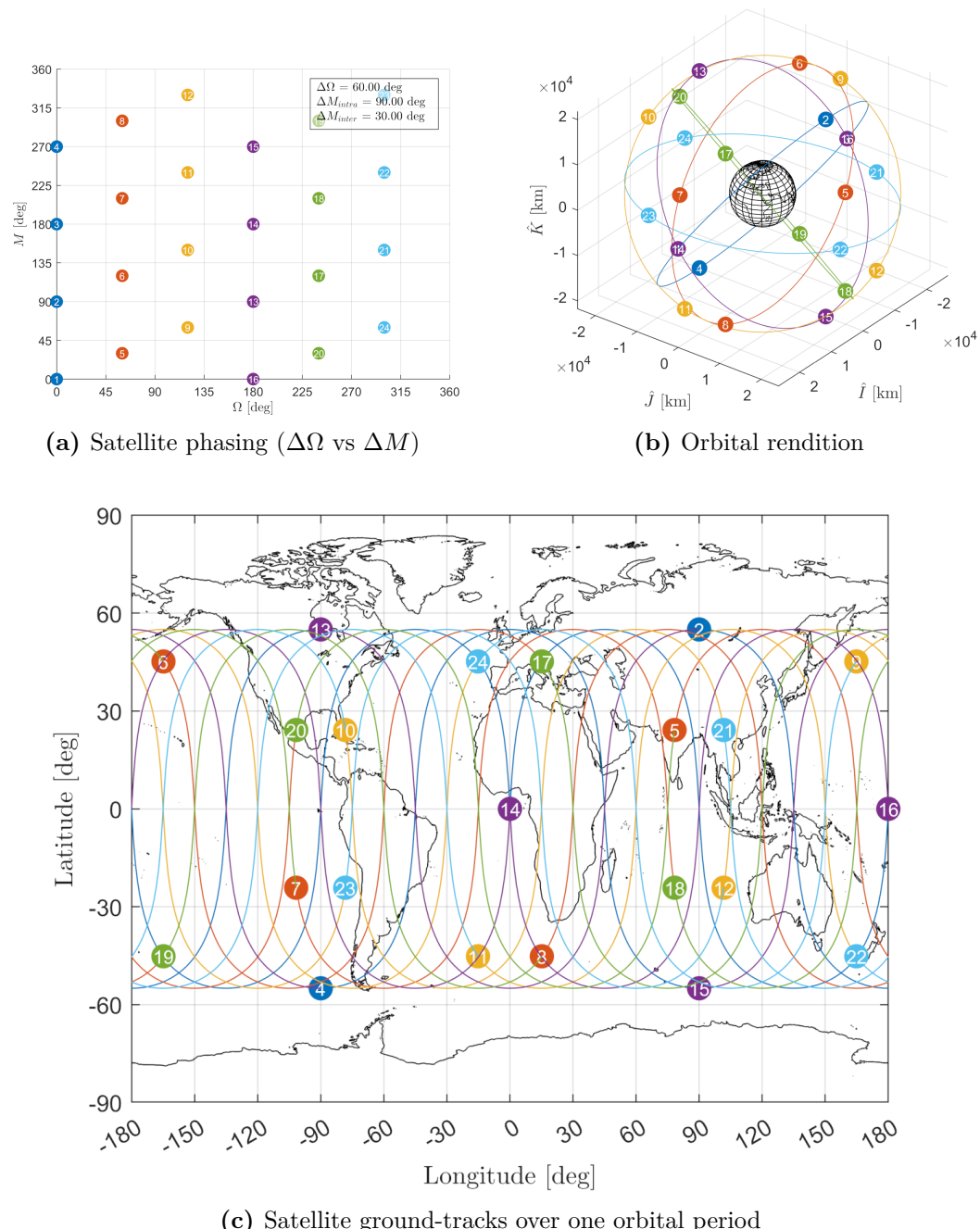


Figure 2.7. Galileo constellation (Walker-Delta 24/3/1)

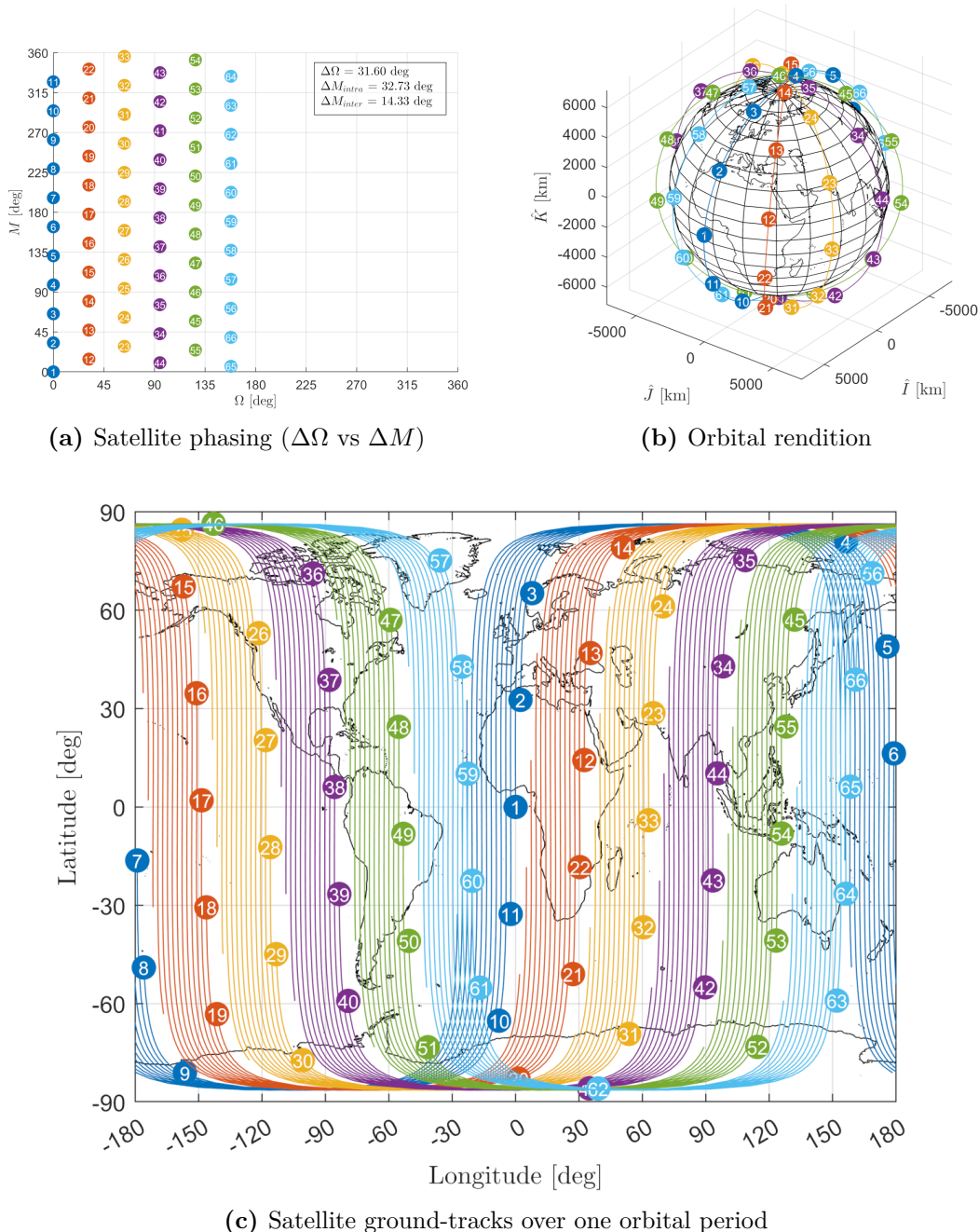


Figure 2.8. Iridium constellation (SoC 66/6)

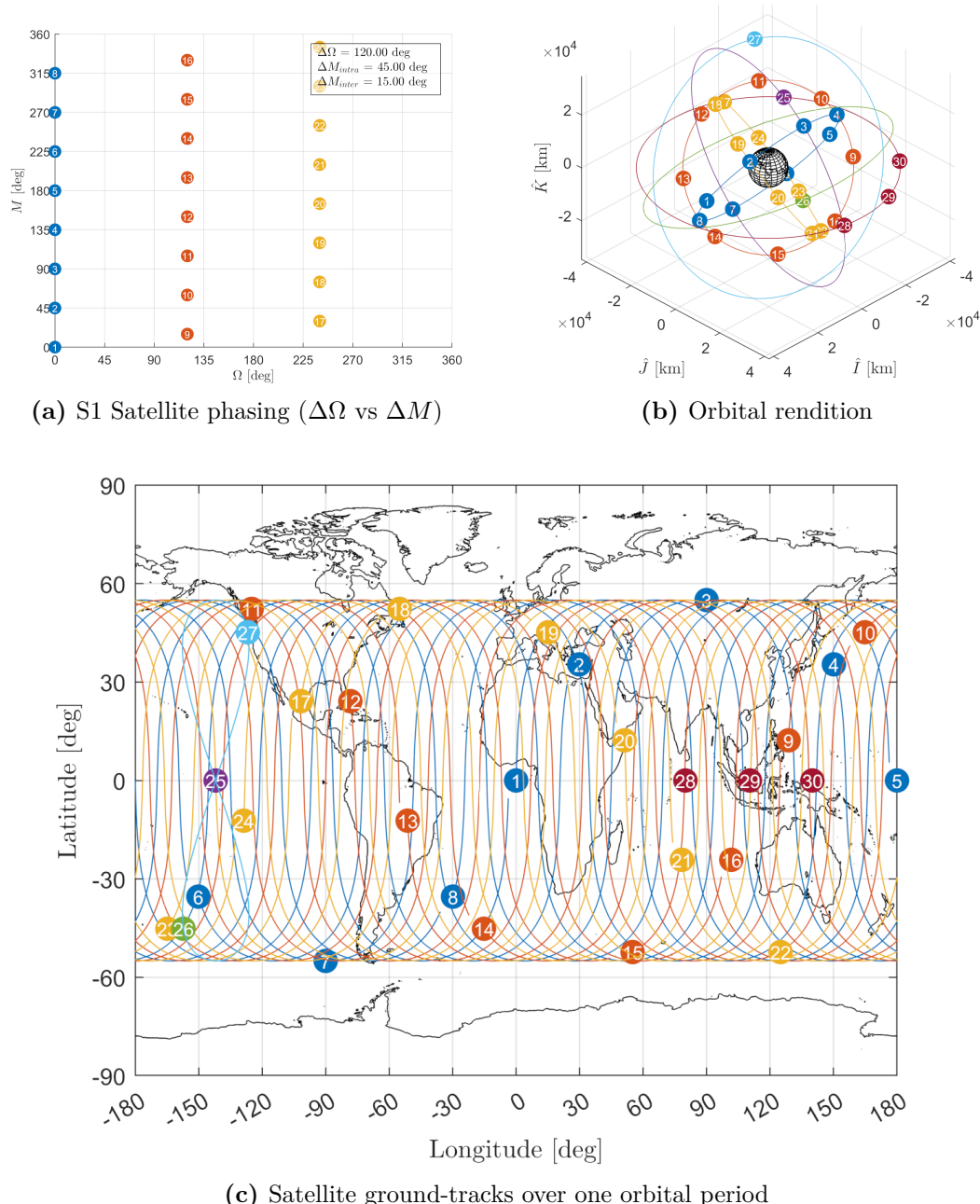


Figure 2.9. BeiDou S1-S3 constellation (Hybrid)

Chapter 3

Orbital mechanics

3.1 Keplerian motion

The motion of an object in space is the result of many acting forces, like gravitational attraction, solar radiation pressure, thrust. It is generally a complex matter to completely describe a satellite motion. Nonetheless, if some assumptions are made, a simpler mathematical expression can be found.

The Keplerian model, named after Johannes Kepler, who formulated the three laws of planetary motion in 1609, is based on several fundamental assumptions: it treats celestial bodies as material points, considers only the central body and the orbiter and ignores all forces except for the gravitational influence of the central body [31].

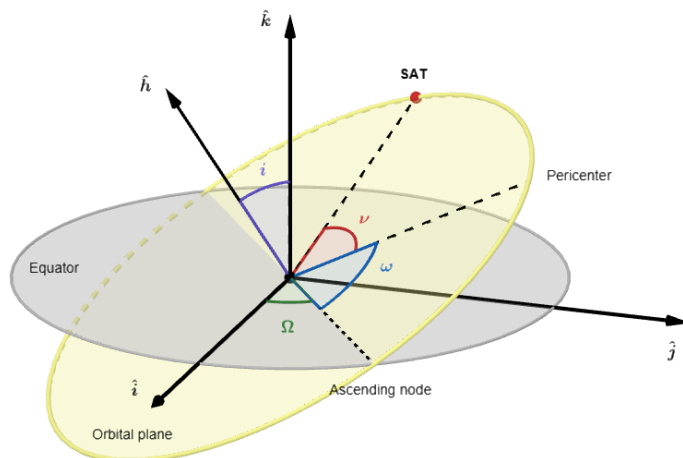


Figure 3.1. Classical orbital parameters

The result is a trajectory, that can analytically expressed as a function of time alone. For an object in proximity of a massive body, this will result in a closed curve, an

orbit.

In this simplified model, constants of motion arise from fundamental physical laws such as the conservation of energy and angular momentum. These constants of motion define the motion of the orbiter and determine the shape, orientation, and energy of its orbit, and are more commonly expressed as the orbital elements, a set of 6 parameters that completely define the trajectory of a satellite.

The parameters that define size and shape of the trajectory are the semi-major axis a and eccentricity e . To have a closed orbit, an eccentricity of less than 1 is necessary. Furthermore, an eccentricity of zero results in a circular orbit.

As it can be seen from Fig. 3.1, three parameters define the orientation in space of the orbital plane on which the satellite motion takes place. These are the inclination i , defined from the equatorial plane, the right ascension of the ascending node Ω , calculated with respect to the vernal axis, and the argument of periapsis ω . Lastly, the true anomaly ν is a function of time and expresses the position of the satellite along its orbit.

Given a set of orbital parameters, it is possible to derive the motion of the satellite. The perifocal frame (PQW) is the easiest frame to describe a satellite position. The frame is centered on the main attractor and has the \hat{X} and \hat{Z} axes oriented along the periapsis direction and the angular momentum direction, respectively.

$$\vec{r}_{PQW}(t_0) = \frac{a(1-e^2)}{1+e\cos\nu(t_0)} \begin{bmatrix} \cos\nu(t_0) & \sin\nu(t_0) & 0 \end{bmatrix}^T \quad (3.1)$$

$$\vec{v}_{PQW}(t_0) = \sqrt{\frac{\mu}{a(1-e^2)}} \begin{bmatrix} -\sin\nu(t_0) & e+\cos\nu(t_0) & 0 \end{bmatrix}^T \quad (3.2)$$

Another angle, the mean anomaly M can be used in place of ν , since it always increases linearly with time, which the true anomaly does not, in general. Nonetheless, if the orbit is circular, mean anomaly and true anomaly coincide.

$$\begin{aligned} M &= E - e \sin E = \\ &= \text{atan2}\left(\sqrt{1-e^2} \sin \nu, e + \cos \nu\right) - e \frac{\sqrt{1-e^2} \sin \nu}{1+e \cos \nu} = \\ &= \nu \end{aligned} \quad (3.3)$$

A new frame, the planetocentric inertial (PCI) is established to express the satellite position and velocity vectors in relation to the planet surface. The frame is centered on the main body, has its \hat{Z} axis along the North Pole direction and the plane

formed by \hat{X} and \hat{Y} is the equatorial plane. In particular the \hat{X} axis is chosen to be oriented along the vernal axis Υ . It is a non-rotating, inertial frame of reference (for all our purposes) and a point in space can be represented through either cartesian coordinates (x, y and z) or polar coordinates (longitude λ , latitude ϕ and altitude h). The rotation matrix that transforms the PWQ coordinates into PCI is a function of the three orbital elements that convey the orbital plane orientation in space: i , Ω and ω .

$$R_{PQW \rightarrow PCI} = \begin{bmatrix} c_\Omega c_\omega - s_\Omega s_\omega c_i & -c_\Omega s_\omega - s_\Omega c_\omega c_i & s_\Omega s_i \\ s_\Omega c_\omega + c_\Omega s_\omega c_i & -s_\Omega s_\omega + c_\Omega c_\omega c_i & -c_\Omega s_i \\ s_\omega s_i & c_\omega s_i & c_i \end{bmatrix} \quad (3.4)$$

$$\vec{r}_{eci}(t_0) = R_{PQW \rightarrow PCI} \vec{r}_{pqw}(t_0) \quad (3.5)$$

$$\vec{v}_{eci}(t_0) = R_{PQW \rightarrow PCI} \vec{v}_{pqw}(t_0) \quad (3.6)$$

The keplerian problem is expressed through the set of Eqs. 3.7 in an inertial frame of reference, that together with a set of initial conditions constitute a Cauchy problem. Consequently, solving it grants the satellite position and velocity vectors over time.

$$\begin{cases} \dot{\vec{v}} = -\frac{\mu}{|\vec{r}|^3} \cdot \vec{r} \\ \vec{r} = \vec{v} \end{cases} \quad (3.7)$$

Should the interest be, on the ground-track of the satellite, another rotation would be needed to a new frame PCPF, centered and rotating with the main body. In this new frame, the \hat{X} is chosen to be oriented along the prime meridian of the planet. The angle α is the right ascension of the prime meridian, and allows to correct for the planet rotation, defined by its angular velocity W_p .

$$\alpha(t) = \alpha_0 + W_p(t - t_0) \quad (3.8)$$

$$R_{PCI \rightarrow PCPF} = \begin{bmatrix} \cos \alpha(t) & \sin \alpha(t) & 0 \\ -\sin \alpha(t) & \cos \alpha(t) & 0 \\ 0 & 0 & 1 \end{bmatrix} \quad (3.9)$$

$$\vec{r}_{PCPF}(t) = R_{PCI \rightarrow PCPF} \vec{r}_{PCI}(t) \quad (3.10)$$

The ground-track of a satellite is the path traced by the SSP on the planetary surface as the satellite moves in its orbit over time. Longitude λ and latitude ϕ can be obtained through a conversion, from cartesian to geographical coordinates.

$$\lambda(t) = \arctan \left(\frac{y(t)}{x(t)} \right) \quad (3.11)$$

$$\phi(t) = \arctan \left(\frac{z(t)}{\sqrt{x^2(t) + y^2(t)}} \right) \quad (3.12)$$

3.2 Earth-Moon system

The Earth and its only natural satellite, the Moon form together a binary system. An artificial satellite in the cis-lunar space is subject to the gravitational effects of both the Earth and the Moon. For satellites that are relatively close to the Moon, keplerian motion can be reinstated. This critical distance is known as the sphere of influence radius D_{SOI} and stands at around 66000 km for the Moon. Within this distance it is possible to neglect Earth's gravitation without deviating much from the real case.

The Moon's mass is about 1/81 of Earth's, resulting in an much weaker attraction, having a surface gravity of 1.62422 m/s², about a sixth of Earth's.

Given that the Moon orbits at an average distance a_M of 384400 km, this greatly limits the region applicable to be considered a Moon's satellite. In reality, the threshold distance is smaller than the value stated, because perturbations grow exponentially with distance from the Moon. The trajectory of the Moon around Earth takes the shape of an ellipse with an eccentricity e_M of around 0.0549, producing to a notable difference between apogee and perigee distances, 405400 and 362600 km respectively.

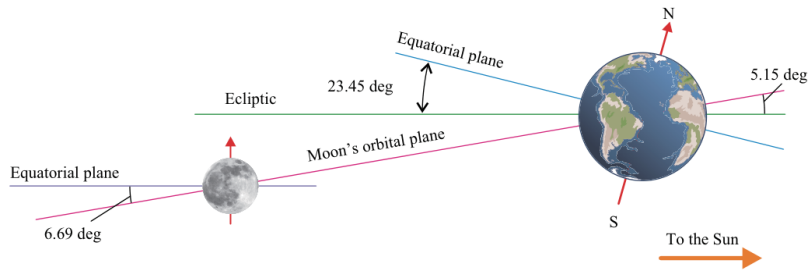


Figure 3.2. Earth-Moon system [5]

Its orbital plane inclination i_M is fixed with respect to the ecliptic plane, the average plane defined by Earth's motion around the Sun, though is not with respect to Earth equatorial plane, itself inclined some 23.4 deg to the ecliptic. The Earth-Moon system is depicted in Fig. 3.2.

The remaining orbital elements that describe the lunar motion orientation undergo secular and periodic changes due to the nature of the dynamical system.

As a matter of fact, the Moon's orbit is perturbed mainly by the third-body, gravitational attraction of the Sun. This perturbation results in apsidal precession, with a period of 8.85 years, and in nodal precession, that causes the lunar orbital plane to rotate with a period of 18.6 years. The values for the Moon's orbit are reported in Eqs. (3.13)-(3.15).

The Moon completes an orbit around Earth in 27.32 days with respect to the fixed stars. This time interval is known as the sidereal period. However, since the Earth-Moon system is moving around the Sun at the same time the Moon is orbiting Earth, it takes longer for the Moon to return to the same lunar phase, around 29.53 days or a synodic period. It is also commonly referred as to the lunar month and is equal to the length of the solar day on the Moon. On the other side, the sidereal day is defined by the complete rotation about its rotational axis with respect to the fixed stars and is solely defined by its rotational speed W_p . This results in a 27.32 days sidereal rotation period.

In fact, the Moon is tidally locked with Earth, meaning it shows a 1:1 orbital resonance. For this reason, only a portion of the Moon's surface is visible from Earth's perspective, the near side. Conversely, the other portion is called the far side of the Moon. In reality, the Moon wobbles a bit, resulting in libration motion that allows for visibility over a greater portion of the lunar surface, about 59% aggregated over time.

$$a_M = 384400 \text{ km} \quad (3.13)$$

$$e_M = 0.0549 \quad (3.14)$$

$$i_M = \begin{cases} 5.15 \text{ deg} & \text{wrt the ecliptic plane} \\ 18.28 \div 28.58 \text{ deg} & \text{wrt Earth equatorial plane} \end{cases} \quad (3.15)$$

The Moon can be approximated at first as a sphere, with a mean radius R_p of 1737.4 km, but a more appropriate description of its shape would be a spheroid, an ellipsoid with circular symmetry. It has both an equatorial a and a polar radius c . Eqs. (3.16)-(3.20) show the Moon's principal physical characteristics [32].

$$R_p = 1737.4 \text{ km} \quad (3.16)$$

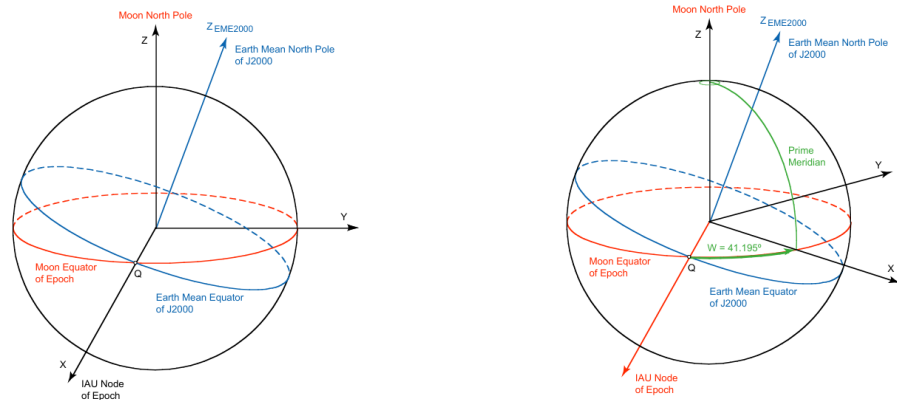
$$a = R_p|_{\text{equatorial}} = 1738.1 \text{ km} \quad (3.17)$$

$$c = R_p|_{\text{polar}} = 1736.0 \text{ km} \quad (3.18)$$

$$W_p = 13.176 \text{ deg/day} \quad (3.19)$$

$$\mu_p = 4904.87 \text{ km}^3/\text{s}^2 \quad (3.20)$$

The general planetocentric frames developed before need to be specialized for the Moon, here assumed a sphere. The new selenocentric frames, called MCI and MCMF respectively, are shown in Fig. 3.3.



(a) Moon Centered Inertial [15]

(b) Moon Centered, Moon Fixed [15]

Figure 3.3. Lunar coordinate systems

While the inertial frame is easy to define based on the lunar equatorial plane and

the vernal axis Υ alone, it is necessary to define a prime meridian on the Moon as a reference datum, from which points on the surface can be located. On Earth it's the meridian passing through Greenwich, UK, and for the Moon it was chosen as the meridian passing through the center of the Moon's disc as seen from Earth, near the crater Bruce [15]. The intersection of the lunar equatorial plane with the prime meridian results in a direction, which is chosen as the \hat{X} direction for the body-fixed frame.

3.3 Perturbations

Accelerations not considered in the keplerian model are considered to be perturbations. Among the sources of perturbations we can have a complex gravitational field of the main body, the presence of third bodies, the solar wind, as well as the drag caused by an atmosphere. Fortunately, the Moon has no atmosphere, so the last perturbation can be easily disregarded. Perturbation accelerations for a satellite in lunar orbit are presented in Fig. 3.4.

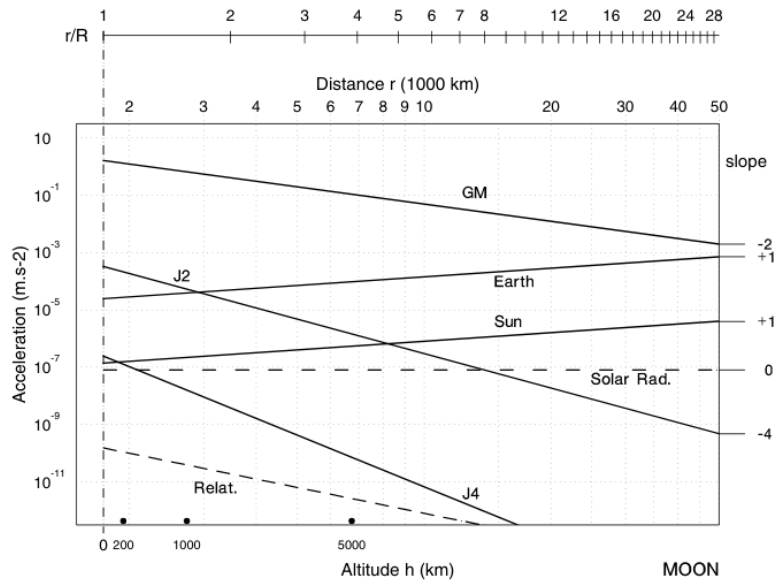


Figure 3.4. Accelerations as a function of the distance r of the satellite from the center of the Moon (logarithmic scale) [33]

It is clear how the main perturbations, for a low orbiting satellite, are due to the J_2 term and the presence of the Earth and Sun as third bodies. Consequently, the solar radiation pressure will be neglected in this study.

Given the presence of perturbations in the dynamical system, a closed-form expression is not available anymore for the trajectory of a satellite around a main body. Therefore

it is necessary to numerically integrate the Eqs. 3.21 to obtain the satellite's position over time.

$$\begin{cases} \dot{\vec{v}} = -\frac{\mu}{|\vec{r}|^3} \cdot \vec{r} + \sum_{j=1}^N \vec{a}_{p,j} \\ \vec{r} = \vec{v} \end{cases} \quad (3.21)$$

where j and N represent the index and the number of considered perturbations respectively.

3.3.1 Selenopotential

The Moon's gravitational field is not uniform, due to its non-spherical shape and its distribution of mass on the planet. In fact, the main lunar gravity features are mascons, or mass concentrations, regions of a planet's crust that contains a large positive gravity anomaly. These anomalies greatly influence the orbit of spacecraft about the Moon.

The gravitational potential for a generic planet can be written as follows.

$$U = \frac{\mu_p}{r} \left\{ 1 - \sum_{n=2}^{\infty} \sum_{m=0}^n \left(\frac{R_p}{r} \right)^n [C_{nm} \cos(m\lambda) + S_{nm} \sin(m\lambda)] P_{nm}(\sin \phi) \right\} \quad (3.22)$$

where C_{nm} and S_{nm} are the harmonic coefficients, P_{nm} are the associated Legendre functions (also shown in Eq. 3.23), λ is the longitude and ϕ is the latitude of the considered point. These harmonic coefficients take on different physical meanings depending on the indexes n and m .

$$P_{nm}(x) = \frac{1}{2^n n!} (1-x^2)^{\frac{m}{2}} \frac{d^{n+m} (x^2-1)^n}{dx^{n+m}} \quad (3.23)$$

Terms with $m = 0$ are called zonal harmonics and their coefficients $J_n = C_{n0}$ are the zonal harmonic coefficients. The zonal harmonics are independent of longitude and have sign changes of n over the full range of latitude. They divide the planet into a series of longitude-independent zones.

Terms with $n = m$ are called sectoral harmonics since they divide the planet into sectors that are independent of latitude.

Lastly, terms with $m \neq 0$ and $m \neq n$ are called tesseral harmonics, since these divide the world into a tiled pattern. All of these harmonics are shown in Fig. 3.5.

Of these, the J_2 term is by far the most influential of the potential terms, as it is the largest. It represents the mass distribution of the equatorial bulge of a planet, since it has two changes of sign between the north and south poles. It has important effects

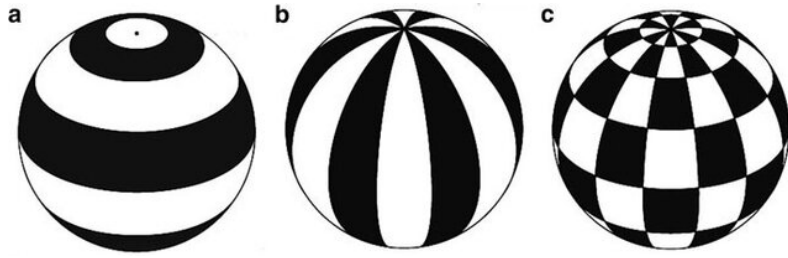


Figure 3.5. Spherical harmonics for the characterization of the gravitational field of a general planet: a. Zonal harmonics ($m = 0$), b. Sectorial harmonics ($m = n$), c. Tesselar harmonics ($m \neq n$) [34]

for the orbit in that it causes both the right ascension of the ascending node and the argument of perigee to rotate at rates of several degrees per day. As central bodies become less spherically symmetric the impact of the higher order harmonics becomes more important. J_2 and other harmonic coefficients are listed in Tables (3.1)-(3.2) for the Moon [15].

Table 3.1. Normalized zonal harmonic coefficients for the Moon [15]

n	m	\bar{J}_n
2	0	$0.909\,011 \times 10^{-4}$
3	0	$0.320\,307 \times 10^{-5}$
4	0	$-0.321\,410 \times 10^{-5}$
5	0	$0.221\,010 \times 10^{-6}$
6	0	$-0.376\,479 \times 10^{-5}$
7	0	$-0.561\,331 \times 10^{-5}$
8	0	$-0.231\,954 \times 10^{-5}$

To use the values reported in Tables (3.1)-(3.2) it is necessary to convert them from normalized to un-normalized values.

$$J_n = \frac{\bar{J}_n}{\Pi_{n0}} \quad (3.24)$$

$$C_{nm} = \frac{\bar{C}_{nm}}{\Pi_{nm}} \quad (3.25)$$

$$S_{nm} = \frac{\bar{S}_{nm}}{\Pi_{nm}} \quad (3.26)$$

where \bar{J} , \bar{C} and \bar{S} are the normalized gravity field coefficients and J , C and S are the

Table 3.2. Normalized sectorial and tesseral harmonic coefficients for the Moon [15]

n	m	\bar{C}_{nm}	\bar{S}_{nm}
2	1	$-0.186\,274 \times 10^{-8}$	$-0.142\,454 \times 10^{-8}$
2	2	$0.346\,376 \times 10^{-4}$	$0.144\,064 \times 10^{-7}$
3	1	$0.263\,418 \times 10^{-4}$	$0.546\,308 \times 10^{-5}$
3	2	$0.141\,853 \times 10^{-4}$	$0.488\,914 \times 10^{-5}$
3	3	$0.122\,863 \times 10^{-4}$	$-0.178\,246 \times 10^{-5}$
4	1	$-0.600\,062 \times 10^{-5}$	$0.165\,956 \times 10^{-5}$
4	2	$-0.709\,370 \times 10^{-5}$	$-0.678\,563 \times 10^{-5}$
4	3	$-0.135\,880 \times 10^{-5}$	$-0.134\,333 \times 10^{-4}$
4	4	$-0.602\,939 \times 10^{-5}$	$0.393\,526 \times 10^{-5}$

un-normalized coefficients. The conversion factor Π appearing in Eqs. (3.24)-(3.26) is given by the following formula.

$$\Pi_{nm} = \sqrt{\frac{(n+m)!}{(2n+1)k(n-m)!}} \quad (3.27)$$

$$k = \begin{cases} 1 & \text{if } m = 0 \\ 2 & \text{if } m \neq 0 \end{cases} \quad (3.28)$$

Since the gravitational force is a conservative force, it is possible to derive the perturbation acceleration from the gravitational potential found before.

$$\vec{a}_G = \nabla U \quad (3.29)$$

with the operator $\nabla = \left(\frac{\partial}{\partial x}, \frac{\partial}{\partial y}, \frac{\partial}{\partial z} \right)$.

3.3.2 Third bodies

The presence of a third body makes the dynamical system more complex than before. This additional body exerts a force both on the satellite and the main body. Fig. 3.6 shows the situation.

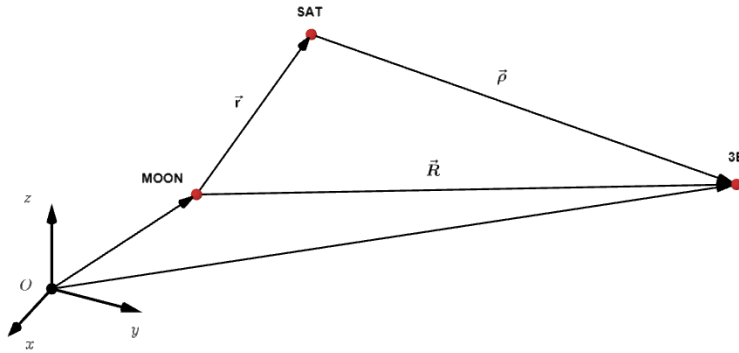


Figure 3.6. Geometry for a satellite orbiting the Moon with a third body present

$$\vec{a}_{3B,j} = \mu_{3B,j} \left(\frac{\vec{\rho}_j}{\rho_j^3} - \frac{\vec{R}_j}{R_j^3} \right) \quad (3.30)$$

$$\vec{\rho}_j = \vec{R}_j - \vec{r}_j \quad (3.31)$$

Eq. 3.30 is the resulting perturbation acceleration due to a generic third body, and is written from the main body's perspective. Two terms are visible: the first is the direct term, result of the gravitational force the third body exerts on the satellite and depends on the distance $\vec{\rho}$ between them. The second term is the indirect term, originating from the non-inertial nature of the frame the motion is described in. This term depends on the distance \vec{R} between the main and third bodies, and is necessary for proper modeling.

For a satellite orbiting the Moon, the Earth and Sun constitute the only contributors to this kind of perturbation. Consequently one can write the following terms.

$$\vec{a}_{3B,1} = \mu_{3B,1} \left(\frac{\vec{\rho}_1}{\rho_1^3} - \frac{\vec{R}_1}{R_1^3} \right) \quad (3.32)$$

$$\vec{a}_{3B,2} = \mu_{3B,2} \left(\frac{\vec{\rho}_2}{\rho_2^3} - \frac{\vec{R}_2}{R_2^3} \right) \quad (3.33)$$

with 1 and 2 being the indexes representing the Earth and the Sun, respectively. The gravitational forces of the Earth and the Sun cause periodic variations in most orbital elements. The most affected parameters are inclination, the longitude of the ascending node, and the argument of pericenter, that see a secular variation as well. Nonetheless, secular variations are associated with the motion of both the satellite and the disturbing body and can be obtained by double averaging the variations along their orbits [35].

3.4 Secular effects of J2

Since the largest term is J_2 , it is interesting to see how perturbation accelerations arise from it. The following equations are written for cartesian coordinates in an selenocentric frame such as MCI [36].

$$U_{J2} = \frac{\mu_p}{r} \left[1 - \frac{J_2}{2} \left(\frac{R}{r} \right)^2 (3 \sin^2 \phi - 1) \right] \quad (3.34)$$

$$\vec{a}_{J2} = \nabla U_{J2} \quad (3.35)$$

$$\vec{a}_{J2} = \frac{J_2 \mu R_p^2}{r^7} \begin{bmatrix} x(6z^2 - \frac{3}{2}(x^2 + y^2)) \\ y(6z^2 - \frac{3}{2}(x^2 + y^2)) \\ z(3z^2 - \frac{9}{2}(x^2 + y^2)) \end{bmatrix} \quad (3.36)$$

If we were to consider only the perturbation due to the J_2 term and using the Cowell's method (i.e. numerical integration) on Eqs. 3.21 to solve for the trajectory of the satellite it is possible to examine the secular and short-time variations on the orbital elements. Fig. 3.7 shows their time variation. It is clear the distinction between metric and angular elements: both are subjected to short-time variations, but while for the metric elements the secular variations are null, it is not the case for the angular elements, which keep increasing linearly with time.

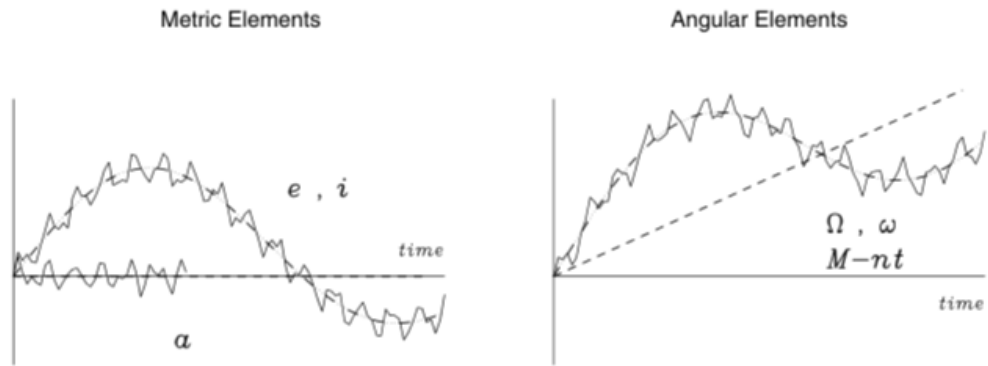


Figure 3.7. Representation of the time variation of the orbital elements due to J_2 perturbation. Secular variation is shown in a dashed line. [33]

Averaging the effects of the term J_2 over an orbital period eliminates the short-time variations, while keeping the secular effects. We can conclude that J_2 produces secular effects on three orbital elements, while the semi-major axis, eccentricity, and inclination stay the same. The following equations can be obtained starting with the

Lagrange planetary equations, substituting for a_{J_2} from Eq. 3.36 and integrating over an orbital period T .

$$\dot{\Omega} = -\frac{3}{2} J_2 \frac{R_p^2}{a^{3.5}} \sqrt{\mu} (1 - e^2)^{-2} \cos i \quad (3.37)$$

$$\dot{\omega} = \frac{3}{2} J_2 \frac{R_p^2}{a^{3.5}} \sqrt{\mu} (1 - e^2)^{-2} \left(2 - \frac{5}{2} \sin^2 i \right) \quad (3.38)$$

$$\dot{M} = \sqrt{\frac{\mu}{a^3}} + \frac{3}{2} J_2 \frac{R_p^2}{a^{3.5}} \sqrt{\mu} (1 - e^2)^{-1.5} \left(1 - \frac{3}{2} \sin^2 i \right) \quad (3.39)$$

3.5 Repeating ground-track orbits

In general a ground-track considered over an orbital period, will remain open, meaning the beginning and end points differ. The reason is that the rotation of the planet ω_p , as well as the long term effects of J_2 shift the planetary surface and the orbital plane, respectively. Therefore, the ascending nodes of the ground-track will be shifted accordingly.

An orbit is a periodic orbit, or repeating ground track orbit (RGTO for short), if in a time interval, is able to complete an integer number of orbits R while the planet beneath completes an integer number of rotations m about its axis. The result is a grid, drawn by the ground-track of the satellite, on the planetary surface, since the initial and final SSP coincide. Various examples are shown in Fig. 3.10. This also means, that the ground-track repeats each subsequent cycle in the exact same manner, allowing for shorter analyses on performance indexes. The mathematical condition for a repeating ground-track orbit is the following [37].

$$mD_{syd} = RT_{orb} \quad (3.40)$$

where D_{syd} and T_{orb} are the sidereal rotational time of the planet, and the orbital period respectively.

If the secular effects of the J_2 term are added to the model, it is possible to express the ground-track of a general satellite through its longitude λ and latitude ϕ . Eqs. (3.41)-(3.42) are obtained by using the values found in Eqs. (3.37)-(3.39) and are written in a PCPF frame.

It is clear from Eq. 3.42 that the maximum and minimum values of the latitude ϕ reached by the ground-track will be determined entirely by the orbital inclination i . If a prograde orbit is considered, the maximum latitude is $\phi_{max} = i$, while the minimum latitude is $\phi_{min} = -i$. These definitions will come in handy later in

Chapter 4 when considerations over physical constellation are made.

$$\lambda(t) = \lambda_0 - (W_p - \dot{\Omega})t + \arctan(\cos i \tan[(\dot{\omega} + \dot{M})t]) \quad (3.41)$$

$$\phi(t) = \arcsin(\sin i \sin[(\dot{\omega} + \dot{M})t]) \quad (3.42)$$

At the same time, the previous condition for a repeating ground-track orbit now becomes:

$$mD_n = RT_n \quad (3.43)$$

$$D_n = \frac{2\pi}{W_p - \dot{\Omega}} \quad (3.44)$$

$$T_n = \frac{2\pi}{\dot{M} + \dot{\omega}} \quad (3.45)$$

where D_n is the nodal day of the planet, or the rotational period with respect to the nodal line, and T_n is the nodal period of the satellite, or the time that passes through two consecutive passes at the ascending node. The same logic can be used to study the effects of higher harmonics and the presence of third bodies on repeating ground-track orbits, as was analyzed by Cinelli [16].

Using the secular variations in Eqs. (3.37)-(3.39) in the expressions (3.44)-(3.45) and both in the repeating ground-track orbit condition we find a polynomial in a , e , i and q . The latter parameter $q = \frac{R}{m}$ is the repeat factor, and describes how many orbits can the satellite complete in an nodal day. For $q = 1$ we obtain synchronous orbits, while for $q > 1$ we obtain supersynchronous orbits.

$$a^{3.5} + b_1 \cdot a^2 + b_2 = 0 \quad (3.46)$$

$$\begin{aligned} b_1 &= -\frac{\sqrt{\mu}}{qW_p} \\ b_2 &= -\frac{K_p}{qW_p}(4\cos^2 i - 1 - q\cos i) \\ K_p &= \frac{3}{2}J_2R_p^2\sqrt{\mu} \end{aligned}$$

Given values for e , i and q , the polynomial transforms in a 7-th degree equation in a , and its only real solution provides the semi-major axis of the corresponding RGTO orbit.

The same equation simplifies for circular orbits, allowing to find a as a function of solely i and q , and therefore the orbital altitude h once the planet radius R_p is known, as shown in Fig. 3.8. In the image, the curve represent a set of possible circular RGTO orbits for both Earth (Fig. 3.8a) and Moon (Fig. 3.8b).

In general, altitude decreases for increasing values of the repeat factor q , since to allow for more orbits per nodal day the satellite would have to be in a lower altitude. On the other hand, the effect that inclination has on the altitude is negligible for small values of q , but not for larger values. Overall, altitude increases along with the inclination i at a given repeat factor q .

Nonetheless, the choice of the planet plays a major role, exemplified by the parameter K_p in the previous equation. A RGTO orbit around Earth is limited to a small range of repeat factor, say between 1 and 15, while a RGTO orbit around the Moon has a much larger range, from 15 up to 300.

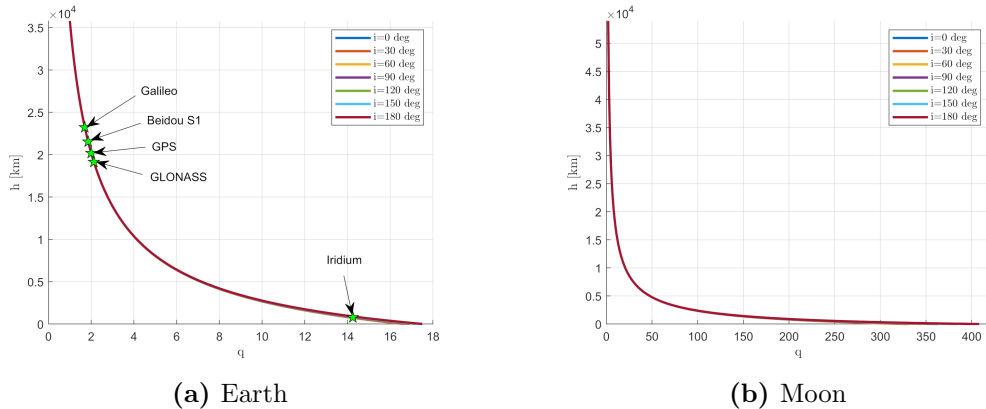


Figure 3.8. Altitude h as a function of the repeat factor q and inclination i for a circular orbit

Similarly, using Eq. (2.2) and having fixed an elevation angle ε it is possible to see how the coverage angle θ behaves for different inclinations and repeat factors. Here the effect that the inclination has on the coverage angle is much more noticeable. Furthermore, by comparing to the five constellations seen before, one concludes that to offer the same coverage performance on the Moon, the repeat factor q should be limited to the range between 25 and 75. The trends are shown in Fig. 3.9 for both Earth and Moon.

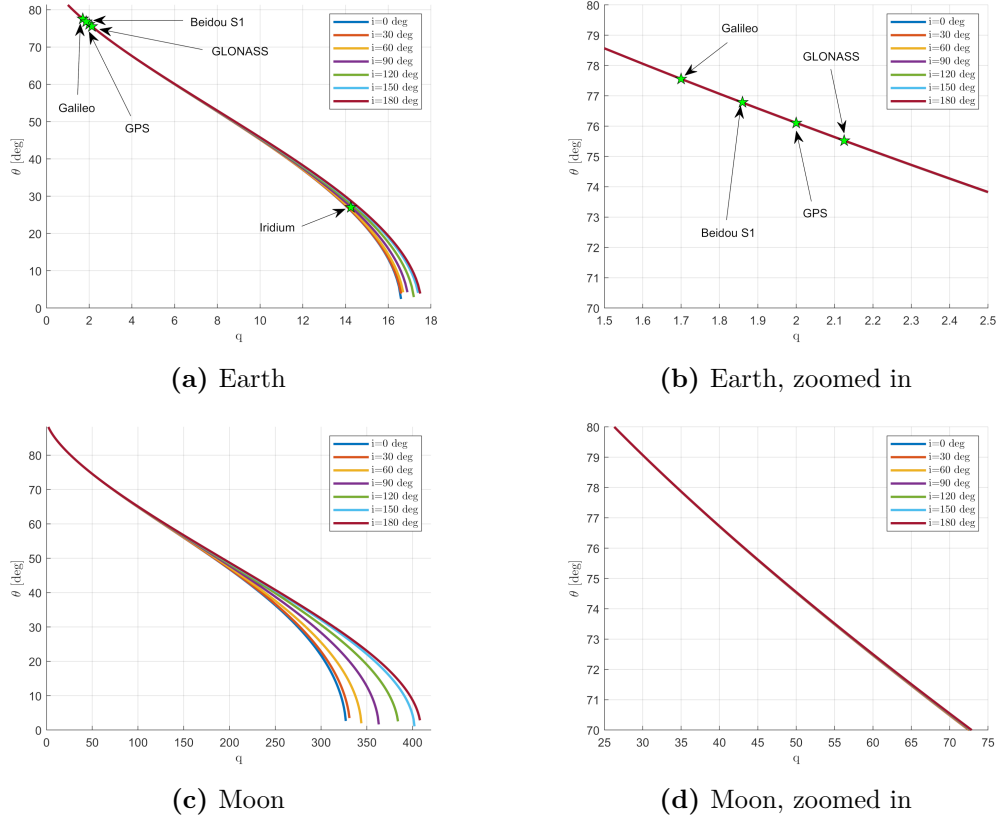


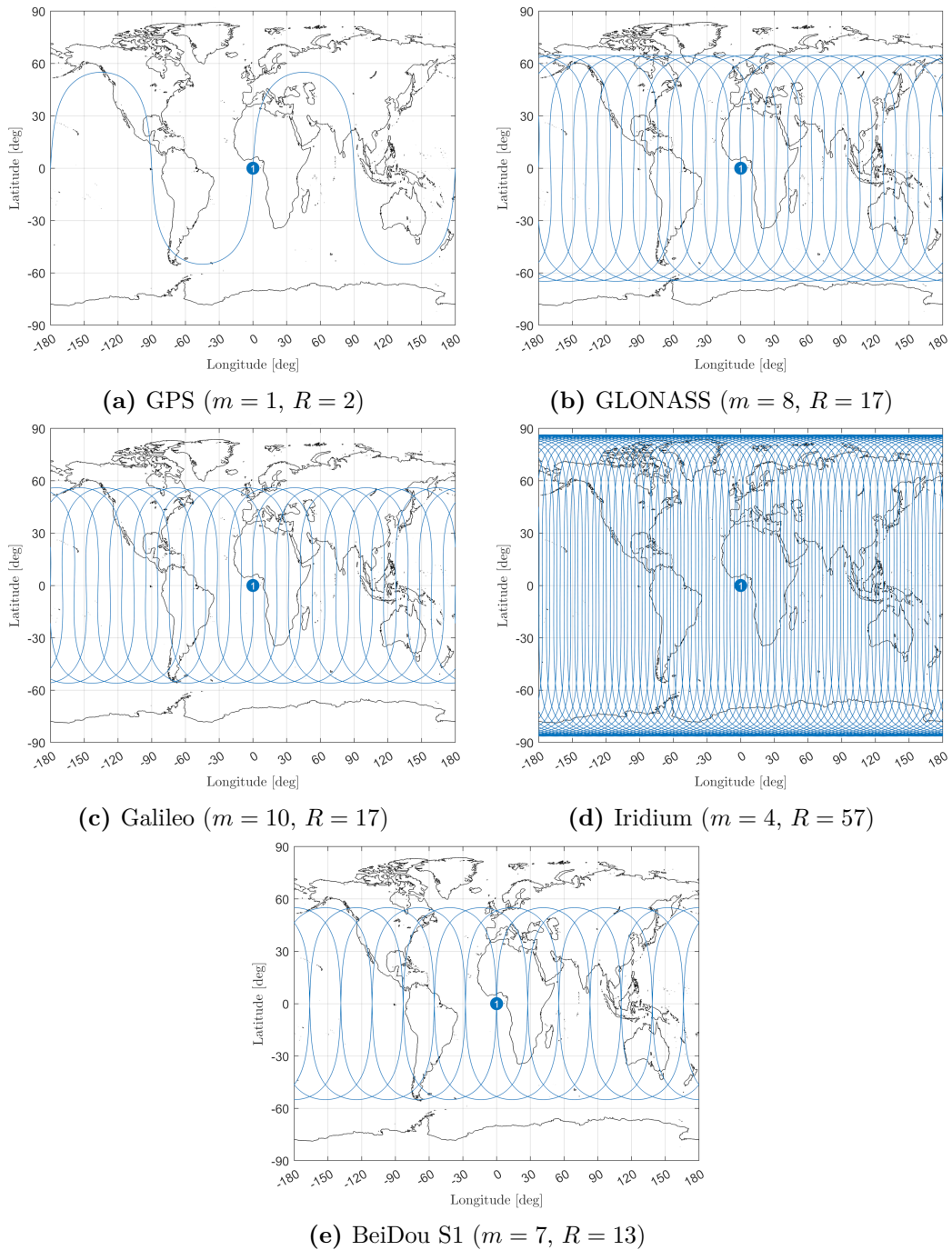
Figure 3.9. Coverage angle θ (for $\varepsilon = 0$ deg) as a function of the repeat factor q and inclination i for a circular orbit

The five constellations seen in Chapter 2 are based on RGTO. Their repeat values are reported in Table 3.3 and the ground-track for a satellite of each constellation is shown in Fig. 3.10.

The four GNSS constellations were designed to be based on RGTO orbits from the start, since it is an advantage to be able to repeat the same pattern over the surface each cycle, meaning that the coverage and navigation performance can be easily predicted and replicated a number of times. For instance, for Galileo the repeat cycle last around 10 solar days. Conversely, the Iridium constellation was not designed as such, and it is clear by just looking at the high value of the repeat factor q .

Table 3.3. Repetition coefficients for the most known constellations [16]

Constellation name	m	R	q
GPS	1	2	2
GLONASS	8	17	$2 + \frac{1}{8}$
Galileo	10	17	$1 + \frac{7}{10}$
BeiDou S1	7	13	$1 + \frac{6}{7}$
Iridium	4	57	$14 + \frac{1}{4}$

**Figure 3.10.** RGTO examples

As seen before, the repeat cycle duration of a RGTO orbit can be defined either as mD_n or as RT_n . It is possible to redefine the nodal period to show its dependence on the variation $\dot{\Omega}$. One can find the following using the definition of nodal day:

$$D_n = \frac{D_{syd}}{1 - \frac{\dot{\Omega}}{W_p}} \quad (3.47)$$

This relation can be studied over a large range of altitudes and can be concluded that, for lunar circular RGTO orbits with an altitude larger than 1000 km, the nodal day is almost exactly equal to the sidereal day, or 27.32 days. A repeat cycle duration can be therefore any multiple m of this value, meaning the advantage of repeated patterns is somewhat negated by the long time intervals, entailing longer and computationally heavy simulations to characterize a certain orbit. For this very reason, it was chosen to consider only RGTO orbits with a factor $m = 1$, which in turn means that $q = R$, leading to the considerations made before for q to be valid for R instead.

3.6 Software used

3.6.1 MATLAB

MATLAB is programming language and numeric computing environment developed by MathWorks. MATLAB is great at working with matrices and vectors, allowing for fast computation and is a favorite for plotting of functions, implementation of algorithms, and numerical simulations. It offers many libraries and toolboxes, both developed in-house and by standards users that expand the domains in which MATLAB can be used. It is mostly used in engineering fields.

In this dissertation MATLAB was used to generate satellite constellations, to propagate them over time, and to calculate access from both the ideal and detailed surface. The methods used are explained in detail in Chapters 3 and 4.

3.6.2 SaVi

SaVi is a constellation simulator and viewer that facilitates the visualization and analysis of coverage. The software is freely available on Linux machines and can be downloaded at the SourceForge website. Lloyd Wood is the current SaVi developer [38]. The software SaVi was used to represent the coverage of the newfound constellations over the Moon. A color-bar has been used to show the degree of coverage guaranteed for a given longitude and latitude on the surface of the planet. An example is shown in Fig. 3.11, the coverage map was calculated with SaVi at

a given time and overlapped with the lunar sea level map. It is clear from the image that the chosen constellation assures 2-fold global coverage for the considered instant.

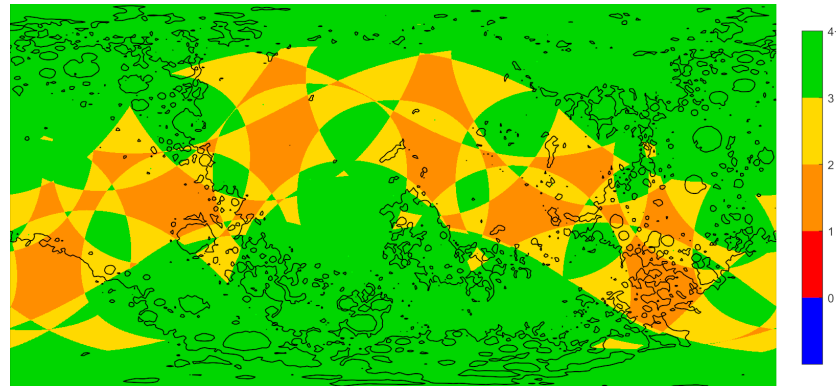


Figure 3.11. Coverage map for a Moon Soc 27/3 (taken at time t_0), made with SaVi

3.6.3 STK

Systems Tool Kit is a proprietary software developed and managed by Analytical Graphics, Inc. (an Ansys company). It allows modeling complex dynamical systems, with "assets" such as ground stations, aircraft, satellites and to perform detailed analyses for mission profiles. It is heavily used in the aerospace and defense fields by governmental, commercial, and defense entities around the world. Notable clients are NASA, ESA, CNES, DLR, Boeing and Airbus.

STK was mostly used to analyze the dilution of precision parameters of the different constellations, and to study the orbital stability of each configurations, through the HPOP built-in propagator, arranged to consider up to the 8th degree harmonics and the Earth and Sun as third bodies.

Chapter 4

Constellation design methods

4.1 Analytical vs numerical methods

Problems can generally be solved either analytically or numerically. An analytical solution involves expressing the problem in a well-defined mathematical form and deriving the solution without using algorithms. On the other hand, a numerical solution involves making approximations and iterating to find an acceptable solution, often introducing errors. Numerical solvers are oftentimes based on algorithms.

The methods discussed in the following sections can be distinguished as either analytical or numerical approaches. While the design methods for a SoC use mathematical equations and geometrical considerations to define the problem and to solve it, and therefore can be considered analytical methods, it is not the case for the design methods for a Walker-Delta. These methods, apart from Walker's, do not solve for an exact solution, and are based on an algorithm that searches for the optimal constellation configuration, making them numerical methods.

4.2 Methods for SoC constellations

A distinction must be made about the design methods for Streets-of-Coverage constellations. Because of the analytical approach, the optimal configuration is the result of an equation given certain parameters.

All of these design methods are direct, which means that one can get the constellation geometry (θ , $\Delta\Omega_{co}$ and ΔM_{inter}), if it exists, from a priori knowledge of number of orbital planes P and number of satellites for each plane N_p . An indirect method can be found using the Equation (4.1), giving the recommended number of planes from knowledge about the expected coverage angle and number of satellites on each plane. Note that $\Delta\Omega_{co}$ and ΔM_{inter} are strictly function of θ and N_p .

$$P = \left\lceil 1 + \frac{\Delta\Omega_{anti}}{\Delta\Omega_{co}} \right\rceil \quad (4.1)$$

where the operator $\lceil x \rceil$ is the ceil operator, resulting in the rounded up value to the greater nearest integer.

4.2.1 Beste coverage method

In 1978 Beste considered the polar orbits to be the most promising orbits to provide regional and global coverage [39]. His work was anticipated by a few years by Lueders, who had first the idea to separate the orbital planes in an uniform manner [40]. Beste's coverage method is able to find an optimal polar SoC constellation capable of 1-fold coverage ($j = 1, k = 1$).

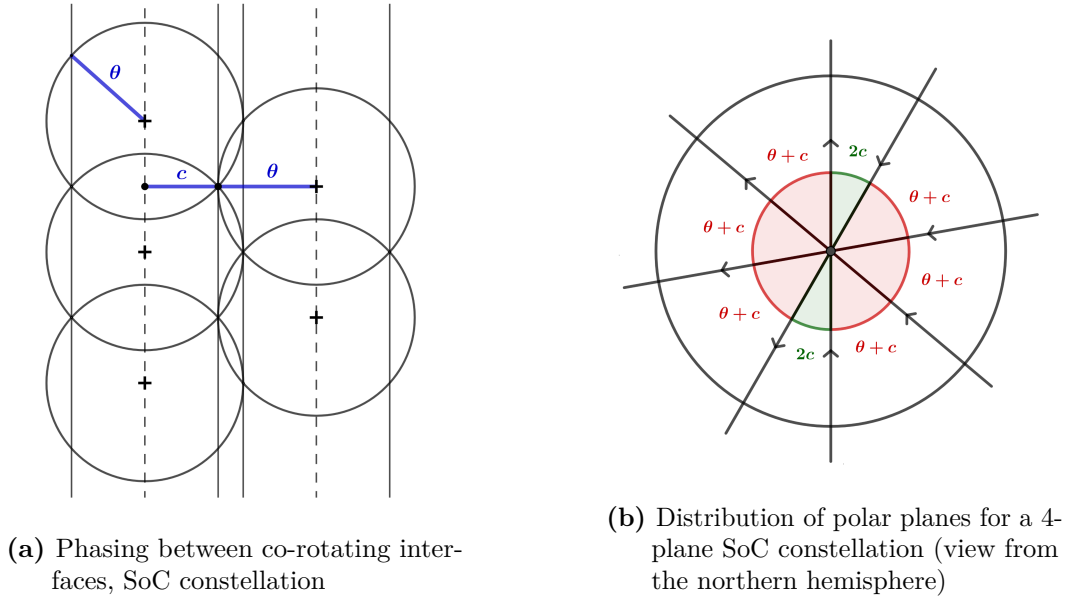


Figure 4.1. Beste's method geometry

The geometry is shown in Fig. 4.1. In the left image we can see the coverage areas, defined by θ of multiple satellites arranged in two streets of coverage. The aim of the method is to find the most efficient way to distribute these streets over an angular spread of π , for given orbital planes P and number of satellites on each plane N_p . A constellation made up P planes has necessarily $(P - 1)$ interfaces between co-rotating streets and 1 interface between counter-rotating streets, as can be seen from the example in the image on the right.

While at the interfaces between co-rotating streets, the relative geometry remains constant, at the one interface where adjacent streets move in opposite directions, it

is not constant, necessitating that the angular separation between the orbital planes must be smaller to maintain coverage.

Overall, if the angular separation between adjacent co-rotating streets is $\Delta\Omega_{co} = \theta + c$ and $\Delta\Omega_{anti} = 2c$ between counter-rotating streets, it follows that the condition that gives the optimal value for c must be attained at the equator, the most demanding place, where streets are the furthest away from each other. The most demanding requirement occurs at the equator, where the following equation must be satisfied:

$$(P - 1)(\theta + c) + 2c = \frac{\pi}{2} \quad (4.2)$$

The parameter c is the half-width of the street and therefore defines the distribution of orbital planes. In reality, c depends on both the phasing between satellites in adjacent streets and the angular separation, as stated before. It was found that, if the satellites of one plane are shifted relative to those of the adjacent plane by one-half of the intraorbit satellite spacing, it is possible to find a distance between co-rotating streets, that clusters the satellites in an optimal manner at the equator. It follows from geometrical analysis that:

$$c_1 = \arccos \left(\frac{\cos \theta}{\cos(\pi/N_p)} \right) \quad (4.3)$$

This configuration minimizes the overlap between coverage from different satellites, as can be seen in the image. Combining the previous two equations it is possible to find an equation where the only unknown is θ , which provides the required coverage angle for 1-fold global coverage, as well as the angular separation between streets $\Delta\Omega_{co}$ and $\Delta\Omega_{anti}$. The relevant equations are provided below for quick reference.

1-fold coverage (1,1) for polar SoC

$$c_1 = \arccos \left(\frac{\cos \theta}{\cos(\pi/N_p)} \right) \quad (4.4)$$

$$\Delta\Omega_{co} = \theta + c_1 \quad (4.5)$$

$$\Delta\Omega_{anti} = 2c_1 \quad (4.6)$$

$$\Delta M_{intra} = \frac{2\pi}{N_p} \quad (4.7)$$

$$\Delta M_{inter} = \frac{\Delta M_{intra}}{2} \quad (4.8)$$

$$(P - 1)\theta + (P + 1)c = \pi \quad (4.9)$$

4.2.2 Ulybyshev coverage method

Ulybyshev's coverage method expanded on the previous one, looking for opportunities to find near-polar, inclined SoC constellations, for 1-fold and 2-fold coverage (respectively $(j, k) = (1, 1), (1, 2)$ and $(2, 1)$). He was also able to develop a general formula for polar SoC constellations for n-fold coverage (j, k) [41].

Starting from the polar SoC capable of n-fold coverage, we need to define the newer streets of coverage, with a half-width c_j . Fig. 4.2 shows this configuration, for $j = 1, 2$. It is clear that the street that guarantees a 2-fold coverage is narrower than the one that guarantees a 1-fold coverage. The same reasoning applies for higher degree j of street coverage. Therefore, the angular separation must reflect this fact, resulting in $\theta + c_j$ for the co-rotating interfaces and $\pi - c_1 - c_j$ for the counter-rotating interfaces.

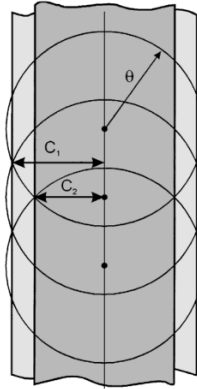


Figure 4.2. Multiple coverage streets

On the other side, the restriction on the angular spread is removed, allowing for an overlap of streets, mixing some ascending streaks with some descending ones. The degree of overlap is controlled by the coverage factor k .

It is important to notice that considering j, k to be 1, these equations simplify to the Beste's coverage method. The relevant equations are provided below for quick reference.

***n*-fold coverage (j, k) for polar SoC**

$$c_j = \arccos \left(\frac{\cos \theta}{\cos(j\pi/N_p)} \right) \quad (4.10)$$

$$\Delta\Omega_{co} = \theta + c_j \quad (4.11)$$

$$\Delta\Omega_{anti} = \pi - c_1 - c_j \quad (4.12)$$

$$\Delta M_{intra} = \frac{2\pi}{N_p} \quad (4.13)$$

$$\Delta M_{inter} = \frac{\Delta M_{intra}}{2} \quad (4.14)$$

$$(P - 1)\Delta\Omega_{co} - \Delta\Omega_{anti} = (k - 1)\pi \quad (4.15)$$

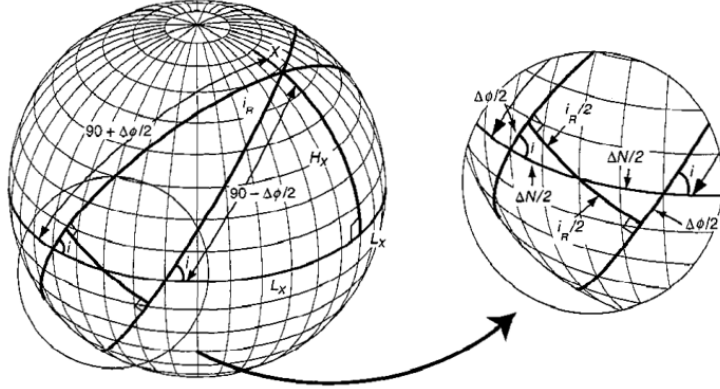


Figure 4.3. Geometry for an inclined SoC [6]

Fig. 4.3 illustrates the geometry for adjacent inclined streets. For polar streets, the RAAN spacing $\Delta\Omega$ is equal to the angular separation D , while for inclined streets the perpendicular angular separation is not the RAAN spacing but is an arc on the great circle 90 deg from the intersection of two orbits. These two values are related by the following equation:

$$\sin \left(\frac{\Delta\Omega}{2} \right) = \sin \left(\frac{D}{2} \right) / \sin i \quad (4.16)$$

As stated before in Chapter 2, to guarantee coverage at the poles, a constellation has to have a minimum inclination in relation with the coverage angle θ provided. For a SoC constellation this relation becomes Eq. (4.17), a necessary condition for attaining global n -fold coverage.

$$i > i_{min} = \frac{\pi}{2} - c_j \quad (4.17)$$

The relevant equations are provided below for quick reference.

1-fold coverage (1, 1) for inclined SoC

$$c_1 = \arccos \left(\frac{\cos \theta}{\cos(\pi/N_p)} \right) \quad (4.18)$$

$$\Delta\Omega_{co} = 2 \arcsin \left(\frac{\sin[(\theta + c_1)/2]}{\sin i} \right) \quad (4.19)$$

$$\Delta\Omega_{anti} = \arccos \left(\frac{\cos(\pi - 2c_1) - \cos^2 i}{\sin^2 i} \right) \quad (4.20)$$

$$\Delta M_{intra} = \frac{2\pi}{N_p} \quad (4.21)$$

$$\Delta M_{inter} = \frac{\Delta M_{intra}}{2} - 2 \arccos \left(\frac{\cos(\Delta\Omega_{co}/2)}{\cos[(\theta + c_1)/2]} \right) \quad (4.22)$$

$$(P - 1)\Delta\Omega_{co} - \Delta\Omega_{anti} = 0 \quad (4.23)$$

A 2-fold global coverage can be attained with two different geometries, as stated in Table 2.2. These geometries defined two overarching families of constellations. The first family, characterized by $j = 1$ and $k = 2$, requires that each orbit plane provide a single street of coverage and that the ascending nodes of said planes be distributed over a 2π range. Conversely, the second family is characterized by $j = 2$ and $k = 1$ and requires that each orbit plane provide a double street of coverage, but the ascending nodes are distributed over a standard π range. The same logic must be applied to higher coverage folds, though there will be more than two families. While the formulas are given below for both families, it was decided to limit the focus to the families sporting $k = 1$ in this dissertation.

2-fold coverage (1, 2) for inclined SoC

$$c_1 = \arccos \left(\frac{\cos \theta}{\cos(\pi/N_p)} \right) \quad (4.24)$$

$$\Delta\Omega_{co} = 2 \arcsin \left(\frac{\sin[(\theta + c_1)/2]}{\sin i} \right) \quad (4.25)$$

$$\Delta\Omega_{anti} = 2\pi - \arccos \left(\frac{\cos(2\pi - 2c_1) - \cos^2 i}{\sin^2 i} \right) \quad (4.26)$$

$$\Delta M_{intra} = \frac{2\pi}{N_p} \quad (4.27)$$

$$\Delta M_{inter} = \frac{\Delta M_{intra}}{2} - 2 \arccos \left(\frac{\cos(\Delta\Omega_{co}/2)}{\cos[(\theta + c_1)/2]} \right) \quad (4.28)$$

$$(P - 1)\Delta\Omega_{co} - \Delta\Omega_{anti} = 0 \quad (4.29)$$

2-fold coverage (2,1) for inclined SoC

$$c_1 = \arccos \left(\frac{\cos \theta}{\cos(\pi/N_p)} \right) \quad (4.30)$$

$$c_2 = \arccos \left(\frac{\cos \theta}{\cos(2\pi/N_p)} \right) \quad (4.31)$$

$$\Delta\Omega_{co} = 2 \arcsin \left(\frac{\sin[(\theta + c_2)/2]}{\sin i} \right) \quad (4.32)$$

$$\Delta\Omega_{anti} = \arccos \left(\frac{\cos(\pi - c_1 - c_2) - \cos^2 i}{\sin^2 i} \right) \quad (4.33)$$

$$\Delta M_{intra} = \frac{2\pi}{N_p} \quad (4.34)$$

$$\Delta M_{inter} = \Delta M_{intra} - 2 \arccos \left(\frac{\cos(\Delta\Omega_{co}/2)}{\cos[(\theta + c_2)/2]} \right) \quad (4.35)$$

$$(P - 1)\Delta\Omega_{co} - \Delta\Omega_{anti} = 0 \quad (4.36)$$

Many versions improving over Ulybyshev's works have been proposed over the years, which was limited to 2-fold coverage for inclined constellations. The version proposed by Huang et al. [42] reinstates to a certain degree the multiple fold coverage, hence it is primarily intended for inclined SoC constellations (with j and $k = 1$). As it can be inferred from Table 2.2 this limits the range over which the planes can be distributed, as it was for the original Beste SoC constellations. Some conditions can be found given the premises of a constellation of T satellites on different P orbital planes. N_p is the number of satellites on each plane. The first condition is about degree of coverage along the street, while the second condition is on the distribution of the streets.

$$N_p\theta \geq j\pi \quad (4.37)$$

$$(P - 1)(\theta + c_j) \leq \pi \quad (4.38)$$

which ultimately leads to the necessary condition:

$$jP(P - 1) \leq T \quad (4.39)$$

n-fold coverage (j, 1) for inclined SoC

$$c_j = \arccos \left(\frac{\cos \theta}{\cos(j\pi/N_p)} \right) \quad (4.40)$$

$$\Delta\Omega_{co} = 2 \arcsin \left(\frac{\sin[(\theta + c_j)/2]}{\sin i} \right) \quad (4.41)$$

$$\Delta\Omega_{anti} = 2 \arcsin \left(\frac{\cos[(\pi - c_1 - c_j)/2]}{\sin i} \right) \quad (4.42)$$

$$\Delta M_{intra} = \frac{2\pi}{N_p} \quad (4.43)$$

$$\Delta M_{inter} = \frac{j\Delta M_{intra}}{2} - 2 \arccos \left(\frac{\cos(\Delta\Omega_{co}/2)}{\cos[(\theta + c_j)/2]} \right) \quad (4.44)$$

$$(P - 1)\Delta\Omega_{co} - \Delta\Omega_{anti} = 0 \quad (4.45)$$

4.2.3 General coverage method

This section presents a novel formulation of the equations for finding the optimal SoC constellation, expanding upon prior research by Beste's and Ulybyshev's.

This new formulation represents an original contribution, enabling the grouping of all previous methods under a unified set of Eqs. (4.46)-(4.50),(4.51).

Therefore, such a method is well suited for both inclined and polar SoC constellations, for multiple global coverage, both along and across the streets. Since it's a broad generalization of the Street-of-Coverage concept, it might encompass other kinds of constellations, such as variants of standard Walker-Delta. Still, more research is needed to prove that increasing the across-coverage factor k is useful in attaining more efficient constellations.

The inclination range of studied constellations has been limited to the range between 0 and 90 deg, due to lesser required ΔV to launch prograde satellites, but should this not be a requisite, it is important to note that the found inclined constellations behave symmetrically with respect to the polar configuration, in such a way that a constellation with planes inclined at 65 deg behaves like the same constellation with the same parameter were to be inclined at 115 deg.

***n*-fold coverage (j, k) for inclined SoC**

$$c_j = \arccos \left(\frac{\cos \theta}{\cos(j\pi/N_p)} \right) \quad (4.46)$$

$$\Delta\Omega_{co} = 2 \arcsin \left(\frac{\sin[(\theta + c_j)/2]}{\sin i} \right) \quad (4.47)$$

$$\Delta\Omega_{anti} = 2\pi \left[\frac{k}{2} \right] + 2(-1)^{k+1} \arcsin \left(\frac{\sin \left[\frac{\pi[1 - (k+1) \bmod 2] - c_1 - c_j}{2(-1)^{k+1}} \right]}{\sin i} \right) \quad (4.48)$$

$$\Delta M_{intra} = \frac{2\pi}{N_p} \quad (4.49)$$

$$\Delta M_{inter} = \frac{j\Delta M_{intra}}{2} - 2 \arccos \left(\frac{\cos(\Delta\Omega_{co}/2)}{\cos[(\theta + c_j)/2]} \right) \quad (4.50)$$

$$(P - 1)\Delta\Omega_{co} - \Delta\Omega_{anti} = 0 \quad (4.51)$$

4.3 Methods for Walker-Delta constellations

All of the methods explained in this section are based on a numerical approach, and therefore require a large number of calculations and heavy computations.

It is important to remember that a Walker-Delta constellation is defined by its three constellation parameters T , P and F and the two orbital parameters, i and h . Setting aside the last two parameters, for a given number of satellites T there exist many possible configurations, that can slow down the search for the global optimum. We define $D(T)$ as the set containing the divisors of T , all possible values for the choice of P . Furthermore, since the phasing factor F can only be an integer number between 0 and $P - 1$, there are P possible values for F (for each considered divisor). Therefore, the number of possible configurations Z for a Walker-Delta constellation made of T satellites can be written as follows:

$$Z = \sum_{P \in D(T)} P \quad (4.52)$$

For instance, given 12 satellites, there are 28 possible configurations, and for 48 satellites, this number increases exponentially to 124 total possible configurations. Since the number of configurations for a Walker-Delta constellation is consistently large, and depends solely on the number of satellites T considered, there is the need to filter out the worst configurations of the bunch. Fortunately, Walker analyzed

many patterns and came up with a list of Walker-Delta patterns to avoid [29].

- $T/1/0$ due to all the satellites being on a single orbital plane, therefore meaning that coverage at the orbital poles (distant 90° at all times from the ground-track) cannot be guaranteed.
- $T/T/0$, $T/T/\frac{T}{2}/0$ and $T/T/\frac{T}{2}$ suffer from the same problem as the last one, since there is at least an instant at which all the satellites pass through one plane, signifying that complete and continuous coverage cannot be achieved as there are zones 90° degrees from the planes not in any satellite's visibility.
- $T/T/\frac{T}{3}$, $T/T/\frac{2T}{3}$ and $T/T/\frac{T}{3}/0$ can be discarded since a most conspicuous configuration happens twice an orbital period: the satellites align on two planes, two thirds of the satellites at latitude $\pm\beta$, and one third at latitude $\mp\beta$. The critical latitude at which this phenomenon occurs can be found from Eq (4.53).

$$\sin \beta = \sin i \sin \left(\frac{\pi}{6} \right) \quad (4.53)$$

Nonetheless, this poses a problem only if the considered constellation is fairly large (i.e. at least 12), as the amount of satellites gathered at a certain latitude might lessen the n-fold coverage, if not disrupt it entirely.

- $T/T/\frac{T}{4}$, $T/T/\frac{3T}{4}$ and $T/T/\frac{T}{4}/0$ can be similarly be ruled out, as there are instances when a two parallel plane configuration takes place, for which one half of the satellites come together at latitude $\pm\beta$, while the other half pass through latitude $\mp\beta$. The critical latitude can be found from Eq (4.54).

$$\sin \beta = \sin i \sin \left(\frac{\pi}{4} \right) \quad (4.54)$$

Consequently, for constellations larger than 12 satellites, these patterns are unlikely to be satisfactory choices to provide complete and continuous coverage.

- $T/T/(T - 1)$ that have an inclination substantially less than 90° degrees and a synchronous orbit as they produce an 8 shaped moving pattern that is not able to cover the other side of the moving constellation.
- patterns with both even values of P and $(N_p - F)$ (such as 6/2/1, 6/6/1, 6/6/3 and 6/6/5 for constellations comprised of 6 satellites) have, due to geometrical reasons, instances in time when two satellites belonging to different orbital planes have their position in space to coincide. For instance, while a satellite is in its ascending node, another one is in its descending node at exactly the very

same longitude. This overlap of both position, and consequently, of coverage areas, produces an inefficient use of coverage.

Thought should be given to the fact that the aforementioned list is not, in any case, an exhaustive tally of all patterns to avoid, nor is it definitive, but simply a thinned out list, in order to speed up the numerical simulation reducing the number of possible sample to compute.

Other patterns could be found that, in a certain way or another, are inadequate to provide a n-fold complete and continuous coverage, such as a three or four parallel planes configuration, but such patterns might jeopardize the coverage only for a much larger number of satellites, and not even then, so they have not been included in this list.

Furthermore, note that a pattern $i/T/P/F$ with an inclination less than 90 degrees behaves the same way as the pattern $(\pi - i)/T/P/(P - F)$, hence the simulation will only consider prograde orbits, considering as well that retrograde orbits are rarely chosen for GNSS purposes.

4.3.1 Walker circumcircle coverage method

Walker's coverage method relies on the geometric properties of spherical triangles and their corresponding spherical circumcircles, making it only partially an analytical approach since determining the optimal coverage angle still requires numerical simulations.

By analyzing all the possible triplets of SSPs over the pattern repetition interval (PRI), it is possible to identify the worst-case scenario for coverage in both time and space, therefore defining the required coverage angle θ for providing global and continuous coverage over the planet surface [28, 29].

Consider 3 satellites, and their SSPs, called A, B and C. Since all of the satellites of a constellation orbit at the same height over the surface, their coverage areas are defined by the same coverage angle θ .

A spherical triangle ΔABC can be defined by using these SSPs as vertices.

A circumcircle for the spherical triangle ΔABC can be defined, with a circumcenter O and circumradius R .

In reality, a triplet of points defines 8 spherical triangles, since the sides can be either the shorter or longer arcs of the great circle passing through two of the vertices. This can clearly be seen in Fig. 4.4.

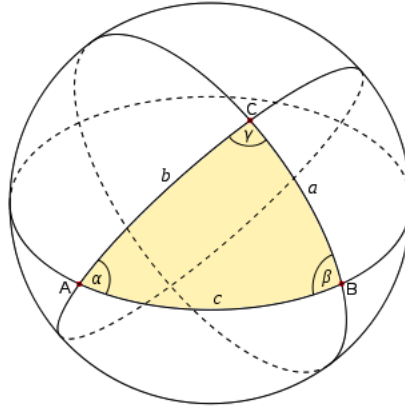


Figure 4.4. Spherical triangles defined by 3 points [7]

However, since the maximum coverage angle providable by a satellite is $\frac{\pi}{2}$ at an infinite distance over the planet. This limits us to the spherical triangle entirely contained within the hemisphere containing all its vertices, with all sides shorter than π , and the corresponding circumradii therefore shorter than $\frac{\pi}{2}$.

A point P within the spherical triangle ΔABC , which is the furthest from any A, B and C can be defined. The distances from the vertices are R_A, R_B, R_C .

The easiest case to consider is when the circumcenter O is a point inside the spherical triangle. In this instance, the furthest point P from any vertex is precisely the circumcenter O.

$$\text{if } O \in \Delta ABC \quad \rightarrow \quad P \equiv O \quad (4.55)$$

For increasing values of the coverage angle θ , obtained through an increasing height of the satellites we can observe how the coverage area expands. For a θ smaller than R , coverage is not provided completely within the spherical triangle (Fig. 4.5a), while for θ exactly R the three coverage circles intersect precisely in the circumcenter O (Fig. 4.5b). In this case, coverage is guaranteed for any point within the spherical triangle, and such configuration is called the critical one, which defines the lower required coverage angle. In the critical case, the point O is on the brim of the three coverage circles, meaning that it has the worst condition for coverage $\varepsilon = \varepsilon_{min}$. Any other point inside the triangle would have consequently a coverage with $\varepsilon > \varepsilon_{min}$. To a further increase in coverage angle corresponds a greater percentage of the spherical triangle are covered by 2 satellites. (Fig. 4.5c).

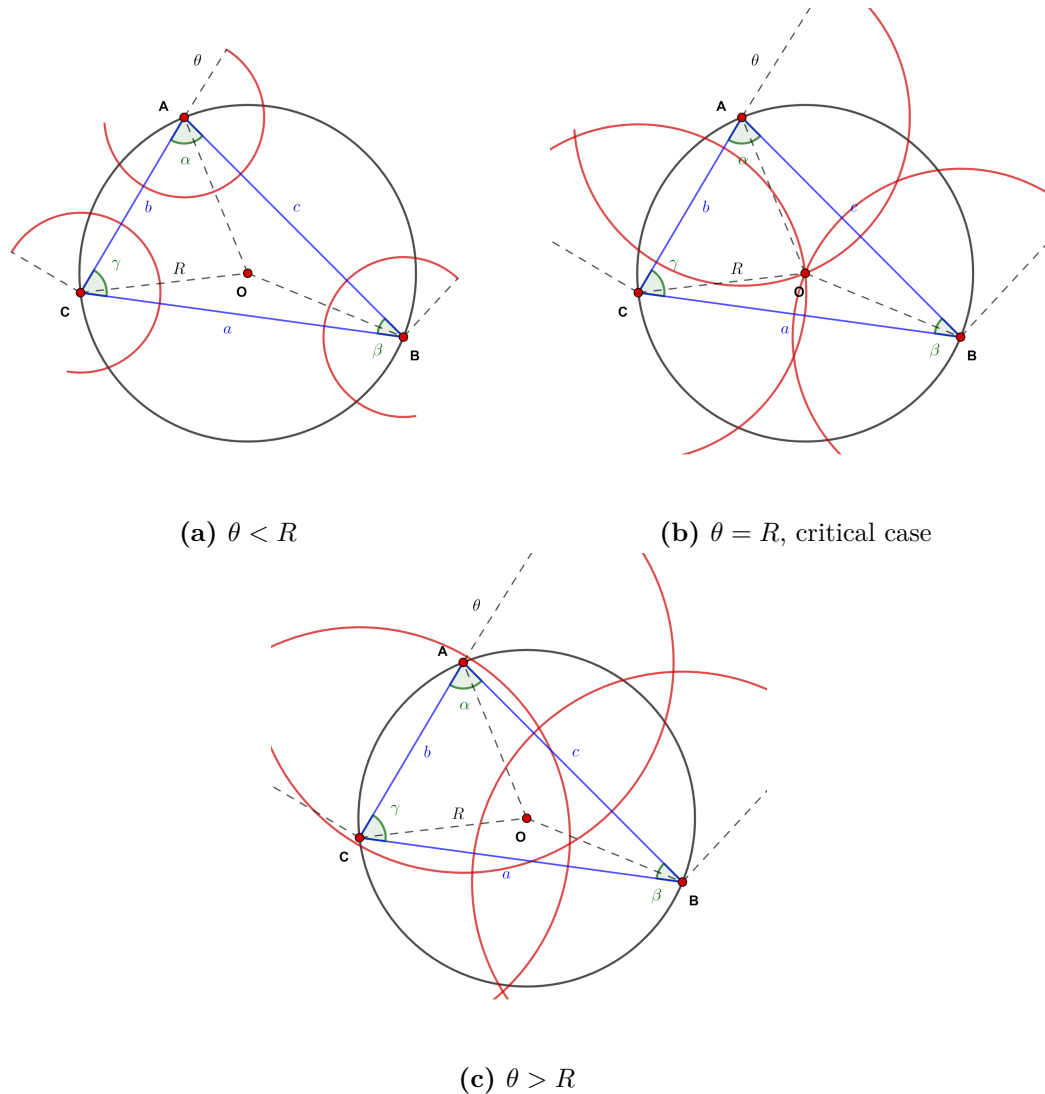


Figure 4.5. Circumcenter inside the spherical triangle

$$\begin{cases} \theta < R & \text{no full coverage for } \Delta ABC \\ \theta = R & \text{full coverage for } \Delta ABC, \text{ critical case} \\ \theta > R & \text{full coverage for } \Delta ABC \end{cases} \quad (4.56)$$

The circumradius R can be calculated from the known positions of the SSPs, both in longitude and latitude (λ_i, ϕ_i) by using the spherical law of cosines [43].

$$a = \arccos(\sin \phi_B \sin \phi_C + \cos \phi_B \cos \phi_C \cos |\lambda_B - \lambda_c|) \quad (4.57)$$

$$b = \arccos(\sin \phi_A \sin \phi_C + \cos \phi_A \cos \phi_C \cos |\lambda_A - \lambda_c|) \quad (4.58)$$

$$c = \arccos(\sin \phi_A \sin \phi_B + \cos \phi_A \cos \phi_B \cos |\lambda_A - \lambda_B|) \quad (4.59)$$

$$\alpha = \arccos\left(\frac{\cos a - \cos b \cos c}{\sin b \sin c}\right) \quad (4.60)$$

$$\beta = \arccos\left(\frac{\cos b - \cos a \cos c}{\sin a \sin c}\right) \quad (4.61)$$

$$\gamma = \arccos\left(\frac{\cos c - \cos a \cos b}{\sin a \sin b}\right) \quad (4.62)$$

$$R = \min \left\{ \arctan \left(\tan \left(\frac{1}{2}a \right) \sec \left(\frac{1}{2}(\beta + \gamma - \alpha) \right) \right), \frac{\pi}{2} \right\} \quad (4.63)$$

where a, b, c are the sides and α, β, γ the angles of the three vertices of the spherical triangle ΔABC .

Therefore we are able to cover any point in the spherical triangle if the following condition is satisfied:

$$\theta \geq R \quad (4.64)$$

If instead the circumcenter O falls outside the spherical triangle ΔABC , then point P does not coincide with the circumcenter and it is found on the triangle's perimeter.

$$\text{if } O \notin \Delta ABC \quad \rightarrow \quad P \in \text{Perimeter}(\Delta ABC) \quad (4.65)$$

The distance from point P to the furthest vertex is then known as R^* .

$$R^* = \max \{R_A, R_B, R_C\} \quad (4.66)$$

Unfortunately the point P must be found iteratively using a numerical approach, and similarly there is no analytical expression for the distance between this point and the furthest vertex. An attempt at solving this problem is reported for a 2-dimensional triangle [44].

In Fig. 4.6 there are 5 images, each representing the situation for an increasing value of the coverage angle θ . The critical configuration happens when the coverage angle equals the distance R^* and further increases only results in increasingly inefficient coverage.

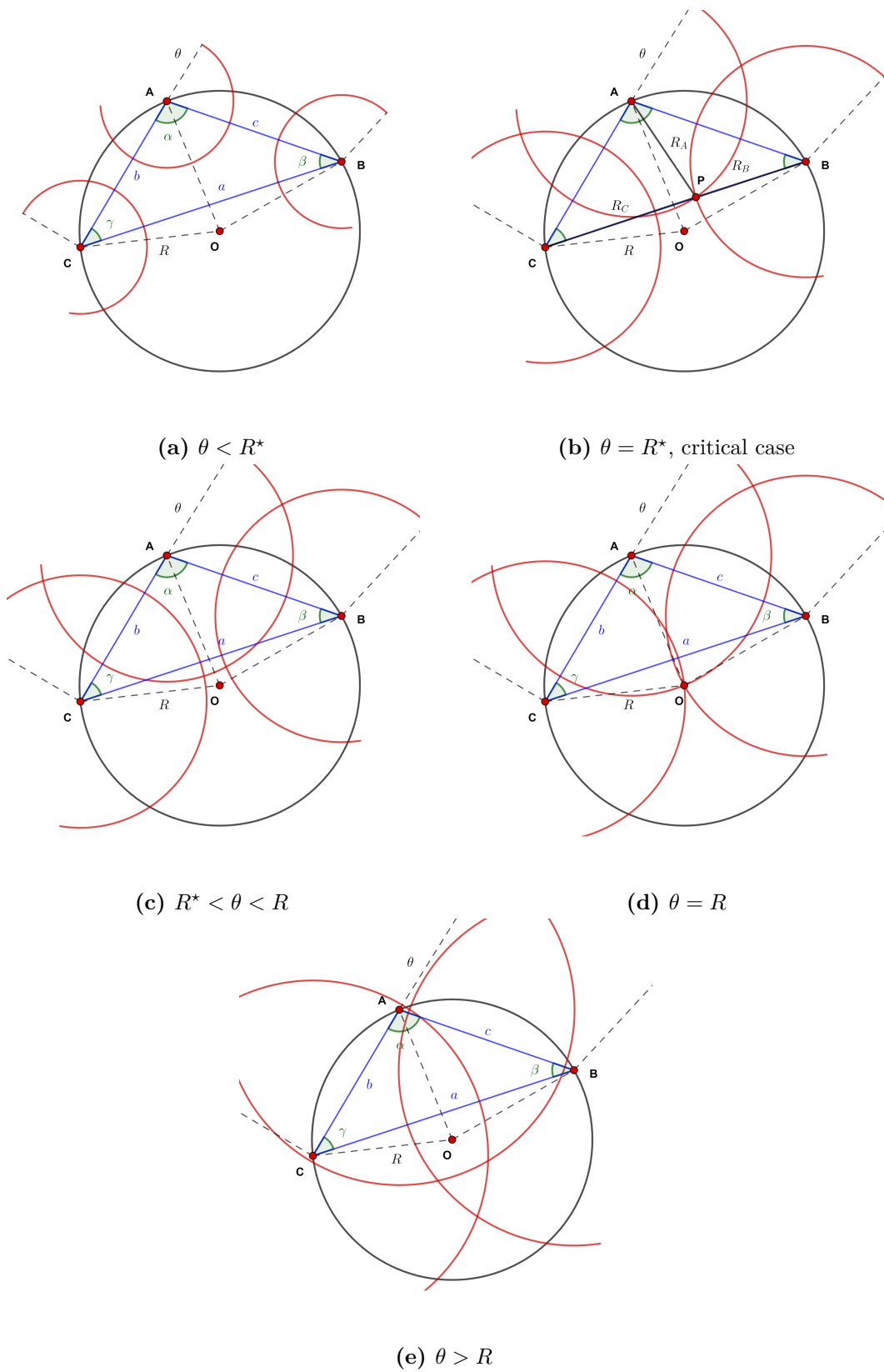


Figure 4.6. Circumcenter outside the spherical triangle

$$\begin{cases} \theta < R^* & \text{no full coverage for } \Delta ABC \\ \theta = R^* & \text{full coverage for } \Delta ABC, \text{ critical case} \\ R^* < \theta < R & \text{full coverage for } \Delta ABC \\ \theta = R & \text{full coverage for } \Delta ABC \\ \theta > R & \text{full coverage for } \Delta ABC \end{cases} \quad (4.67)$$

Therefore we can guarantee coverage for any point within the spherical triangle ΔABC only if:

$$\theta \geq R^* \quad (4.68)$$

Regardless of where the circumcenter O falls with respect to the spherical triangle ΔABC , we can write a generalized approach, for the general point that minimizes the maximum of the distances to these vertices [45]. If Eq. (4.70) is satisfied, any point within the triangle is covered.

$$R_{\Delta ABC} = \min \{R, R^*\} \quad (4.69)$$

$$\theta \geq R_{\Delta ABC} \quad (4.70)$$

It is important to note that if there are more than 3 SSPs, the critical configuration must be found for the spherical triangle that encompasses no other SSP, otherwise it would not result in the worst coverage angle.

We can extend the triangle concept to the entire planet surface, since a sphere surface can be divided into spherical triangles. If 1-fold coverage is guaranteed for each triangle, this would entail 1-fold global coverage.

Given a constellation of T satellites, there are necessarily T SSPs. These points define on the sphere L sides of G spherical triangles, meaning that to ensure global coverage at most G triplets should be analyzed.

$$L = \binom{T}{2} \quad (4.71)$$

$$G = \binom{T}{3} \quad (4.72)$$

Consequently, defining R_{max} as the circumradius corresponding to the worst coverage among all triplets at a given time, we can obtain the new relations that guarantee global coverage.

$$R_{max} = \max \{R_{\Delta ABC}(j)\} \quad \text{for } j = 1, \dots, G \quad (4.73)$$

$$\theta \geq R_{max} \quad (4.74)$$

If continuous coverage is required, the process must be applied to all points in time during the above mentioned *PRI*. The circumradius corresponding to the worst coverage condition over time is called R_{Max} . The Eq. (4.76) guarantee 1-fold global and continuous coverage over the planet for any given Walker-Delta constellation $T/P/F$.

$$R_{Max} = \max \{R_{max}(t)\} \quad \text{for } t = t_0, \dots, T_{orb}, \Delta T_{PRI} \quad (4.75)$$

$$\theta \geq R_{Max} \quad (4.76)$$

While the optimal value R_{Max} for the coverage angle has been determined for a Walker-Delta constellation $T/P/F$, it is not necessarily the most efficient configuration achievable with the same constellation setup. By just varying the inclination i of the constellation, an additional degree of freedom is introduced, which must be analyzed to identify the minimal Walker-Delta constellation. The minimal configuration requires the lowest possible altitude which in turn provides the lowest value for the coverage angle. This resolves in searching for the configuration with the smallest possible coverage angle R_{MAX} among all inclined configurations of the same pattern. The inclination that corresponds to this minimum coverage angle is denominated as the optimal inclination i_{opt} . This process is illustrated in Fig. 4.7, which shows the evolution of the coverage angle for a 5/5/1 pattern across a range of inclinations.

$$R_{MAX} = \min \{R_{Max}(i)\} \quad \text{for } i = 0, \dots, 90 \text{ deg} \quad (4.77)$$

$$\theta \geq R_{MAX} \quad (4.78)$$

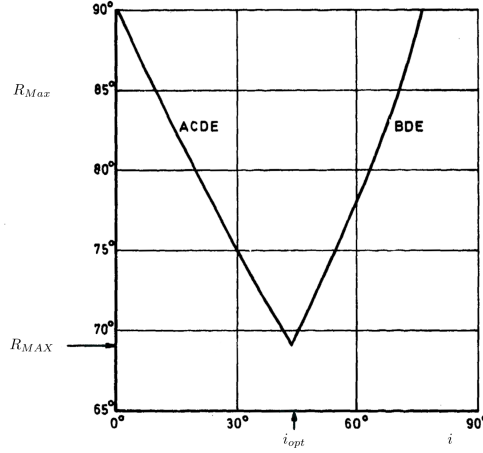
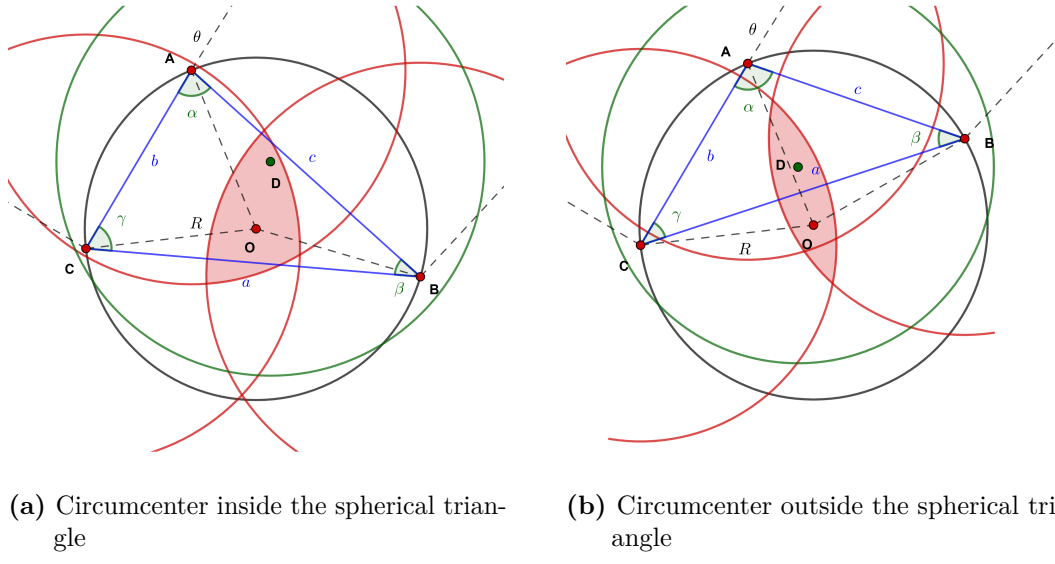
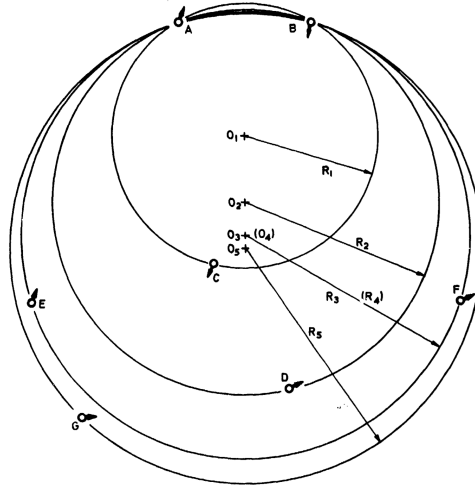


Figure 4.7. Evolution of R_{Max} for a range of inclinations δ for pattern 5/5/1 [29]

The same logic can be extended to higher degrees of coverage, although this requires additional SSPs to be in close proximity of the spherical triangle.

To achieve 2-fold coverage, imagine adding another SSP within the circumcircle. The optimal scenario occurs when this additional SSP is located in the region defined by the intersections of the coverage circles of the SSPs at the vertices of the spherical triangle. This situation is illustrated in Fig. 4.8 for the cases in which the circumcenter lies inside and outside of the spherical triangle.

In both cases these regions are not strictly confined within the spherical triangle; their size varies with the coverage angle and can extend beyond the triangle's confines. Therefore, it is sufficient for the additional SSPs to fall within the circumcircle defined by the three original SSPs to ensure local coverage of the area within the spherical triangle.

**Figure 4.8.** 2-fold coverage**Figure 4.9.** Multiple coverage

More in general, to guarantee n -fold coverage in the considered spherical triangle, its circumcircle must enclose at least $n - 1$ other SSPs. [29, 46]. An example is shown in Fig. 4.9. Needless to say, the process to determine the optimal coverage angle $R_{MAX,n}$ for a constellation requiring a n -fold global coverage follows the same approach, with some adjustments to make to account for the additional SSPs to consider at each step.

Lastly, following studies made by Walker [47] tried to find a way to extrapolate for larger constellation delta patterns. At the time, all he was able to compute

were the optimum patterns for constellations up to 15 satellites, so he tried to comparing its delta patterns with ideal constellations made by regular polyhedra and tessellations, that demonstrate a large inter-distance between its vertices, a characteristic appreciated in constellation design.

The trend he found is exemplified by Eq. (4.79) and it is indeed a good estimation for the minimum number of satellites required to obtain a n -fold global coverage for an effective central angle θ . The parameters p and q are obtained by the previous comparison, and are valued at 0.26 and 0.08 respectively.

$$T = \frac{4n}{[\theta(1 - pe^{-nq})]^2} \quad (4.79)$$

4.3.2 Lang coverage method

This coverage method works in a similar manner to the preceding one, albeit it uses a grid of points on the surface to check for distances to the SSPs, instead of using the points defined by triplets of SSPs.

For the simple reason of using a grid set, the obtained results will not be exact, and they will be highly dependent on the choice of step size for the grid.

Normally, a grid would have to be defined over the whole surface, but since the trend of a single satellite ground-track is symmetric with respect to the equator, we can consider only the norther portion of the planet.

If we were to consider the planet co-rotating with the whole constellation, we would soon find out that the single ground-track follow a curve that correspond to a synchronous orbit ($m = 1$, $R = 1$), for any orbital altitude considered [42, 46].

And since, the inclination is more than zero, the ground-track takes the shape of a figure eight curve, as can be seen in Fig. 4.10.

Consequently, for a constellation made up of T satellites, we can expect a number of ground-tracks equal to T , however not all of them are independent.

Under these assumptions, each configuration $T/P/F$ has a number of independent ground-track that can be determined using Eq. (4.80) since each and every orbit can be considered a RGTO orbit as needed. Therefore, parameters R and m are defined, even if the result is a unfathomable large repeat cycle.

$$N_p = \frac{T}{P} \quad (4.80)$$

$$J = \gcd(N_p, m) \quad (4.81)$$

$$G = N_p R + Fm \quad (4.82)$$

$$K = \gcd(G, PJ) \quad (4.83)$$

$$N_{ind,gt} = \frac{T}{K} \quad (4.84)$$

Using this neat stratagem, we are able to reduce further the test grid size, speeding up the simulation [29].

If a given constellation presents $N_{ind,gt}$ independent ground tracks, we need only to consider a part of the region in between two adjacent curves, since the same pattern will repeat many times over the complete period.

Therefore the grid of points is delimited as follows.

$$\Delta\lambda \in \left[0, \frac{\pi}{N_{ind,gt}}\right] \quad \Delta\phi \in \left[0, \frac{\pi}{2}\right]$$

Fig. 4.10 shows the grid size for simulations concerning a Walker-Delta 12/4/3 constellation. In this case the latitude is limited to the northern part, while the longitude is limited to the range between 0 and 30 degrees.

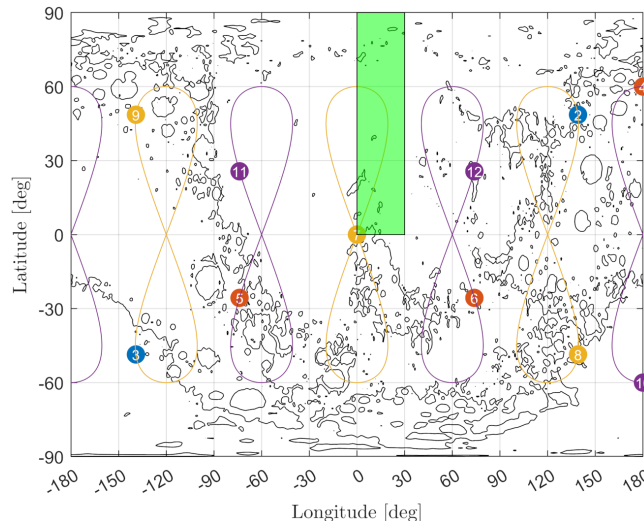


Figure 4.10. Lang coverage test grid (for a Walker-Delta 12/4/3 constellation)

The entire simulation is run over an orbital period. The inputs are the configuration, meaning $T/P/F$ and the inclination i . At each time instant, the positions of the satellite and their underlying SSPs are calculated, and the distances between the latter and the grid points are determined. For each point, the distances are calculated using Eq. (2.4) and the n smallest values are stored for the time instant considered. When all the distances are computed for a given time, the largest value among these is chosen and renamed $R_{max,n}$. At the end of the simulation, the largest value in time is $R_{Max,n}$, dependent on the inclination chosen. This value represents the worst condition for the given constellation configuration. If the constellation is able to provide a coverage angle θ more or equal than $R_{Max,n}$, said constellation can guarantee n -fold global coverage at all times. To find the corresponding altitude from the coverage angle we can use Eq. (2.3).

The same algorithm is then run for a range of different inclinations. The inclination for which we have the smallest value of $R_{Max,n}$ is the optimal inclination i_{opt} and the corresponding value is $R_{MAX,n}$. Ultimately, this angular distance $R_{MAX,n}$ will set the lower bound for the coverage angle θ for a given constellation, and therefore the lowest possible altitude to achieve n -fold global coverage.

4.3.3 RGTO coverage method

The repeating ground-track orbit (RGTO) coverage method works with a grid limited to a quarter of the planetary surface, as depicted in Fig. 4.11.

Contrary to the preceding case, the simulation is run over the entire repeating ground-track period, which for lunar orbits is around 27 days.

Moreover, each constellation is run for different values of inclination i and altitude h , generating a large number of configurations to check for.

A simulation made this way is certainly slower, but it is able, through repeated orbit analysis, to eliminate, or at the very least, to reduce the bias from the previous method, which stems from the selection of both the grid step size and the grid coverage.

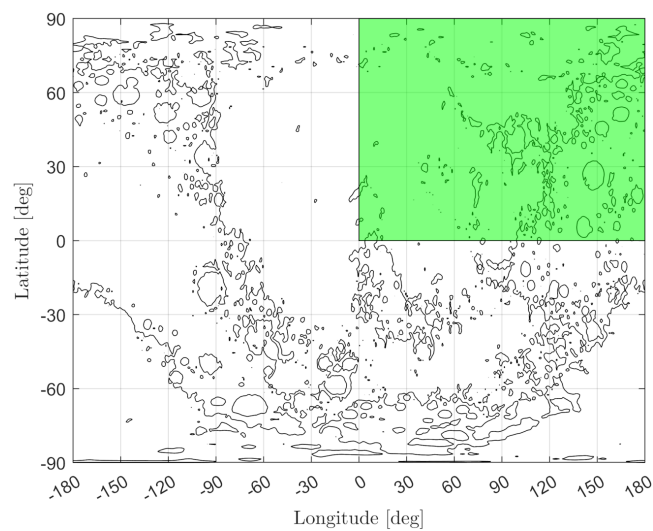


Figure 4.11. RGTO coverage test grid

Chapter 5

Global Navigation Satellite System

5.1 Overview

A Global Navigation Satellite System (GNSS) is a satellite-based system that provides global coverage, enabling autonomous positioning through radio signals transmitted from the constellation satellite. To determine a user's position, signals from at least four satellites are required, as they provide the necessary data to calculate longitude, latitude, altitude, and the clock offset.

GNSS relies on the time-of-arrival (TOA) ranging method to determine user location. This technique involves measuring the time it takes for a signal, transmitted from a satellite at a known position, to reach the user's receiver. The signal propagation time is then multiplied by the speed of light to compute the distance traveled by the signal. By analyzing signals from multiple satellites, the receiver can accurately determine its position through a process known as trilateration. [11]

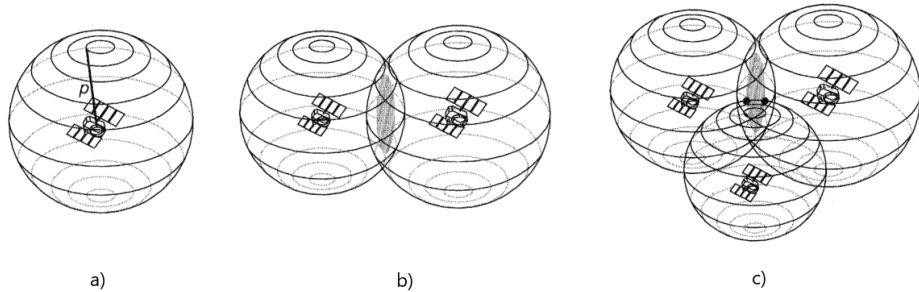


Figure 5.1. 3D trilateration geometry [8]

An example of the trilateration process is illustrated in Figure 5.1.

An explanation The simplest case to consider is the ideal scenario, where the user's clock is perfectly synchronized with the satellite. A single satellite transmits a radio signal that propagates uniformly as a sphere. Upon receiving the signal, the user is able to calculate the signal propagation time and, consequently, the distance to the satellite. This places the user somewhere on a sphere centered on the satellite.

With a second satellite, the user now receives two signals and calculates two distances, placing itself at the intersection of two spheres, that is a circle in space. A third satellite further refines the position, as the user must be on both this circle and a third sphere, reducing the possible locations to two points. Since these two point are symmetric with respect to the plane passing through the three satellites, one of these can be excluded, as it will be in space, while the other one will be in proximity to the planet surface, therefore determining the correct position [11].

Nonetheless, there is newfound interest in serving space users, as was shown in Chapter 1. The region in which an user can utilize the services provided by the GNSS is called "service volume" [9]. Two regions can be properly defined: the Planet Service Volume (PSV) and the Space Service Volume (SSV). Since only terrestrial GNSS exist and operate, these regions have been defined only for the Earth, shown in Fig. 5.2. Nonetheless, a similar concept, albeit with different altitudes as limits, can be easily formalized for different planets if need be. The Terrestrial Service Volume (TSV), as formulated by the GPS standard is the near-Earth region extending from the surface up to an altitude of 3000 km, and takes the form of a spherical shell. The Space Service Volume is instead defined as the outer spherical shell, between the altitudes of 3000 and 36000 km (approximately the GEO altitude).

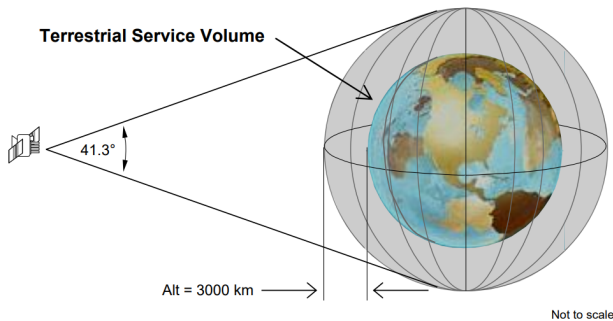


Figure 5.2. Terrestrial service volume [9]

A major challenge arises when the user's clock is not synchronized with the satellites. This clock offset introduces position uncertainty, as when time inaccuracies are present, the distance calculations between satellites and the receiver are incorrect, propagating into errors in determining the user's exact location.

Furthermore, these offsets affects each satellite-user pair differently, adding further ambiguity to the position calculation.

The services provided to the user are collectively known as Positioning, Navigation and Timing (PNT). GNSS performance can be evaluated through four different parameters [48].

- Accuracy: the difference between a receiver's measured and real position.
- Integrity: the capacity of a system to provide a threshold of confidence for the measured position.
- Continuity: the ability of the system to operate in a continuous manner.
- Availability: the ability to maintain the previous three parameters over time.

5.2 Requirements

The space segment of a GNSS is constituted by a satellite constellation, but not any constellation can be chosen due to stringent constraints.

In fact, satellite navigation constellations have very different geometrical constraints from satellite communications systems, among these the most obvious is the need for more multiplicity of coverage. The GNSS navigation solution, as explained before, requires a minimum of four satellites to be in view of an user at any given time to determine three-dimensional position and time.

Therefore, a critical constraint on a GNSS constellation is that it must provide a minimum of 4-fold global coverage at all times. In order to ensure this level of coverage even for a satellite failure, a nominal GNSS constellation is designed to provide more than fourfold coverage so that the minimum of four satellites in view can be maintained.

Also, having an additional satellite can prove useful even when failure is not considered, since if a GNSS satellite is experiencing a signal or timing anomaly, it can be excluded from the navigation solution. Therefore, a practical constraint for coverage of a GNSS constellation is minimum 6-fold coverage above a minimum elevation angle.

A 5 degree minimum elevation angle is generally used as a threshold value for GNSS systems, to minimize the errors related to a signal transmitted at an angle a little over the horizon. Common sources of errors for low elevation angles are the ionosphere (ionospheric delay) and the presence of reflective surfaces (multipath), and can easily add uncertainties on the assumed receiver position. Also, a mask angle is defined to account for obstacles, either of natural (mountains, trees, ...) or

artificial (skyscrapers, buildings, ...) origin that could impede the visibility of GNSS satellites.

In short, the requirements for the existing terrestrial GNSS constellation are as follows: [11]

1. 6-fold global and continuous coverage of the planet.
2. A minimum elevation angle of 5 degree.
3. Good geometric properties, that is sufficient angular separation between satellites at all time, to prevent signal degradation. This results in a perceived dispersion of satellites in both azimuth and elevation angle from the point of view of users.
4. The constellation should keep operating nominally even with a single satellite failure.
5. The constellation must be flexible, meaning that its satellites can be arranged and repositioned to expand or change the constellation configuration.
6. The constellation must be relatively stable, in order to minimize stationkeeping requirements, such as the frequency and magnitude of maneuvers. For the latter, ΔV per year is a good performance indicator.
7. Orbital altitude must be chosen in accordance with the payload mounted, since higher altitudes require increased transmitter power and antenna size to maintain signal strength.

This thesis aims to design a minimal GNSS constellation with the fewest satellites needed to satisfy the navigation equations. However, some of the aforementioned requirements will have to give way to achieve this goal.

A lunar GNSS must ensure a 4-fold global and continuous coverage, maintaining a minimum 5 degree elevation angle. It should also have good geometric properties, with wide angular separation between satellites to minimize positioning uncertainties. Finally, the constellation should reduce stationkeeping maneuvers in both frequency and magnitude.

5.3 Navigation equations

5.3.1 Timekeeping

Accurate timekeeping is of great importance to the correct functioning of positioning services, as the performance of a GNSS constellation depends heavily on it. Clocks

measure time through regular oscillations, but over time, differences in oscillation frequency can cause clocks to drift. The quality factor of a clock measures the stability and precision of these oscillations, serving as a key metric to differentiate high-quality clocks from less accurate ones. Modern systems rely on atomic clocks, which can achieve exceptional precision.

Clocks on GNSS satellites need to be extremely accurate because even small time errors can lead to significant positioning errors, as explained before.

GNSS systems rely on synchronized clocks across the whole constellation to ensure that the transmitted signals are precisely timestamped. The timestamp is then passed to the receiver either in the form of digital data within the GNSS signal itself, or alternatively can be transmitted at regular times with the receiver. Therefore even lost synchronization between GNSS satellites or failure to correctly relay timestamps between a satellite and a receiver can severely degrade positioning accuracy.

The transmission time, recorded from the satellite's point of view, against the on-board clock reference time is $\{t\}_t$, while

The time of the signal transmission, recorded from the clock on-board the satellite, is $\{t_1\}_t$, while the same instant, viewed from the receiver's clock is instead $\{t_1\}_r$. The difference in time is the clock offset ΔT between the satellite and user, and must be included as part of the positioning solution, as an unknown.

$$\Delta T = \{t\}_r - \{t\}_t \quad (5.1)$$

Large de-synchronizations which cannot be accounted for lead to significant errors or even complete service loss. The critical importance of reliable timekeeping was evidenced in 2016, when failures in the onboard clocks of ISRO's NavIC satellites disrupted positioning services for many months, requiring new satellites to restore functionality.

5.3.2 Pseudorange

The pseudorange PR is the measured distance between a satellite and a GNSS user. It is termed "pseudo" due to errors in time measurement caused by clock offset. Additionally, the term reflects the one-way nature of the GNSS signal, unlike a true range, which is measured over a two-way link, as in telemetry.

Fig. 5.3 shows how a pseudorange is calculated in the time reference frames, denominated He and Hr for the transmission and receiver clock, respectively. In the same image the $t_1 = te$ is the transmission time, unassociated with any reference time frame, and $t_2 = tr$ is the receiving time, again independent of the frame.

Since a signal travels at the speed of light c , and considering D its path length, it is possible to write the following expression for the general pseudorange.

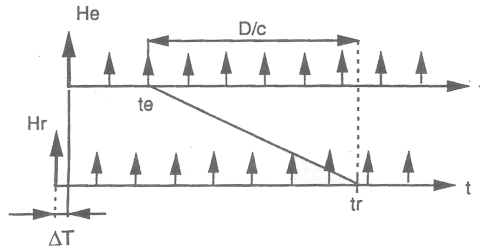


Figure 5.3. Pseudorange measurement [10]

$$PR = c(\{t_2\}_r - \{t_1\}_t) \quad (5.2)$$

$$PR = c(\{t_2\}_r - \{t_1\}_r + \Delta T) \quad (5.3)$$

$$PR = c(\{t_2\}_r - \{t_1\}_r) + c\Delta T \quad (5.4)$$

$$PR = D + c\Delta T \quad (5.5)$$

5.3.3 Non-linear model

Assume a scenario where 4 satellites are in view of a user. The exact positions of the satellites in space are assumed as known (x_i, y_i, z_i) , along with their respective time frames He_i , used by the onboard clock.

Let ΔT_i represent the clock offset between each satellite clock He_i and the user's clock Hr . The unknowns of the problem are:

- The user's coordinates (x, y, z)
- The clock offsets between satellite and the user $\Delta T_1, \Delta T_2, \Delta T_3, \Delta T_4$

Meanwhile the measurements are PR_1, PR_2, PR_3, PR_4 , the pseudoranges measured through each satellite. Therefore, this problem resolves in a system with 4 governing equations and 7 unknowns, making it unsolvable.

$$He = He_1 = He_2 = He_3 = He_4 \quad (5.6)$$

$$\Delta T = \Delta T_1 = \Delta T_2 = \Delta T_3 = \Delta T_4 \quad (5.7)$$

However, by assuming the satellite clocks are synchronized, meaning that all clock offsets are equal, the problem simplifies to a system, exemplified by Eq. 5.9, with 4 equations and 4 unknowns $(x, y, z, \Delta T)$, allowing a unique solution to be determined. Also, for ease of writing consider the following:

$$\tau = c\Delta T \quad (5.8)$$

This system, which serves as the model for the navigation equations, is nonlinear in the unknowns, and must be solved either through linearization, or numerical methods. When the number of available satellites is greater than four, the system is overdetermined and a fitting method must be used.

$$\begin{cases} PR_1 = \sqrt{(x_1 - x)^2 + (y_1 - y)^2 + (z_1 - z)^2} + \tau \\ PR_2 = \sqrt{(x_2 - x)^2 + (y_2 - y)^2 + (z_2 - z)^2} + \tau \\ PR_3 = \sqrt{(x_3 - x)^2 + (y_3 - y)^2 + (z_3 - z)^2} + \tau \\ PR_4 = \sqrt{(x_4 - x)^2 + (y_4 - y)^2 + (z_4 - z)^2} + \tau \end{cases} \quad (5.9)$$

5.4 Dilution of Precision

The dilution of precision (*DOP*) is a metric that quantifies the uncertainty in determining a user's position. This uncertainty typically arises from clock offsets and various error sources. However, since the most common error sources were not accounted for in the model and the clocks were assumed synchronized, the *DOP* describes the uncertainties caused solely by the geometry of the satellite constellation. For example, if a GNSS receiver were to be coplanar with all of the satellites being used, then the out-of-plane component of the position of the receiver would be essentially unknown, since they could not provide information along that direction and the resulting position measurement would be singular and corresponding *DOP* infinite [6].

Precision is considered "diluted" when the trilateration process fails to pinpoint a single location, instead indicating a broader region. The extent of this region is generally defined by the *DOP* value. Different satellite geometries can magnify or lessen the position error, varying its *DOP* value.

The non-linear system needs to be linearized to establish a simpler relationship between pseudorange errors and position errors [49]. This can be achieved using a first-order Taylor series expansion, as seen in (5.10). The same linearized model can be written in a reduced form, defining ∂Y as the vector of range measurement errors and ∂X the vector of position errors.

$$\begin{bmatrix} \partial PR_1 \\ \partial PR_2 \\ \partial PR_3 \\ \partial PR_4 \end{bmatrix} = \begin{bmatrix} A_{11} & A_{12} & A_{13} & 1 \\ A_{21} & A_{22} & A_{23} & 1 \\ A_{31} & A_{32} & A_{33} & 1 \\ A_{41} & A_{42} & A_{43} & 1 \end{bmatrix} \begin{bmatrix} \partial x \\ \partial y \\ \partial z \\ \partial \tau \end{bmatrix} \quad (5.10)$$

$$\partial Y = A \partial X \quad (5.11)$$

The matrix A is the Jacobian matrix of the range measurements residuals equations, with respect to the unknowns X , and is strictly related to the constellation geometry. It is important to note that the last column is full of ones, because the receiver clock offset shifts each pseudorange measurement the same way.

Therefore, to obtain a solution for the non-linear navigation equations, the receiver modifies an initial estimate of X using ∂X and iterates until convergence is achieved. Assuming ∂X to be a zero-mean vector, which is plausible, then its covariance reveals the expected position errors. To find the covariance of ∂X the generalized inverse of the Jacobian matrix A must be used, as well as the covariance of ∂Y , the pseudorange errors.

$$\partial X = (A^T A)^{-1} A^T \partial Y \quad (5.12)$$

$$cov(\partial X) = E[(\partial X \partial X^T)] = \dots \quad (5.13)$$

$$= \dots = \quad (5.14)$$

$$= (A^T A)^{-1} A^T E[(\partial Y \partial Y^T)] A (A^T A)^{-T} \quad (5.15)$$

Fortunately, since the pseudorange errors are assumed to be uncorrelated, Gaussian random variables, they are statistically independent which results in a diagonal covariance matrix multiplied by σ_0 , also known as the standard deviation of the measurements, which can be considered one for ease of writing, since it is the same for all pseudorange measurements.

$$\text{cov}(\partial Y) = \sigma_0^2 I \quad (5.16)$$

$$\text{cov}(\partial X) = \sigma_0^2 (A^T A)^{-T} \quad (5.17)$$

$$Q = (A^T A)^{-1} \quad (5.18)$$

$$Q = \begin{bmatrix} \sigma_x^2 & \sigma_{xy} & \sigma_{xz} & \sigma_{xt} \\ \sigma_{yx} & \sigma_y^2 & \sigma_{yz} & \sigma_{yt} \\ \sigma_{zx} & \sigma_{zy} & \sigma_z^2 & \sigma_{zt} \\ \sigma_{tx} & \sigma_{ty} & \sigma_{tz} & \sigma_t^2 \end{bmatrix} \quad (5.19)$$

From the covariance matrix Q we are able to obtain the DOP values, starting from $GDOP$, the geometric DOP . Other values are the DOP depending solely on physical coordinates ($PDOP$) and on time ($TDOP$).

$$GDOP = \sqrt{\sigma_x^2 + \sigma_y^2 + \sigma_z^2 + \sigma_t^2} \quad (5.20)$$

$$PDOP = \sqrt{\sigma_x^2 + \sigma_y^2 + \sigma_z^2} \quad (5.21)$$

$$TDOP = \sigma_t \quad (5.22)$$

Alternatively, using a different frame of reference we can express the same relations in the local tangent plane coordinates, meaning that the three axes are in the direction of the local east, local north and the zenith, formally up direction. We can therefore find the horizontal HDOP, the vertical HDOP, if need be.

$$Q = \begin{bmatrix} \sigma_e^2 & \sigma_{en} & \sigma_{eu} & \sigma_{et} \\ \sigma_{ne} & \sigma_n^2 & \sigma_{nu} & \sigma_{nt} \\ \sigma_{ue} & \sigma_{un} & \sigma_u^2 & \sigma_{ut} \\ \sigma_{te} & \sigma_{tn} & \sigma_{tu} & \sigma_t^2 \end{bmatrix} \quad (5.23)$$

$$VDOP = \sigma_u \quad (5.24)$$

$$HDOP = \sqrt{\sigma_n^2 + \sigma_e^2} \quad (5.25)$$

$$PDOP = \sqrt{HDOP^2 + VDOP^2} \quad (5.26)$$

Each DOP value represents the goodness of a solution in the given direction, while the $GDOP$ is a composite measure taking into account the geometrical impacts on both time and position.

In general, the dilution of precision values can range from 1 to about 100. A DOP of over 6 is typically regarded as poor performance for that measurement. Some values and their corresponding interpretation are reported in Table 5.1.

Table 5.1. Interpretation of DOP values [17]

Value	Quality
20-100	Poor
10-20	Fair
5-10	Moderate
2-5	Good
1-2	Excellent
<1	Ideal

Similarly, if the average DOP value offered by a constellation is 10, or higher, then that configuration suffers from bad geometry (small angular separation between satellites), and it can be disregarded as a GNSS candidate. Furthermore, it is sufficient for the geometry to be poor over short time intervals, leading to high $DOPs$ values, to skew the average results. For instance, the mean value for the GPS constellation is about 2.7. Examples of both good and bad geometries are shown in Fig. 5.4. As a rule of thumb, the higher the DOP is, the worse the constellation geometry is.

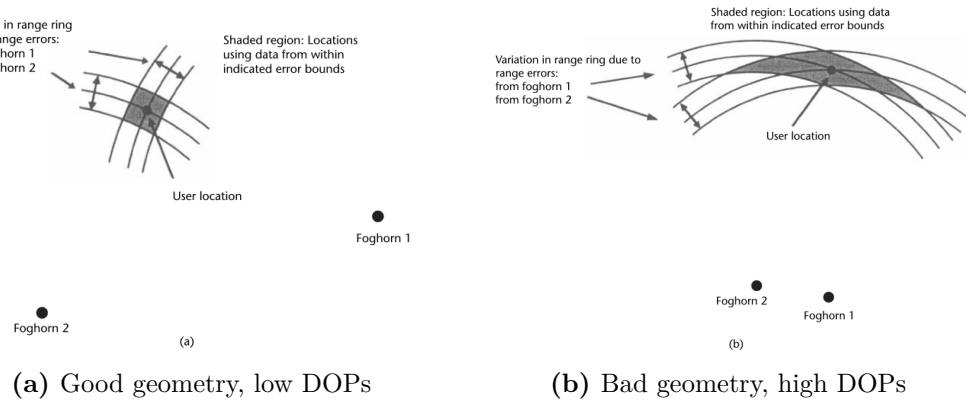


Figure 5.4. DOP geometry [11]

Fig. 5.5 shows the average values of the $DOPs$ attained by the Galileo constellation,

over its repeat cycle (around 10 days), for different latitudes. There is an obvious symmetry about the equation, as a result of the symmetric nature of the constellation, while the small differences between left and right side can be attributed to the topography of the planet.

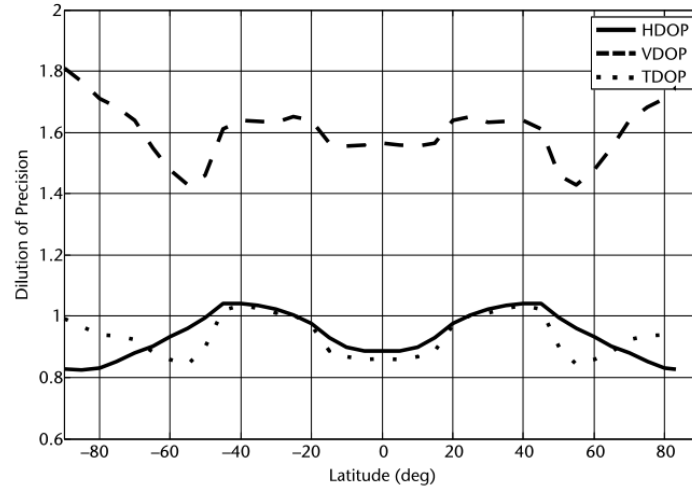


Figure 5.5. Average DOPs as a function of latitude for the Galileo constellation [11]

Navigation performance can be therefore measured through metrics like the *DOPs*. Other performance parameters are the user equivalent range error (*UERE*) and a combined error value, that combines both values into one [50].

Chapter 6

Results

6.1 Streets-of-Coverage

Using the general coverage method outlined in Chapter 4, a wide range of SoC constellations, both inclined and polar, can be identified.

We focused on constellations with an across coverage factor $k = 1$, as these families are well-studied and documented in literature. This choice was driven by the observation that polar geometries within this family consistently outperform inclined orbits in terms of efficiency, that is the lowest possible altitude.

The other families, which increase in number with the considered degree of coverage n , might not exhibit the same behavior and would therefore require more specialized analysis. Therefore, it is recommended to study these families in a future work to uncover potentially valuable insights for designing even more efficient constellations. The superior efficiency of polar geometries is demonstrated in Fig. 6.1 for 1, 2, 3, and 4-fold configurations of selected constellations, a trend consistent across all configurations with $j = n, k = 1$.

In this analysis, various inclinations were considered, shown on the x-axis and selected constellations, consisting of P orbital planes with N_p satellites per plane (denoted as $P \times N_p$), were generated. The results, shown on the y-axis, represent the minimum coverage angle required for the specific constellation to ensure n -fold global coverage.

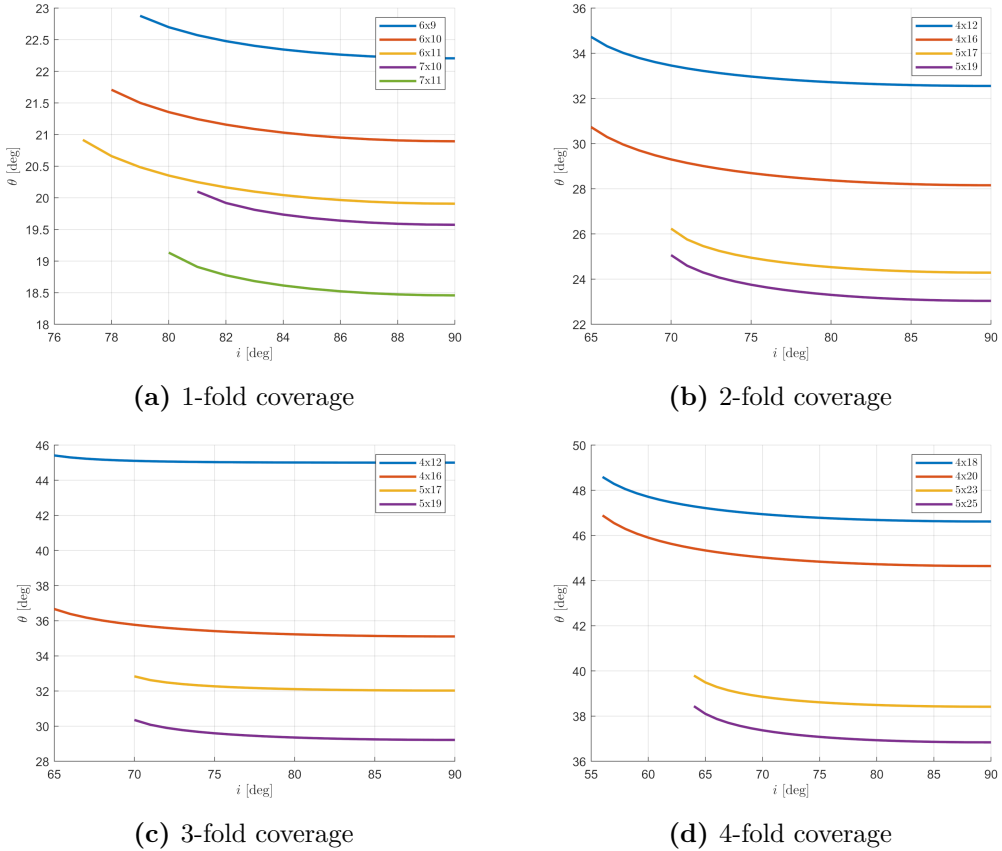


Figure 6.1. Streets-of-Coverage for different inclinations

Given the relationship between the coverage angle θ and the orbital altitude h as described by Eq. (2.2), and once fixed the minimum elevation, the configuration with the lower altitude is always preferred. The reasoning is that if the same altitude were considered for all configurations, (differing only in inclination) the one identified here would exhibit a larger coverage circle and overall superior coverage properties. This definition of more efficient constellations originates from Ulybyshev's work [41], which identifies minimal constellations as those with the fewest satellites at the lowest possible orbital altitude while still meeting the required coverage needs. It can be clearly seen that the coverage angle (or orbital altitude for the matter) is a monotonic function of the inclination. This also means that the minimum coverage angle is always found at the polar inclination. For instance, in the 1-fold image, it can be seen that the blue line represents the many configurations the SoC constellation, comprised of 6 orbital planes with 9 satellites per plane, can assume. While this constellation inclined at 79 degrees has a coverage angle of approximately 23 degrees, the corresponding polar constellation achieves a coverage angle of 22.3 degrees.

Lastly, the inclinations here considered were limited to prograde orbits. If retrograde orbits were considered, the graph would exhibit symmetry for configurations with inclinations larger than 90 degrees.

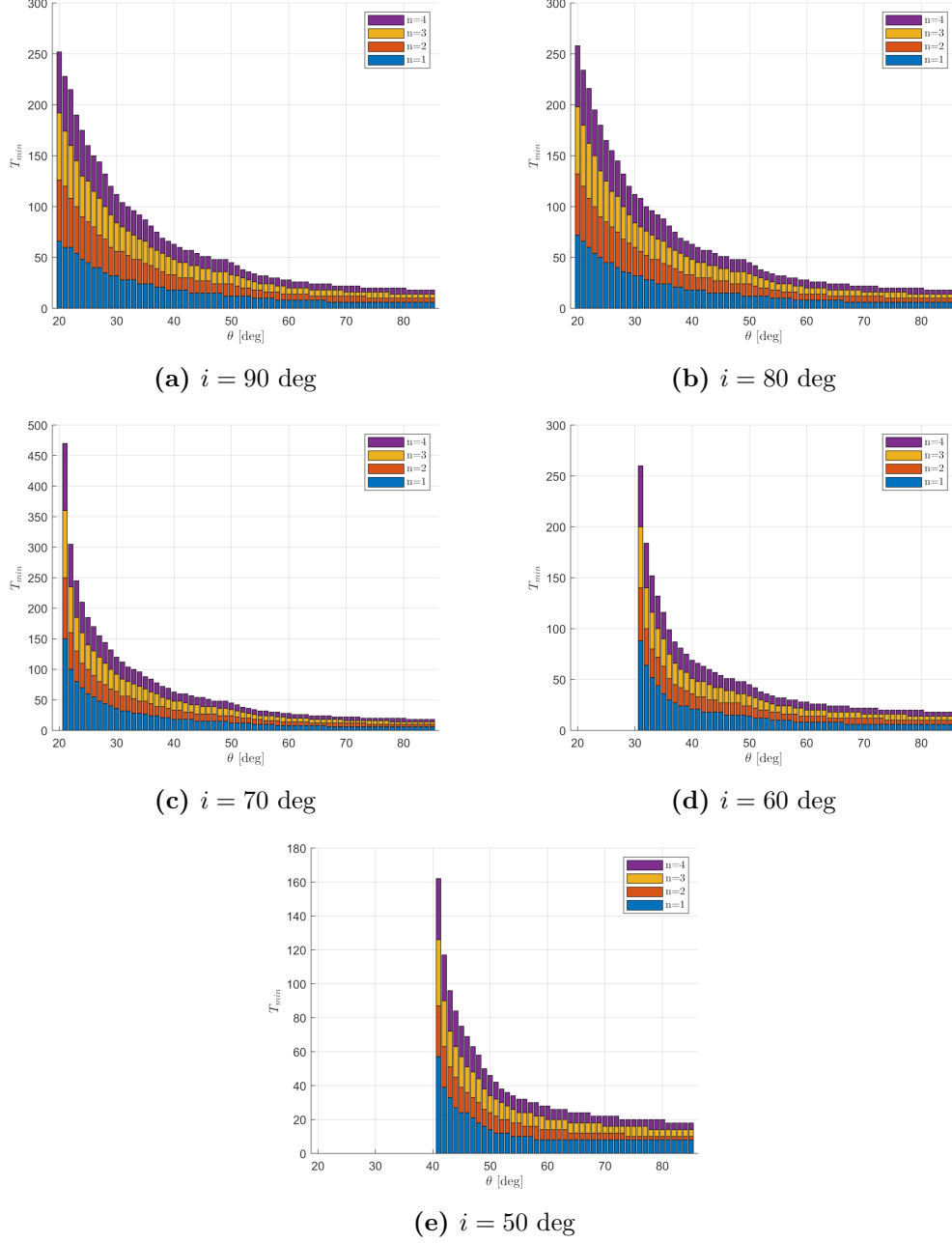


Figure 6.2. Minimum number of satellites in a SoC constellation to guarantee n -fold coverage with fixed value θ

Fig. 6.2 presents the results of an extensive analysis encompassing all possible SoC constellations composed of T satellites, irrespective of the number of streets P . As

previously explained, the first image is the most significant, since it represents the best overall polar SoC constellations.

This analysis also reveals that the least inclined (closer to the equatorial plane) SoC constellations cannot be built with small coverage angles, as it renders them unable to reach and cover the polar regions, as explained in Eq. (2.5). Therefore, to reach the poles these constellations must necessarily rely on a higher altitude to attain a larger coverage angle θ .

In the context of comparing the best SoC constellations with the best Walker constellations, it makes sense to consider only the best polar SoC constellations, excluding less efficient configurations.

6.1.1 More SoC solutions

A consideration must be made regarding the general coverage Eq. (4.45), which defines the unique minimal SoC constellations, if they exist, for specific initial values such as the number of planes P , the number of satellites per plane N_p , and the requested degree j of global coverage.

For a broader search, Eq. (6.1) can be used when the focus is not strictly on minimal constellations. This inequality solution yields a set of constellations similar in size to the previously identified minimal ones (same total number of satellites T) and capable of meeting the same coverage requirements for different coverage angles and therefore orbital altitudes h .

$$(P - 1)\Delta\Omega_{co} - \Delta\Omega_{anti} \geq 0 \quad (6.1)$$

This is demonstrated in Fig. 6.3 for a 2-fold SoC 27/3 constellation. The unique minimal constellation is depicted as a green dot in the first image, while all the possible configurations of the same constellation can be seen to its right, with increasing values of θ .

Overall, the first two images illustrate how the spacing values $\Delta\Omega_{co}$, $\Delta\Omega_{anti}$ and ΔM_{inter} vary for these configurations, which will therefore assume different spatial geometries. Similarly, the last image shows the corresponding variations of the half-widths c_1, c_2 .

The gray box represents the limits for what we call a proper SoC constellation, since for larger values we would find streets spanning more than the maximum angular spread π . And since, we started with considering the across coverage factor $k = 1$, this result would contradict it.

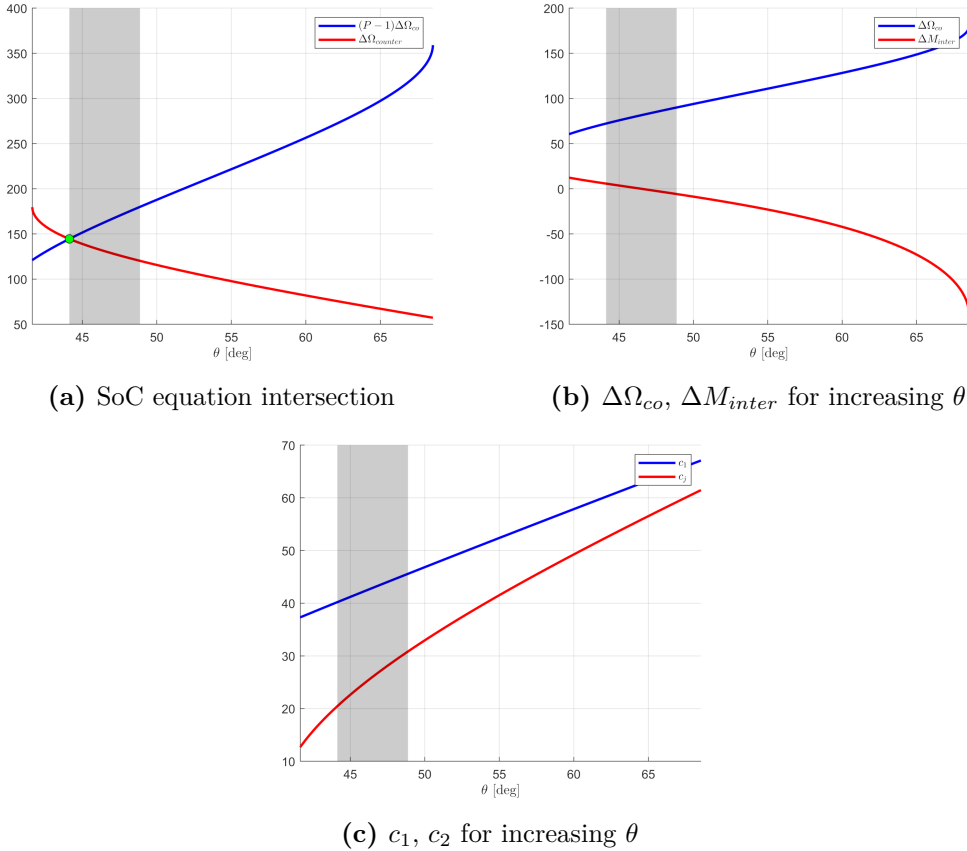


Figure 6.3. Search for a lower bound SoC 27/3 solution

6.2 Walker-Delta

Since the methods for designing Walker-Delta constellations rely on numerical approaches, some inaccuracies in coverage calculations are inevitable.

Common issues in numerical simulations for evaluating constellation coverage, as noted by Wertz [6], include:

1. Grid points, since both the step size and the distribution of points on a sphere can cause inaccuracies. Obviously a finer grid would result in lesser approximate and better results, (in our case coverage angles), but it would also significantly increase computation time, so a compromise is needed. Regarding the distribution of points on a sphere there is no easy manner to distribute them in an uniform manner [51]. Otherwise, if considering a simple rectangular grid in both latitude and longitude, points would cluster at the poles, thus biasing the simulation results.
2. Incorrect time step, since the step size selection is important since it allows for

a greater detail of the results, and must be carefully chosen as not to resonate with the selected repeat cycle of the constellation. It is for this reason that the RGTO coverage method was preferred to design Walker constellation, since it minimizes the bias that any choice in the time step could have generated.

3. Incorrect interpretation of results, since it must not be forgotten that both the simulations and constellations are deceitful, as an optimum cannot be predicted a priori.

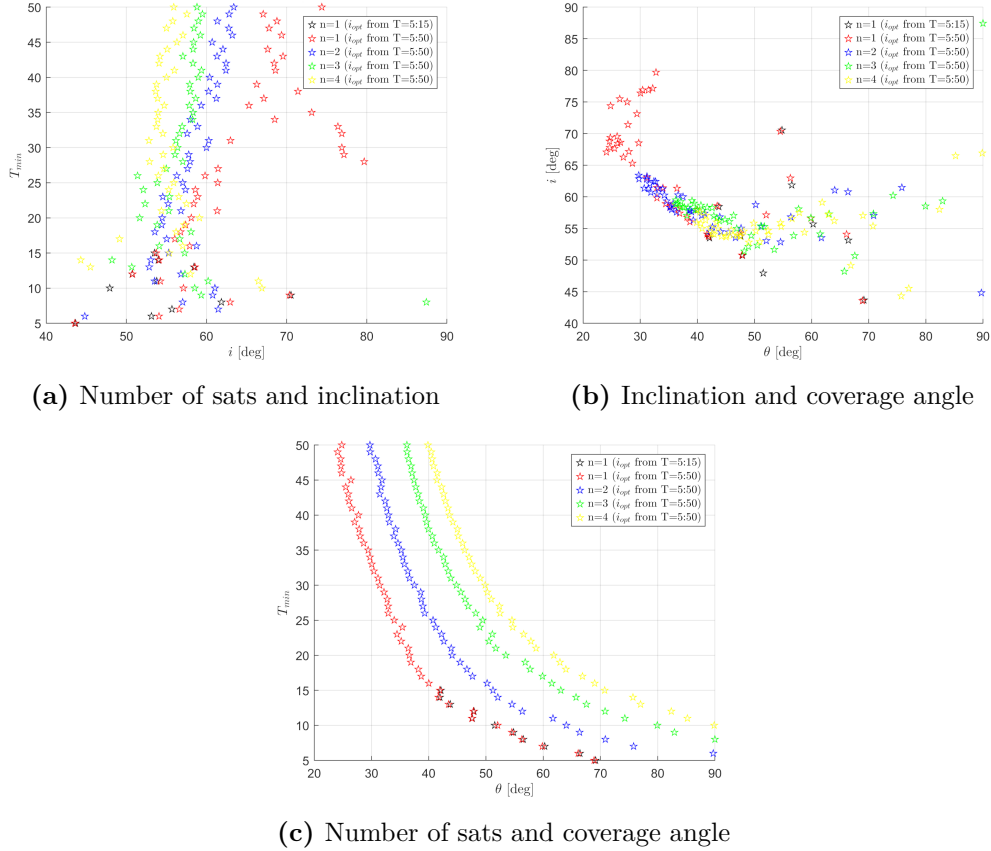


Figure 6.4. Walker-Delta optimal configurations

Similarly as was done with the SoC constellations, the best Walker-Delta constellations must be found to subsequently compare them. Earlier simulations were done by Walker and Ballard [29, 47, 52], but they focused on smaller constellations, up to 15 satellites in total. Since then, computers improved significantly and larger analysis are possible with manageable computation times.

The results obtained through the RGTO coverage method agree with the discoveries of the earlier authors, as it can be seen from Fig. 6.4 from the proximity of black

and red solutions. Each star represents an optimal Walker-Delta constellation, as it was defined in Chapter 4, for an increasing number of satellites T , up to 50. While a trend can be surmised for each of the pairs of optimal values, it is only for the number of satellites T and the coverage angle θ that a relation can be defined. This relation (4.79), alongside Eq. (2.2), allows us to predict the minimum number of satellites required for global coverage starting from an orbital altitude [47]. The Walker relation has been developed for a mask angle of zero. However, they can be easily expanded to the general case by repeating the coverage analysis for different values of ε . Typically, as the mask angle increases, the trends observed in Fig. 6.4c shift to the right, necessitating more satellites in the constellation.

$$T_{min} = f(\theta, n) \quad (6.2)$$

$$T_{min} = f(\theta, n = 4) \quad (6.3)$$

$$= f(\theta) \quad (6.4)$$

which can also be written in the similar form with altitude h and ε

$$T_{min} = f(h, \varepsilon, n) \quad (6.5)$$

$$T_{min} = f(h, \varepsilon = 0, n = 4) \quad (6.6)$$

$$= f(h) \quad (6.7)$$

A similar analysis can be seen in Fig. 6.5, which shows the minimum number of satellites required to guarantee a n -fold global coverage given an inclination i and a coverage angle θ .

A vertical asymptote for coverage angle θ approaching $90 - i$ degrees is visible in the first three images. The limit is a consequence of the inclination, and means that a global coverage constellation with θ in the range between 0 and $90 - i$ is physically impossible, as it cannot reach the polar regions. At the same time, it makes it harder for constellations to guarantee global coverage, therefore requiring more satellites. The same phenomenon was observed before for SoC constellations.

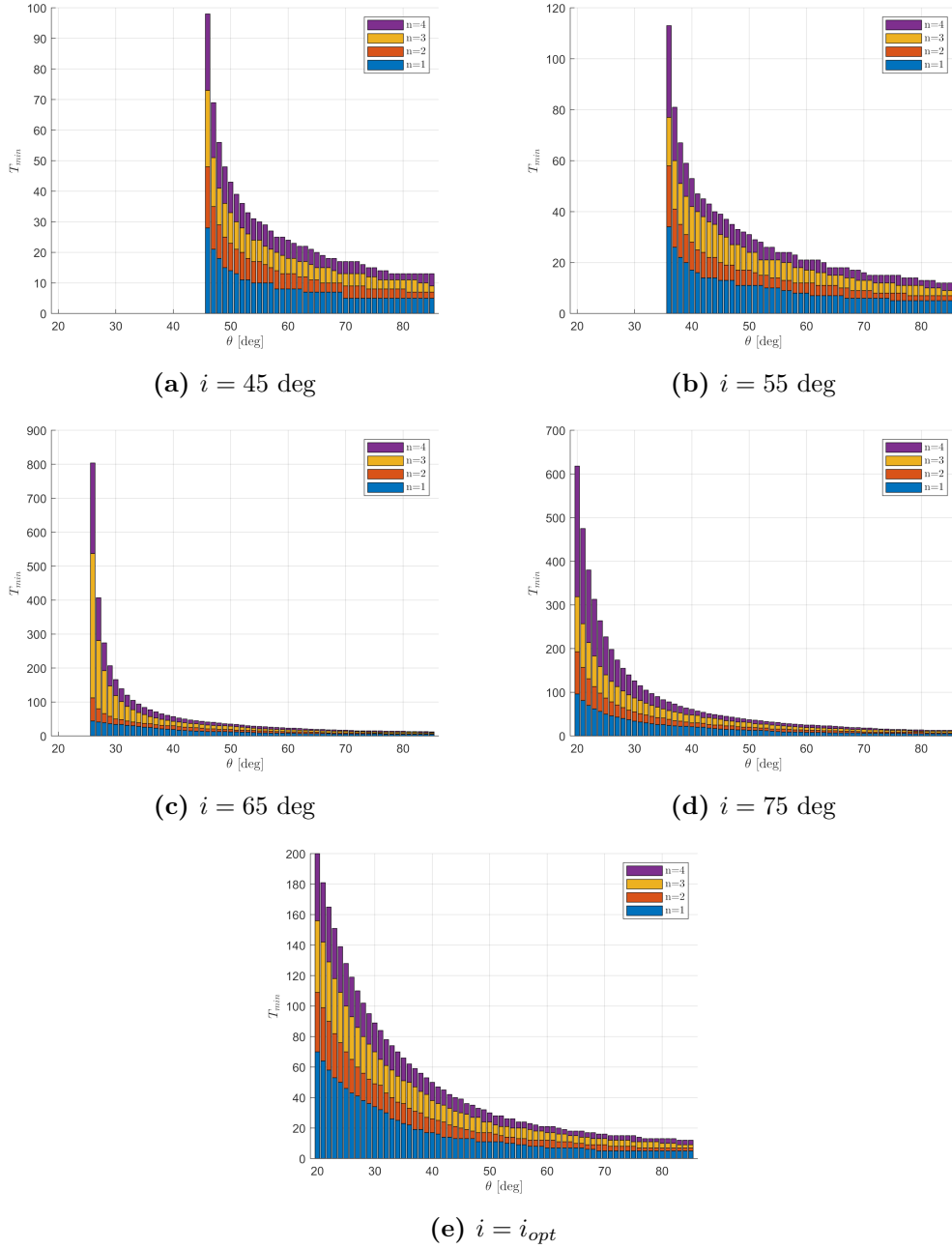


Figure 6.5. Minimum number of satellites in a Walker-Delta constellation to guarantee n -fold coverage with fixed value θ

6.3 Moon Walker tables

The relation found in the previous section is a general one, applicable to any planet assumed to be a sphere.

Using the data from either coverage analysis or directly from the fitted Walker

relation, it is possible to tabulate the minimum number of satellites as a function of either altitude or coverage angle, resulting in a Walker table. These tables can be generated for different requirements, such as the degree n of global coverage and the minimum elevation angle ε .

An original contribution of this dissertation is the specialization of Walker tables for application on the Moon. These tables are presented as a function of the repeat factor q , a characteristic of the Moon, and the inclination i in Fig. 6.6 for minimum elevation angles of 0, 5, and 10 degrees, respectively and for a 4-fold coverage.

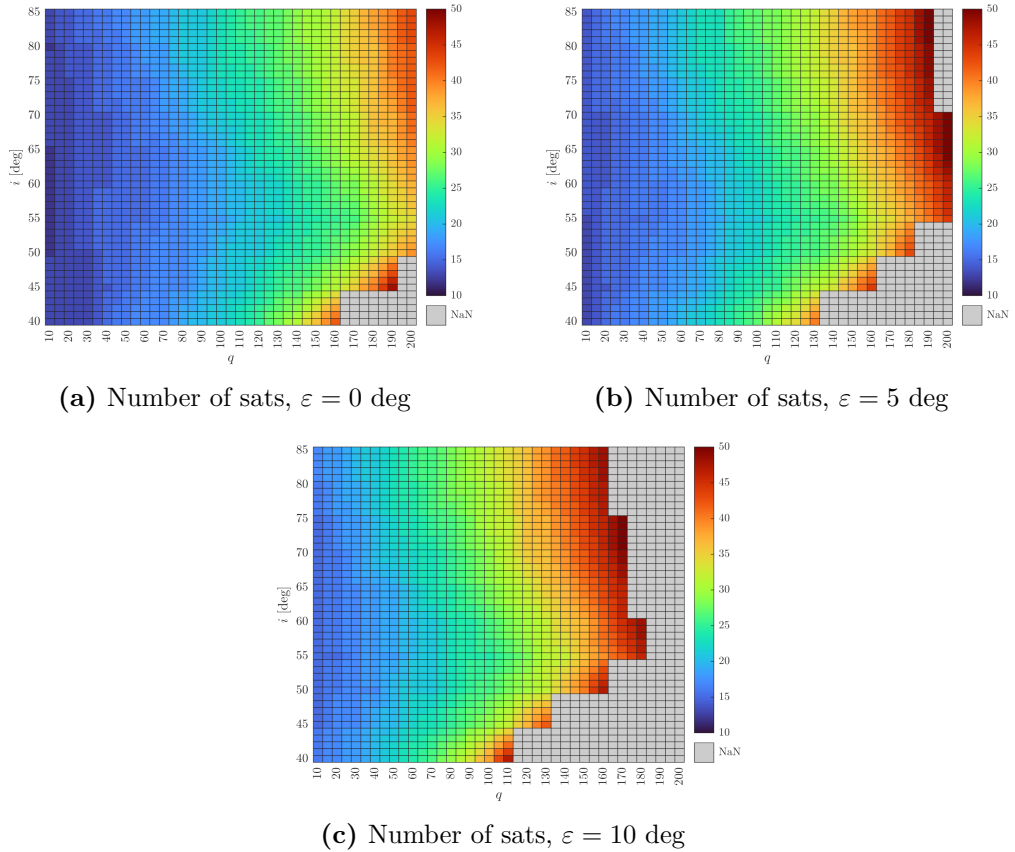


Figure 6.6. Moon Walker-Delta tables

The tables are presented in heatmap mode, displaying values through a color scale. Gray values indicate that more than 50 satellites were required. The values reported were obtained using the RGTO coverage method, for constellations where $m = 1$. Moreover, the research domain was limited to inclinations between 40 and 85 degrees, with the repeat factor ranging from 10 to 200, based on considerations made from Fig. 3.9c.

It is evident that the required number of satellites T increases with the repeat factor q , while the relationship with inclination i is more complex.

The relation between altitude, inclination and repeat factor can be seen in Fig. 3.8b. While the effect of inclination on altitude is minimal for the considered range of repeat factor, it surprisingly has a significant impact on the number of satellites required as it can be observed on the tables.

The minimum number of satellites for an elevation angle $\varepsilon = 0$ degrees is reported in Fig. 6.7 for each inclination considered. This figure helps discern the optimal constellations and their corresponding inclinations.

It is evident that the optimal constellations, which require fewer satellites, often have an optimal inclination value of 55 degrees. There is some overlap for these lines for low repeat factors, indicating that good alternatives with the same number of satellites can be found at higher inclinations if necessary.

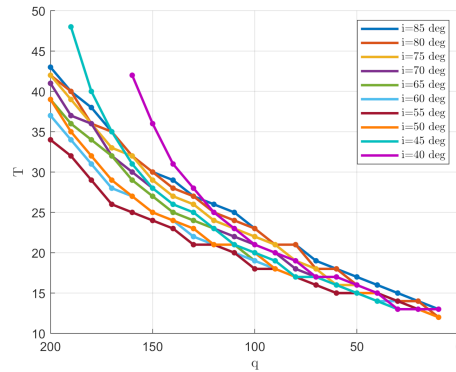


Figure 6.7. Moon Walker-Delta optimum ($\varepsilon = 0$ deg)

Ultimately, the aim is to generate from these table an expression of the form:

$$T_{min,\varepsilon,n} = f(q, i, \varepsilon, n) \quad (6.8)$$

$$T_{min} = f(q, i, \varepsilon = 0, n = 4) \quad (6.9)$$

$$= f(q, i,) \quad (6.10)$$

Leaving the most general case aside, we need to find a way to express the results for the case obtained for ε equal to 0 degrees and $n = 4$, since it's the limiting case for GNSS applications. While an elegant expression could not be found at this time, efforts have been made to fit the data using surface fitting techniques. Several options are available, from custom equations to polynomial surface fitting. A minimum of a 3-by-5 parameter polynomial would be necessary for an adequate fit. Alternatively, a custom equation can be developed based on the knowledge from the one-dimensional Eq. 4.79.

From observation we can surmise a exponential trend along the q direction. An option is therefore a bi-exponential function with parameters a_1, b_1, c_1, d_1, q_0 .

$$T_{min}|_{i=const} = f(q) \quad (6.11)$$

$$T_{min} = a_1 \exp(-(q - q_0)b_1) + c_1 \exp(-(q - q_0)d_1) \quad (6.12)$$

Similarly, at least a 3-degree polynomial should be considered along the i direction with parameters a_2, b_2, c_2, d_2 .

$$T_{min}|_{q=const} = f(i) \quad (6.13)$$

$$T_{min} = a_2 i^3 + b_2 i^2 + c_2 i + d_2 \quad (6.14)$$

And finally a set of surface equations can be generated by combining together the behaviors along the axes q and i . If T behaves independently in the two directions, we might use addition, assuming that the two effects contribute separately, while if T is affected by both factors simultaneously, we use multiplication. This assumes that the growth in one direction scales the effect of the other. The available options have been written down below:

$$T_{min} = \exp(ax) \cdot (b_0 + b_1 y + b_2 y^2 + b_3 y^3) \quad (6.15)$$

$$T_{min} = \exp(ax) + (b_0 + b_1 y + b_2 y^2 + b_3 y^3) \quad (6.16)$$

$$T_{min} = (c_1 \exp(a_1 x) + c_2 \exp(a_2 x)) \cdot (b_0 + b_1 y + b_2 y^2 + b_3 y^3) \quad (6.17)$$

$$T_{min} = (c_1 \exp(a_1 x) + c_2 \exp(a_2 x)) + (b_0 + b_1 y + b_2 y^2 + b_3 y^3) \quad (6.18)$$

As previously mentioned, it was not possible to fit the collected data with a simple and effective function.

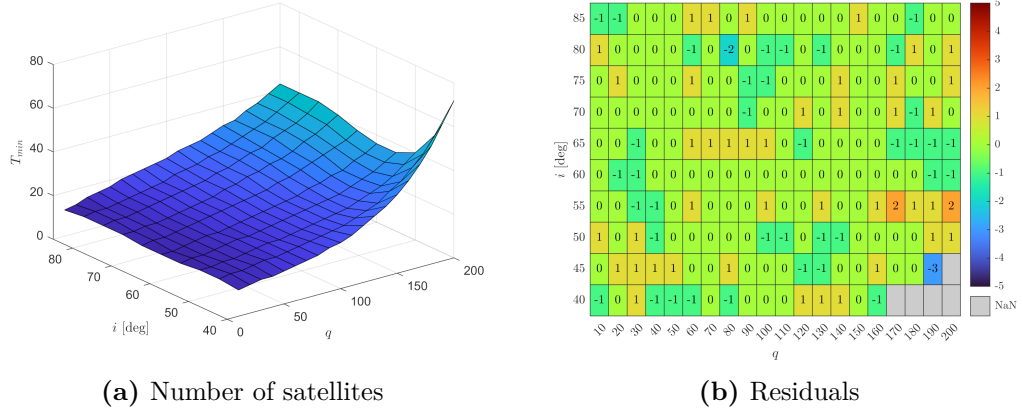
Otherwise, a polynomial of degree 5 in both the q (repeat factor) and i (inclination) axes, known as a poly55 expression, can be used to fit the collected data. The fitting required normalization on both axes over the ranges previously considered. The inclination was normalized by mean $\mu(i) = 102.9$ and standard deviation $\sigma_i = 56.94$, while the repeat factor was normalized by mean $\mu_q = 63.05$ and standard deviation $\sigma_q = 14.15$. The converged fit shows a coefficient of determination $R^2 = 0.994$. The coefficient values found are reported in Table 6.1.

$$\begin{aligned}
T_{min} = & p_{00} + p_{10}x + p_{01}y + p_{20}x^2 + p_{11}xy + p_{02}y^2 + p_{30}x^3 + \\
& + p_{21}x^2y + p_{12}xy^2 + p_{03}y^3 + p_{40}x^4 + p_{31}x^3y + \\
& + p_{22}x^2y^2 + p_{13}xy^3 + p_{04}y^4 + p_{50}x^5 + p_{41}x^4y + p_{32}x^3y^2 + \\
& + p_{23}x^2y^3 + p_{14}xy^4 + p_{05}y^5
\end{aligned} \tag{6.19}$$

Table 6.1. Coefficients value for poly55 fit

Coeff	Value	Coeff	Value
p_{00}	20.0561575585217000	p_{31}	-0.5008454938300830
p_{10}	6.3820941877479300	p_{22}	0.8988660879185690
p_{01}	2.3084051002624600	p_{13}	-1.5790062389984900
p_{20}	0.6858214290098480	p_{04}	0.3935858887831520
p_{11}	3.0444293465804800	p_{50}	-0.0127007092182069
p_{02}	0.1073795575002700	p_{41}	-0.0930254201081384
p_{30}	0.3514246491987080	p_{32}	0.4775225871546660
p_{21}	0.8828167430104950	p_{23}	-0.9332710087248280
p_{12}	-0.5397632076196500	p_{14}	0.5528882781340900
p_{03}	-1.1488614628753600	p_{05}	0.2063042306707840
p_{40}	0.2951142995907080		

Fitting the data in the Moon Walker table results in the surface shown in Fig. 6.8a, while the residuals range from (-3) to (+2) in Fig. 6.8b. This surface can be used therefore to forecast the minimum number of satellites for a lunar constellation given different initial conditions.

**Figure 6.8.** Poly55 fit

6.4 Comparison and selection

The best SoC constellations are compared with the best Walker-Delta constellation for 1, 2, 3, and 4-fold coverage in Fig. 6.9.

The analysis shows that while SoCs outperform Walker-Delta constellations for single coverage with more than 20 satellites, they fall short for higher degrees of coverage. Therefore, for 4-fold global coverage, Walker-Delta constellations are the more efficient choice and should be the only class to consider for designing a GNSS constellation

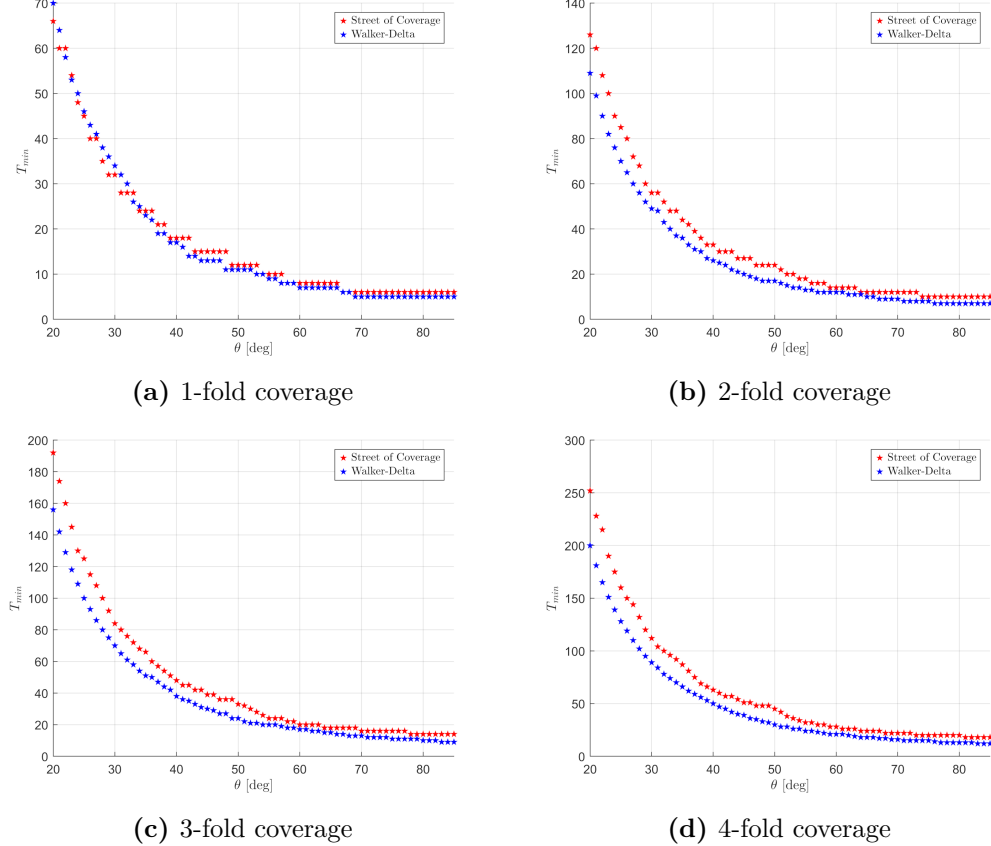


Figure 6.9. Streets-of-Coverage vs Walker-Delta comparison

A total of 54 Walker-Delta constellations constellations were considered, to find the most suitable configuration for a lunar GNSS constellation. Of these 10 were physically unfeasible, due to their high orbital altitudes, resulting decisively in poor stability performance over the long period.

Below in Tab. 6.2 we reported the best 18 configurations and the additional 8 optimal constellations from 13 to 20 satellites.

Table 6.2. List of GNSS constellation candidates

ID	h [km]	i [deg]	T	P	F	R	θ [deg]
1	11142.21	45.51	13	13	2	18	77.2771
2	9200.07	44.31	14	14	2	23	75.8950
3	5358.44	55.37	15	15	2	44	70.8822
4	4609.79	57.03	16	16	10	52	69.1758
5	3845.54	49.15	17	17	11	63	66.9399
6	3103.01	56.21	18	3	1	78	64.0489
7	2868.85	57.21	19	19	5	84	62.9295
8	2694.16	59.12	20	10	7	89	62.0107
9	9200.32	61.70	14	7	4	23	75.8952
10	10268.57	58.51	14	7	4	20	76.7113
11	6375.33	62.57	15	5	1	36	72.6817
12	6529.00	56.26	15	5	1	35	72.9142
13	12807.22	72.39	16	8	3	15	78.1657
14	5358.64	59.29	16	8	5	44	70.8826
15	5358.68	60.01	16	8	5	44	70.8827
16	3621.71	61.87	18	6	2	67	66.1579
17	4302.94	51.65	18	6	2	56	68.3492
18	4231.67	47.84	18	9	2	57	68.1445
19	7038.98	80.63	18	9	3	32	73.6262
20	3674.69	50.64	18	9	5	66	66.3491
21	4376.89	62.58	18	9	6	55	68.5563
22	4609.95	59.33	18	9	6	52	69.1763
23	9884.70	84.99	18	9	7	21	76.4355
24	5953.67	65.94	20	4	0	39	71.9948
25	3906.73	61.90	20	4	2	62	67.1424
26	3517.77	65.02	20	5	1	69	65.7707

6.5 Coverage performance

As was stated before in Chapter 2 the coverage angle can be used as a performance index, enabling us to filter out the constellations that display an inefficient use of the coverage. This coverage performance is exemplified by the excess coverage parameter cov , which depends on both the number of satellites T , and the coverage angle θ .

$$cov = \frac{T \times 2\pi R_p^2 (1 - \cos \theta)}{4\pi R_p^2 \times n} \quad (6.20)$$

and since we considered 4-fold coverage, using $n = 4$ gives us the final relation:

$$cov = \frac{T(1 - \cos \theta)}{8} \quad (6.21)$$

This coverage index was calculated for all 26 configurations previously chosen. For each of these, the average values of the DOP and the minimum number of satellites in view at any given time were calculated and reported in Table 6.3.

The optimal constellations (IDs 1 to 8) are unimpressive due to poor geometry and low DOP values. Their only advantage is the high number of visible satellites, attributed to them having a single satellite per orbital plane. While efficient on paper, as shown by the low excess coverage parameter cov , they are impractical due to the excessive number of planes.

Similarly, configurations like 13 and 18 are discarded for having too many orbital planes, leading to low DOP values.

Configuration 19 is considered to be excessively inclined, and that would degrade coverage and positioning over the middle latitudes and is therefore discarded.

Only four configurations (12, 16, 17, and 26) have been selected for their superior geometric properties, evidenced by low DOP values. Notably, their inclination range is between 50 and 65 degrees, similar to existing terrestrial GNSS constellations.

Table 6.3. List of GNSS constellation candidates - coverage efficiency

ID	cov	GDOP	PDOP	TDOP	HDOP	VDOP	Min T
1	1.2671	9.2061	7.8129	4.8264	2.6082	7.2379	5.6246
2	1.3235	12.7585	10.5290	7.1297	3.4342	9.8377	5.8905
3	1.2609	6.2742	5.3623	3.2059	2.1178	4.8373	5.6735
4	1.2890	12.9443	10.8752	6.5493	4.9346	9.3986	5.8211
5	1.2926	19.5191	18.6410	5.6582	14.3245	9.5039	5.8678
6	1.2654	19.7352	16.3486	10.9671	5.8123	15.1130	4.2661
7	1.2942	3.9659	3.4973	1.8426	1.5682	3.0637	4.1467
8	1.3267	4.0137	3.5465	1.8566	1.3578	3.2120	4.1973
9	1.3235	4.9929	4.2751	2.5417	1.6189	3.8687	4.0122
10	1.3477	4.6275	3.9746	2.3367	1.4744	3.5971	4.0453
11	1.3169	4.8352	4.1308	2.4642	1.9166	3.5736	4.2230
12	1.3241	4.5101	3.8943	2.2409	1.8724	3.3536	4.2648
13	1.5898	3.5185	3.1176	1.6204	1.6191	2.6273	4.7230
14	1.3450	3.0476	2.6953	1.4045	1.1542	2.3751	4.4321
15	1.3450	3.1507	2.7817	1.4609	1.1564	2.4613	4.4321
16	1.3405	2.5960	2.3295	1.1338	1.1833	1.9902	4.5261
17	1.4199	2.4345	2.1913	1.0511	1.1251	1.8671	4.8345
18	1.4124	4.9077	4.2937	2.3492	1.7080	3.8671	4.7195
19	1.6157	3.1641	2.8284	1.3951	1.4790	2.3556	4.9791
20	1.3474	5.0175	4.4030	2.3565	1.7757	3.9280	4.1603
21	1.4274	2.7154	2.4230	1.2131	1.1186	2.1115	4.9495
22	1.4501	2.6182	2.3463	1.1529	1.0969	2.0395	4.8868
23	1.7223	2.4610	2.2200	1.0335	1.2311	1.8057	5.1307
24	1.7272	2.8695	2.5472	1.3084	1.2371	2.1950	5.9878
25	1.5289	2.8779	2.5883	1.2475	1.2586	2.2324	4.9251
26	1.4740	2.6497	2.3943	1.1208	1.2022	2.0417	4.6220

6.6 Orbital stability

The orbital stability of the four remaining configurations was analyzed using simulations in STK, through the HPOP propagator and over many repeat cycles. The HPOP propagator accounts for disturbances from the Earth and Sun, as well as the Moon's non-spherical shape.

Given that the primary perturbations arise from third bodies, the Kozai-Lidov mechanism can broadly describe the system's dynamical evolution. If a single satellite is considered, this phenomenon states that a component of the satellite's angular momentum is conserved (if the orbit-averaged equations of motion are considered). This quantity C can be expressed in terms of the satellite's eccentricity e and inclination i as follows:

$$C = \sqrt{1 - e^2} \cos i = \text{constant} \quad (6.22)$$

It can be concluded from this relation that the effect of third bodies on the satellite's eccentricity is significantly greater than on its inclination. Consequently, correcting for the eccentricity is more important than adjusting the inclination to prevent further degradation of the satellite's orbit.

As a confirmation of this phenomenon it was observed that over long propagation times, the satellites diverged from their nominal conditions, initially slowly and then rapidly, following a marked increase in the eccentricity.

Thus, to maintain stability, a frequency of one maneuver per repeat cycle was chosen to prevent further degradation of the constellation geometry.

Gauss planetary equations were employed to calculate the necessary stationkeeping ΔV .

$$\Delta a = \frac{2\sqrt{a^3}}{\sqrt{\mu(1 - e^2)}} (e \sin \nu \cdot \Delta V_r + (1 + e \cos \nu) \cdot \Delta V_t) \quad (6.23)$$

$$\Delta e = \sqrt{\frac{a(1 - e^2)}{\mu}} \left(\sin \nu \cdot \Delta V_r + \frac{e + e \cos^2 \nu + 2 \cos \nu}{1 + e \cos \nu} \cdot \Delta V_t \right) \quad (6.24)$$

$$\Delta i = \sqrt{\frac{a(1 - e^2)}{\mu(1 + e \cos \nu)}} \cos(\omega + \nu) \cdot \Delta V_n \quad (6.25)$$

Since each satellite in a constellation experiences unique perturbations based on its position relative to disturbance sources, only the first satellite per orbital plane has been considered. This decision was motivated by the similar evolution shared by satellites within the same plane.

The tables below present the variations in orbital elements Δa , Δe and Δi at

the end of each cycle for each orbital plane, as well as a mean value for each constellation. Additionally, the required cost ΔV per maneuver and per year (a total of 13 maneuvers) are reported, to make it easier to compare the total cost of stationkeeping.

Table 6.4. Configuration ID12 - orbital stability

Plane	Δa [km]	Δe	Δi [deg]	ΔV [m/s]	ΔV_{year} [m/s]
1	-1.1569	-0.0025	-0.0011	2.0920	27.1964
2	10.8263	-0.0024	-0.0007	2.1132	27.4717
3	3.0800	-0.0027	-0.0067	7.3726	95.8444
4	4.3204	-0.0016	0.0005	1.2735	16.5555
5	-18.5468	-0.0028	0.0108	9.5181	123.7358
mean	7.5861	0.0024	0.0040	4.4739	58.1608

Table 6.5. Configuration ID16 - orbital stability

Plane	Δa [km]	Δe	Δi [deg]	ΔV [m/s]	ΔV_{year} [m/s]
1	0.0345	-0.0007	0.0000	0.6465	8.4050
2	1.5317	-0.0005	-0.0004	0.6907	8.9790
3	-2.4948	-0.0007	-0.0022	2.8483	37.0279
4	0.3992	-0.0005	-0.0023	2.4281	31.5654
5	-0.6629	-0.0002	0.0027	5.9297	77.0863
6	2.5849	-0.0007	0.0026	5.2075	67.6978
mean	1.2847	0.0005	0.0017	2.9585	38.4602

Table 6.6. Configuration ID17 - orbital stability

Plane	Δa [km]	Δe	Δi [deg]	ΔV [m/s]	ΔV_{year} [m/s]
1	-0.6948	-0.0011	0.0003	1.0544	13.7077
2	2.9957	-0.0008	-0.0011	1.5163	19.7125
3	-4.0479	-0.0011	-0.0036	4.3803	56.9433
4	1.3665	-0.0008	-0.0033	3.1779	41.3126
5	-1.7607	-0.0004	0.0041	60.4302	785.5927
6	-0.6702	-0.0014	0.0040	24.6803	320.8444
mean	1.9226	0.0009	0.0027	15.8732	206.3522

Table 6.7. Configuration ID26 - orbital stability

Plane	Δa [km]	Δe	Δi [deg]	ΔV [m/s]	ΔV_{year} [m/s]
1	0.1576	-0.0006	-0.0001	0.5834	7.5847
2	1.7979	-0.0005	-0.0003	0.6427	8.3545
3	0.7681	-0.0006	-0.0024	3.6453	47.3889
4	0.2004	-0.0003	0.0003	0.3928	5.1068
5	-2.7892	-0.0010	0.0032	3.4822	45.2687
mean	1.1426	0.0006	0.0012	1.7493	22.7407

Both configurations 16 and 26 exhibit lower average stationkeeping costs, reflecting their greater stability due to lower altitudes.

Although configuration 26 has the lowest stationkeeping cost, it consists of 20 satellites, contradicting the initial requirement for a minimal constellation. Therefore, configuration 16, with 18 satellites, is preferred as it balances the number of satellites with stationkeeping costs.

Lastly, Fig. 6.10 illustrates the evolution of the orbital elements for the first satellite of configuration 16 over two repeat cycles. The effects on these elements of the stationkeeping maneuver at the end of the first repeat cycle should not be visible, since a "reset" of sorts is expected. However, the evolutions for each repeat cycle are not identical due to differences in the directions of the disturbance sources.

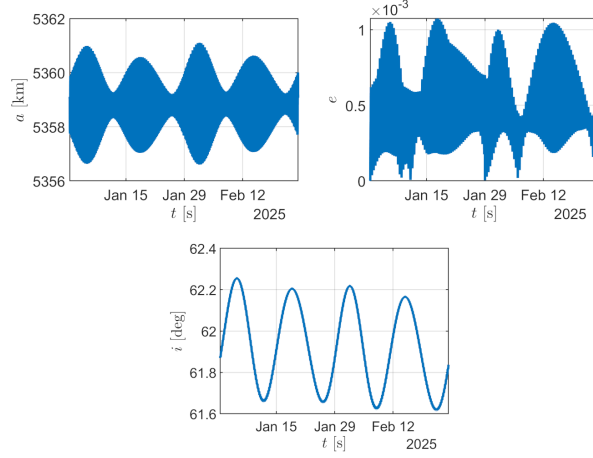
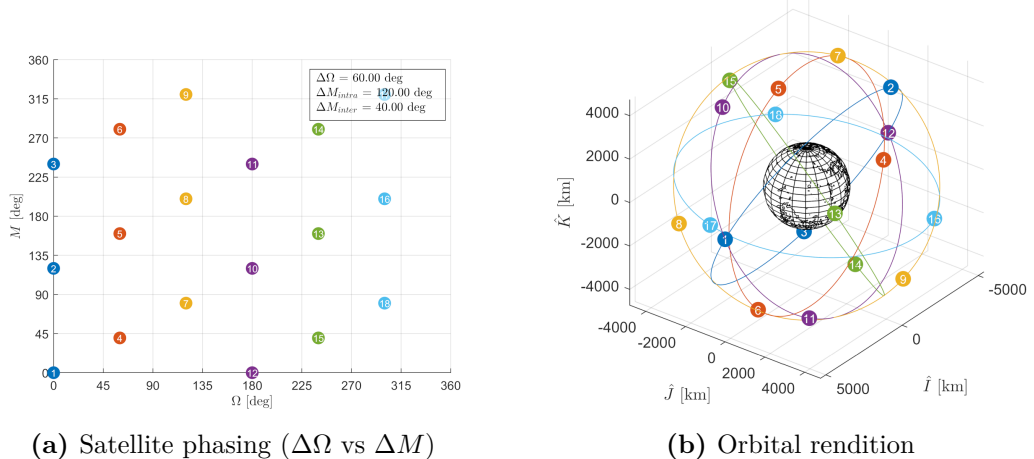
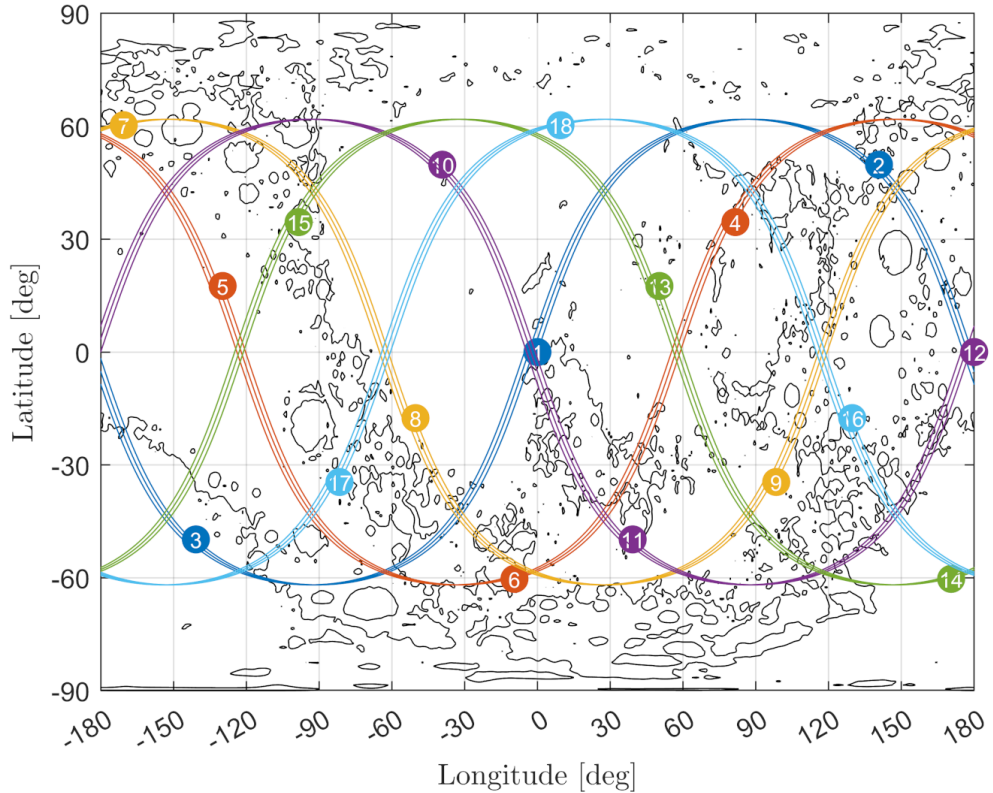


Figure 6.10. Evolution over two repeat cycles of the orbital elements with the considered stationkeeping maneuvers, for plane 1 of the configuration 16

6.7 Proposed constellation

The best overall constellation is therefore configuration 16, the Walker-Delta 18/6/2 constellation, based on a RGTO orbit at an altitude of 3621 meters over the lunar surface and with an inclination of 61.87 degrees with respect to the lunar equator. The constellation geometry is depicted in Fig. 6.11.

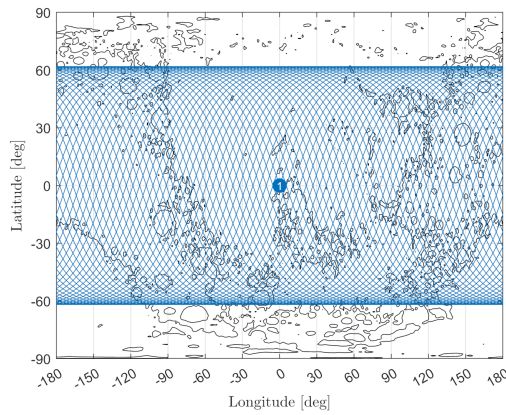




(c) Satellite ground-tracks over one orbital period

Figure 6.11. Lunar GNSS constellation (Walker-Delta 18/6/2)

This lunar constellation is capable of providing a 4-fold global coverage at all times over the lunar surface. The satellites are always visible from the surface with an elevation angle greater than 5 degrees, providing some leeway against adverse local topography.

**Figure 6.12.** Lunar GNSS ground-track grid ($m = 1$, $R = 67$)

Furthermore, in Fig. 6.13 we can see the *DOP* values and the minimum number of visible satellites for a range of latitudes. It can be observed how the best performance is obtained over the polar regions, as a minimum of 6 visible satellites and low values of *DOP* are guaranteed. Conversely, the worst conditions are obtained over the medium latitudes, where the number of visible falls to four and therefore no additional measurements for solving the navigation equations can be utilized, resulting in worse value for *DOP*. Nevertheless, these visible spikes are small in magnitude and do not undermine the overall excellent properties of the constellation.

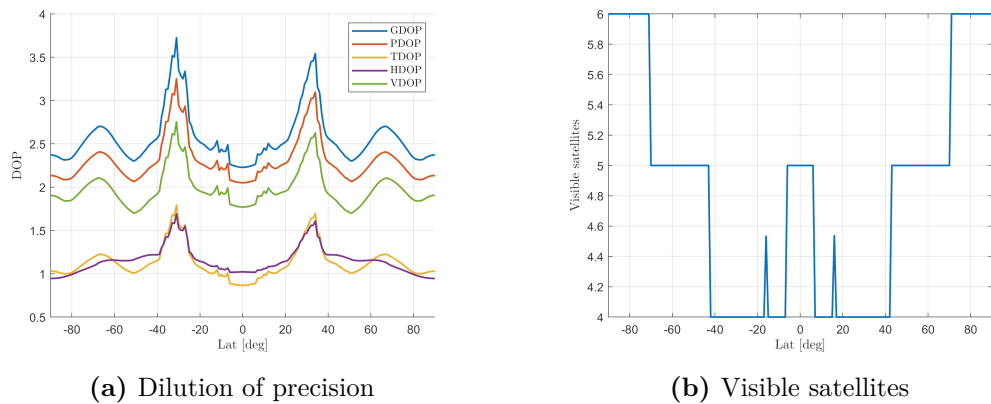


Figure 6.13. Lunar GNSS constellation properties

A brief analysis was made in case of a single satellite failure, to see how the constellation would cope in its degraded form. It was demonstrated that on average, any satellite failure would heavily deteriorate the constellation, halving its global coverage percentage.

Table 6.8. Failure of a satellite for the lunar GNSS constellation

CONFIG	% cov	GDOP	PDOP	TDOP	HDOP	VDOP	Min T
mean	48.57	3.9738	3.5401	1.7761	1.6487	3.0728	3.5650
worst	46.55	4.2947	3.8341	1.9063	1.7952	3.3637	3.5436
best	52.71	3.7551	3.3517	1.6663	1.5673	2.8951	3.6098
variability	13.23%	12.57%	12.58%	12.59%	12.70%	13.93%	1.87%

Given all these premises, the proposed constellation has been demonstrated as a strong contender for a lunar GNSS.

Chapter 7

Determination of gray areas for coverage

7.1 DEM

The Moon has a complex shape that can be approximated with a sphere at first instance. To provide a better approximation, the Moon can be considered an oblate spheroid, with the equatorial radius a that is different from the polar radius c . [32]

$$a = 1738.1 \text{ km} \quad (7.1)$$

$$c = 1736.0 \text{ km} \quad (7.2)$$

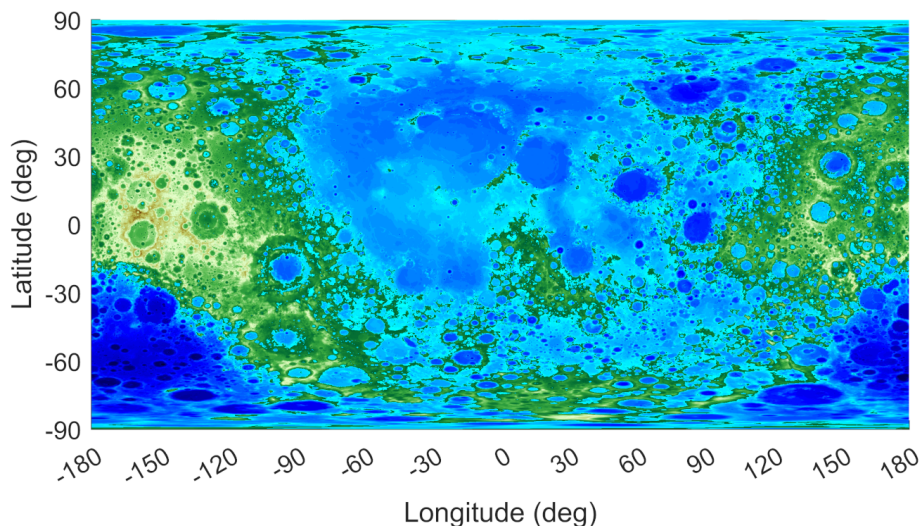


Figure 7.1. Moon DEM (450 arcsec)

A Digital Elevation Model (DEM) is a representation of a planet's surface topography. It consists of a grid of pixels, with each pixel storing an elevation value, representing the height of the terrain at a specific location. Therefore, a DEM can approximate the Moon surface better than any simple geometric shape.

The lunar DEM was obtained through the Lunar Orbiter Laser Altimeter (LOLA) aboard the Lunar Reconnaissance Orbiter (LRO) that collected over 6.3 billion measurements of surface height with a vertical precision of 10 cm and an accuracy of 1 m. A cylindrical map projection of the lunar DEM is depicted in Fig. 7.1, with the areas below the standard radius $R_p = 1737.4$ km colored in blue, and the areas above colored in green.

Many versions of the lunar DEM are available online, differing for the precision offered. A higher precision corresponds to a larger grid, which entails longer calculation times [53].

For a DEM, the precision is expressed either in a unit of length (meters, centimeters) or in angles (rad, deg). For polar regions it is more convenient to define the precision in meters, while for middle latitudes, it is easier to use angles, as the longitudinal distance varies wildly with near-polar latitudes, but not so much for middle ones, as it can be seen from Table 7.1, written for the Moon.

If s is the distance expressed in meters, θ is expressed in arcsec and ϕ the considered latitude, the governing equation for the conversion of longitudinal distances can be found:

$$s = R_p \cos \phi \cdot \left(\theta \frac{1}{3600} \frac{\pi}{180} \right) \quad (7.3)$$

Table 7.1. Longitudinal distance by latitude and precision (in arcsec)

θ	$\phi = 0$ deg	$\phi = 0$ deg	$\phi = 30$ deg	$\phi = 60$ deg	$\phi = 85$ deg
1 arcsec	8.42 m	8.14 m	7.29 m	4.21 m	0.73 m
3 arcsec	25.27 m	24.41 m	21.88 m	12.63 m	2.20 m
5 arcsec	42.12 m	40.68 m	36.47 m	21.06 m	3.67 m
15 arcsec	126.35 m	122.04 m	109.42 m	63.17 m	11.01 m
30 arcsec	252.69 m	244.08 m	218.84 m	126.35 m	22.02 m
225 arcsec	1.90 km	1.83 km	1.64 km	947.60 m	165.18 m
450 arcsec	3.79 km	3.66 km	3.28 km	1.90 km	330.36 m

Values in between grid points can be obtained in a series of different ways. In this dissertation, the method used was bilinear interpolation among the four points that

surround the selected point.

7.2 LOS algorithm

An algorithm to find the intersection between a satellite line-of-sight and the planet beneath was developed by Puccinelli [54].

The algorithm is mostly used in observation missions, as there is the need to associate a location with the pixel carrying its data. To each pixel corresponds a line-of-sight vector that intersects somewhere the area observed. For instrumentation working in the visible range, this intersection is indeed the planetary surface, which is turn approximated by its DEM.

The algorithm explained below is defined in a PCPF frame, since it permits to not consider the planet, and the corresponding DEM rotating. The planet itself is assumed to be a spheroid, an ellipsoid with circular symmetry and with an equatorial radius a and a polar radius c .

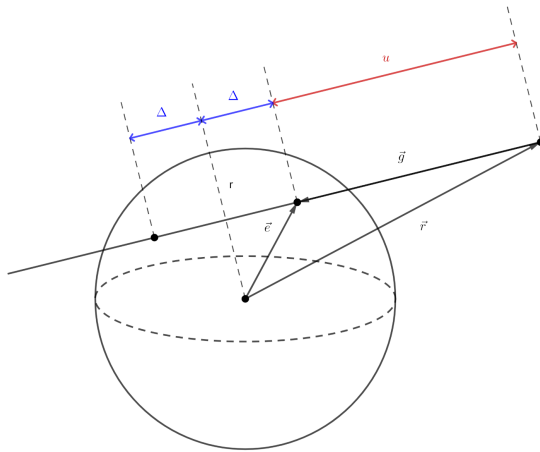


Figure 7.2. LOS algorithm

Fig. 7.2 shows the situation, where \vec{r} is the satellite position, \vec{g} is the line of sight direction, and \vec{e} is the intersection position to find, with respect to the ellipsoid. Comparing the surface equation of any ellipsoid with the definition of the intersection position, for which $\vec{e} = \vec{r} + u\vec{g}$ holds true, it is possible to find a 2nd degree equation in the distance u along the line-of-sight vector. Once this distance is found, the intersection vector \vec{e} is defined for given ellipsoid, and the corresponding geographic coordinates can be found.

$$A = (c + h_*)^2(g_x^2 + g_y^2) + (a + h_*)^2g_z^2 \quad (7.4)$$

$$B = 2 \left[(c + h_*)^2(r_x g_x + r_y g_y) + (a + h_*)^2 r_z g_z \right] \quad (7.5)$$

$$C = (c + h_*)^2(r_x^2 + r_y^2) + (a + h_*)^2(r_z^2 - (c + h_*)^2) \quad (7.6)$$

$$u = \frac{-B - \sqrt{B^2 - 4AC}}{2A} \quad (7.7)$$

$$\vec{e} = \vec{r} + u\vec{g} \quad (7.8)$$

$$\lambda_{int} = \text{atan2}(e_y, e_x) \quad (7.9)$$

$$\phi_{int,geoc} = \text{atan2}(e_z, \sqrt{e_x^2 + e_y^2}) \quad (7.10)$$

$$\phi_{int,geod} = \arctan\left(\frac{a^2}{c^2} \cdot \phi_{int,geoc}\right) \quad (7.11)$$

$$h_{int} = \text{interp2}(\lambda_{int}, \phi_{int,geod}) \quad \text{on the DEM grid} \quad (7.12)$$

having defined the operators $\text{atan2}(x, y)$ as the 2-argument arctangent, commonly used in computing.

$$\text{atan2}(x, y) = \begin{cases} \arctan\left(\frac{y}{x}\right) & \text{if } x > 0, \\ \arctan\left(\frac{y}{x}\right) + \pi & \text{if } x < 0 \text{ and } y \geq 0, \\ \arctan\left(\frac{y}{x}\right) - \pi & \text{if } x < 0 \text{ and } y < 0, \\ +\frac{\pi}{2} & \text{if } x = 0 \text{ and } y > 0, \\ -\frac{\pi}{2} & \text{if } x = 0 \text{ and } y < 0, \\ \text{undefined} & \text{if } x = 0 \text{ and } y = 0. \end{cases} \quad (7.13)$$

and the $\text{interp2}(\lambda, \phi)$ as the function that operates a bilinear interpolation on the DEM grid, as can be seen in Fig. 7.3. It is a built-in MATLAB function.

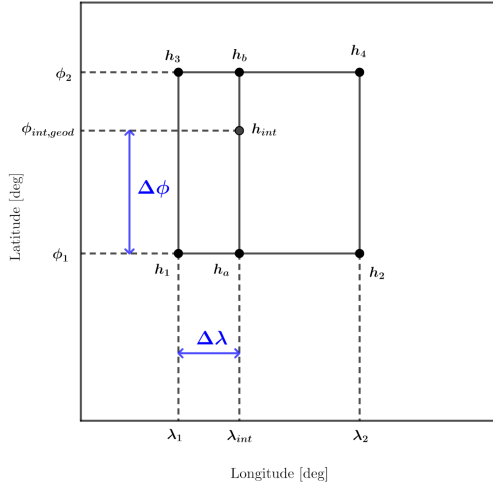


Figure 7.3. Bilinear interpolation for the DEM

It is itself an algorithm that permits finding a value within a well-defined grid. Some useful definitions are the DEM resolution m_{pix} , expressed in pixels per degree (or ppd), the pair of indexes (i, j) indicating a certain pixel on the DEM grid, and the minimum latitude and longitude in the grid λ_1, ϕ_1 .

$$i_1 = \lfloor (\lambda_{int} - \lambda_1)m_{pix} + 1 \rfloor \quad (7.14)$$

$$i_2 = i_1 + 1 \quad (7.15)$$

$$j_1 = \lfloor (\phi_{int,geod} - \phi)m_{pix} + 1 \rfloor \quad (7.16)$$

$$j_2 = j_1 + 1 \quad (7.17)$$

$$h_1(i = i_1, j = j_1) \quad (7.18)$$

$$h_2(i = i_2, j = j_1) \quad (7.19)$$

$$h_3(i = i_1, j = j_2) \quad (7.20)$$

$$h_4(i = i_2, j = j_2) \quad (7.21)$$

$$h_a = h_1 + m_{pix}\Delta\lambda(h_2 - h_1) \quad (7.22)$$

$$h_b = h_3 + m_{pix}\Delta\lambda(h_4 - h_3) \quad (7.23)$$

$$h_{int} = h_a + m_{pix}\Delta\phi(h_b - h_a) \quad (7.24)$$

For DEM implementation, an initial altitude h_0 is chosen, usually a mean value for the DEM grid considered. An ellipsoid with axes $a + h_0$ and $c + h_0$ is drawn and used to find its intersection with the LOS vector. The coordinates of the intersection are input in the DEM grid, and the resulting altitude $h_1 = DEM(\lambda_0, \phi_0)$ is instead

used for a new ellipsoid, with radii $a + h_1$ and $c + h_1$. The same process is applied until the intersection location eventually converges [55].

The algorithm used for the SPOT mission is shown in Fig. 7.4. Variations of this algorithm were employed in different observation missions [56, 57, 58].

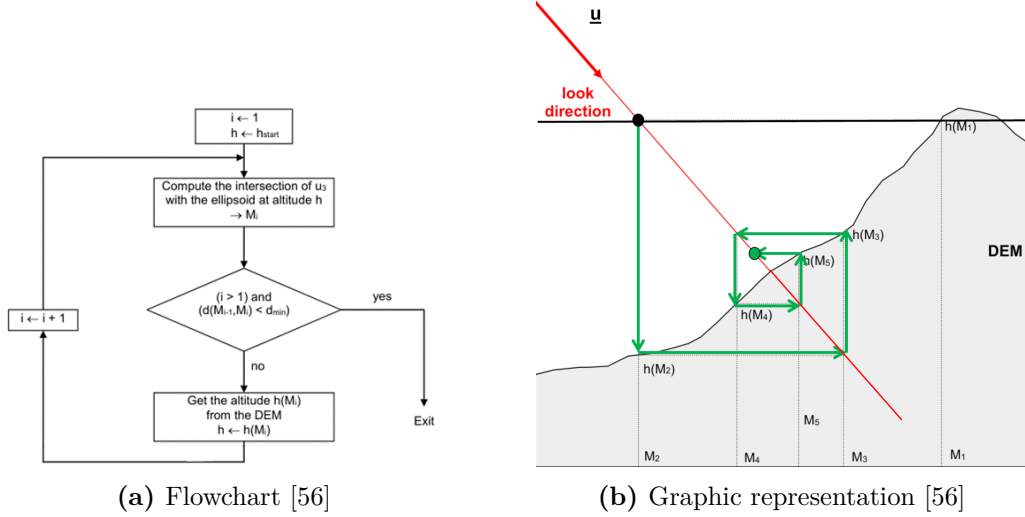


Figure 7.4. LOS algorithm employed by the mission SPOT

7.3 Gray areas

The same LOS algorithm can be used to determine the extent of regions of the planet, where coverage is limited due to the topography [59].

In the context of GNSS constellation, a region in space is called a gray area, when it is not covered simultaneously by the 4 satellites necessary for positioning. These regions can be defined at a given time, or for a time interval. The latter definition was chosen for the application.

This part is an original contribution, and it makes use of the number of intersections between the LOS vector \vec{g} and the DEM to flesh out these regions.

Instead of using the LOS algorithm to find the intersection through convergence, it is possible to employ the same algorithm to find the change in altitude at the start h_* and at the end h_{int} . The same process is applied for multiple starting altitude. Many ellipsoids are therefore considered in succession, each with an equatorial radius $a + h^*$ and a polar radius $c + h^*$. In the simulation a step of 20 m was chosen.

By looking at the trend of H , defined by the starting and end heights, it is possible to determine at which altitudes an intersection occurs. In fact, it occurs when said function changes sign for an increasing starting height h_* .

The highest intersection, is the only one that is able to see the satellite, and be seen

by it. All the others, if there are, are covered by either moon craters or mountains. For instance, in the case of 3 intersections, the region between the two deepest intersections is a not-covered area by the considered satellite.

This algorithm works for a pair comprised of a satellite and a test grid point. The test grid point is defined through its geodetic coordinates, longitude λ_{tg} , latitude ϕ_{tg} , altitude h_{tg} which together define the vector \vec{r}_{tg} having considered the ellipsoidal shape of the planet. The satellite position is instead defined by \vec{r}_{sat} .

$$e = 1 - \frac{c^2}{a^2} \quad (7.25)$$

$$N = \frac{a}{\sqrt{1 - e^2 \sin \phi_{tg}}} \quad (7.26)$$

$$\vec{r}_{tg} = \begin{bmatrix} (N + h_{tg}) \cos \phi_{tg} \cos \lambda_{tg} \\ (N + h_{tg}) \cos \phi_{tg} \sin \lambda_{tg} \\ ((1 - e^2)N + h_{tg}) \sin \phi_{tg} \end{bmatrix} \quad (7.27)$$

$$\vec{g} = \frac{\vec{r}_{tg} - \vec{r}_{sat}}{|\vec{r}_{tg} - \vec{r}_{sat}|} \quad (7.28)$$

$$H(h_\star) = h_\star - h_{int} \quad (7.29)$$

7.4 Application: Shackleton crater

In this section, the algorithm developed earlier was implemented in a real-case scenario, to determine gray areas for the final constellation in the South Pole region. More specifically, the Shackleton crater in the South Pole–Aitken basin was chosen, as it is an area of great interest due to its nature as a permanent shaded area, meaning that sunlight never reach the crater, and therefore makes it a probable place to find ice and other minerals.

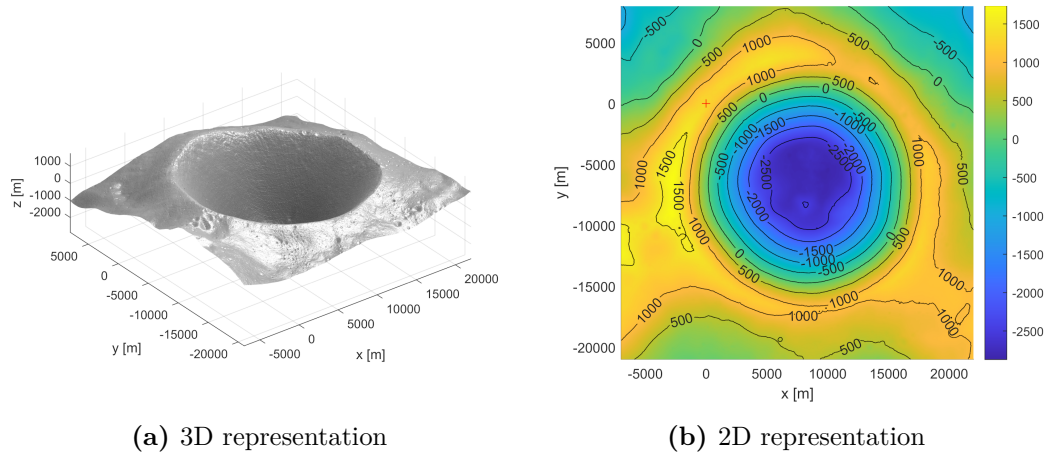


Figure 7.5. Shackleton crater DEM (20 m)

Shackleton crater is located at 89.67°S 129.78°E , very close to the pole, has an almost perfect circle shape, and its diameter measures around 21 km. Fig. 7.5a visualize the crater through the use of the DEM, obtained by the instrument LOLA. It is evident from 7.5b that the crater ridge mostly reaches a height of 1000 meters over the sea level, while grows up to 1500 meters on the "eastern side". The basin depth is fairly flat, with a depth of 2800 meters below sea level, however a hilltop stands around 200 meters over the basin, on the "southern side". Overall, the height difference between the basin and the ridge is around 4000 meters, over two times as deep as the Grand Canyon, a physical feature that already proves to be a challenging obstacle to PNT services here on Earth.

The constellation found in Chapter 6 is capable to guarantee an average of 6 satellites over the South Pole, as it can be seen from Fig. 6.13b, if considered over the whole repeating ground track period and for an ideal planet, devoid of physical features like mountains and canyons.

Naturally, the lunar surface elevation must be considered and therefore there could be moments in time when the service falters. Unfortunately, since the constellation was chosen considering coverage over a perfect sphere, it is unavoidable that such situations arise. It is the aim of this section to investigate those situations, to predict them, in order not to compromise human activities on the lunar surface that would depend on GNSS services.

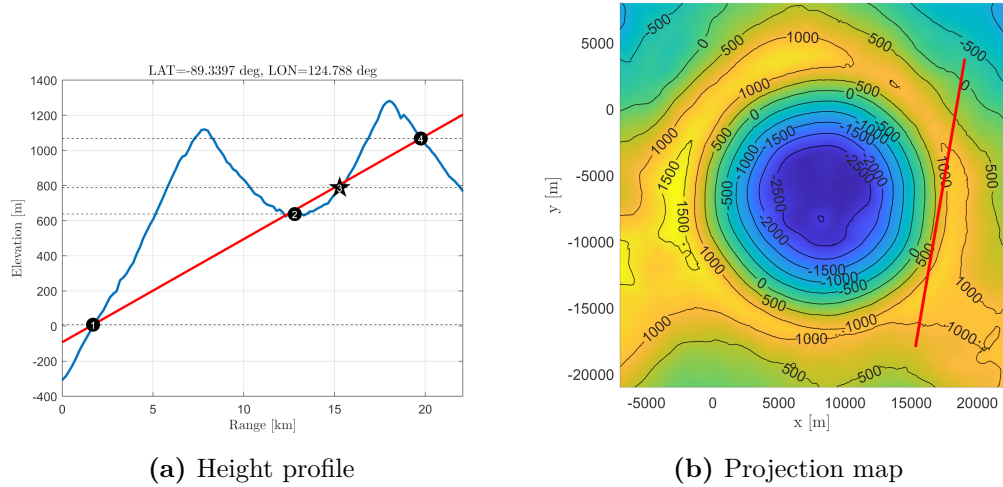


Figure 7.6. LOS and DEM intersections around Shackleton crater

Fig. 7.6 presents a first attempt to demonstrate the effectiveness of the algorithm for determining intersection points. The simulation was performed for a specific grid point-satellite pair, and the results shown here correspond to a single instant in time.

In the left image, the projection of the LOS vector is shown alongside the DEM, revealing four intersections along the same direction. However, only the fourth intersection provides access to the satellite at that moment, while the first three do not. Notably, the simulation was run for the surface point represented by the star, which corresponds to the third intersection.

The right image illustrates the same scenario but from a top-down perspective, within the xy grid of the polar stereographic map. Here, the LOS projection is represented by the red line.

It can be concluded that the regions around the three non accessible intersections are critical areas for the instant in time considered, since they lose access to one satellite. Were the number to fall under four satellites in total, the same areas would be called gray areas.

A larger simulation was conducted for every satellite-surface point pair on the grid over an entire repeat cycle of the constellation (approximately a lunar month). This simulation allows us to identify the so-called gray areas, where satellite access is limited.

The satellites were propagated using a 2 minute time step, with a grid spacing of 500 meters for surface points, and a vertical resolution of 20 meters for detecting intersections with the DEM.

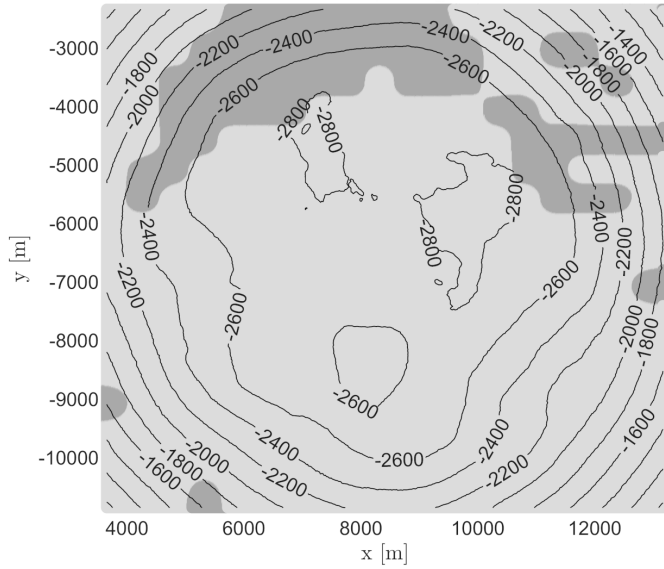


Figure 7.7. Gray areas, Shackleton crater

Fig. 7.7 presents the minimum number of satellites visible at each grid point. The lighter areas maintain access to at least four different satellites throughout the entire period, while the darker regions do not. These darker regions correspond to the gray areas, which remain inaccessible to four satellites for at least part of the simulation duration.

In particular, the northern ridge of the crater exhibits difficulty in maintaining a line of sight to overhead satellites. Additionally, smaller northeastern regions experience similar inaccessibility.

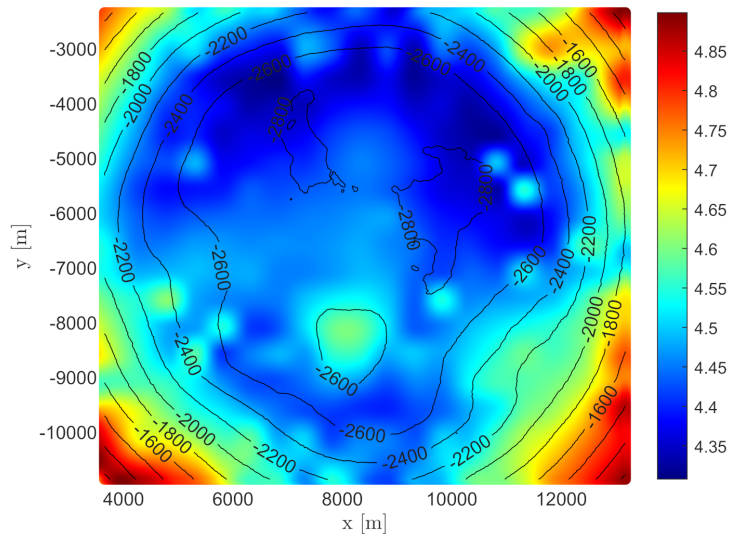


Figure 7.8. Average number of visible satellites, Shackleton crater

Fig. 7.8 instead displays the average number of visible satellites at each grid point. While each location typically has access to at least four satellites on average, there are periods when this number drops to three, as seen in the previous figure. Furthermore, visibility generally increases with elevation, as higher locations have fewer obstacles along the line-of-sight direction.

For the observed crater basin, the southern hill stands out as a relatively more accessible area, with an average of 4.6 visible satellites, compared to 4.4 or even 4.3 satellites in the surrounding terrain.

Throughout the entire simulation, satellite access was recorded under both ideal conditions and with terrain obstructions from the DEM. It was found that, on average, a grid point could see 6.27 satellites in the ideal case, but this number dropped to 4.49 satellites when accounting for the topography.

Chapter 8

Conclusions

8.1 Key results

In this thesis, we have examined the coverage problem for satellite constellations, demonstrating the positive correlation between altitude and the coverage angle. The spherical distance was evidenced to be a valuable index, useful to design more efficient constellations. Another index to evaluate GNSS constellation designs, the *DOP* has been explained, along with its relation between constellation geometry and the uncertainty on positional data.

Two classes of constellations were studied: Streets-of-Coverage and Walker-Delta. For each, we have outlined the fundamental concepts and principles.

The methodologies for designing SoC constellations have been reviewed and improved upon. Specifically, a more general approach has been developed by incorporating the across-track coverage factor k into the formula, thereby expanding the research domain.

Additionally, the design of Walker-Delta constellations has been examined, and the general idea for determining the optimal coverage value has been detailed. A novel approach utilizing RGTO orbits has been introduced, drawing from parallels from existing GNSS constellations.

It was demonstrated that polar SoC constellations are more efficient than their inclined counterparts, but are overall inefficient at providing global coverage, carving a niche for 1-fold coverage for larger-sized constellations.

In contrast, Walker-Delta constellations were found to be preferable for higher degrees of coverage due to their minimal configurations, which provide greater flexibility in designing constellations to meet specific mission requirements.

An original contribution of this work is the development of the Moon Walker Tables which specialize the optimal Walker-Delta configurations for lunar GNSS applications. These tables report the minimum number of satellites required to achieve 4-fold

global coverage over a wide range of inclinations and repeat factors.

From these tables many minimal configurations have been compared in terms of constellation geometry, number of satellites, coverage efficiency, and orbital stability. These configurations have been presented in tables, providing a vast overview of potential lunar constellations. Nonetheless, the optimal configurations for 13-20 satellites were proved to be inadequate choices due to poor satellite distribution and consequently constellation geometry. Additionally, a strategy for the stationkeeping of these candidate lunar constellations has been proposed, to ensure long-term stability.

Lastly, a detailed coverage analysis incorporating a DEM was conducted to identify potential critical areas. The algorithm used for this analysis is another original contribution, adapted from a LOS algorithm initially developed for observation missions.

8.2 Final remarks

In conclusion, the Walker-Delta pattern is undeniably the superior choice for a GNSS constellation, also supported by extensive experience, given as all the four extant terrestrial GNSS solutions are based entirely or partially on this constellation class. The proposed lunar constellation, a Walker-Delta 18/6/2, is found to meet all the requirements outlined in Chapter 5 while still qualifying as a minimal constellation. Relaxing these strict requirements, particularly the minimal constellation criterion, would likely yield constellations with improved coverage and stability, as demonstrated by the Walker-Delta 20/5/1 (the one with $ID = 26$) being among the top configurations.

Nonetheless, the chosen GNSS constellation is a strong candidate, chosen in order to compromise between total number of satellites and orbital stability.

Regarding the presence of gray areas, it is inevitable that a minimal satellite constellation have them, due to the low count of satellites by design. However, simulations have demonstrated that these areas are limited in extent and pose no significant risk to human or robotic activities on the lunar surface, particularly in terms of extended intervals when autonomous positioning might be interrupted. Moreover, the knowledge gained from the detailed coverage analysis can be leveraged to avoid these areas altogether during those specific intervals when access to a satellite is lost.

8.3 Future work

Nevertheless, future developments in lunar exploration may favor SoC constellations over Walker-Delta, particularly for applications that prioritize the lunar poles.

Additional research is certainly required to review SoC families with an across coverage factor $k > 1$, which were not considered in this dissertation.

Furthermore, more work is needed to develop a simple and elegant expression for the Moon Walker-Delta constellations detailed in Chapter 6 that accurately fits the obtained data. Additional simulations are necessary, covering a broader range of inclinations i and repeat factors q , with a finer grid for enhanced precision.

Regarding future exploration, it is worth investigating the feasibility of establishing a lunar surface base within the Shackleton crater, specifically near the hill on the southwestern edge. The coverage analysis has shown that an observer in this location would have access to an average of more than four satellites in a repeating ground track cycle (i.e., a lunar month), thereby ensuring reliable GNSS services. In fact, the very same area has been identified as rich in ice deposits, as reported by a 2018 study that confirmed the presence of ice within the South Pole-Aitken basin. The research utilized data from NASA's M3 spectrometer [12]. As illustrated in Figure 8.1, a substantial amount of ice is present on the southwestern inner edge, in close proximity to the aforementioned prominence.

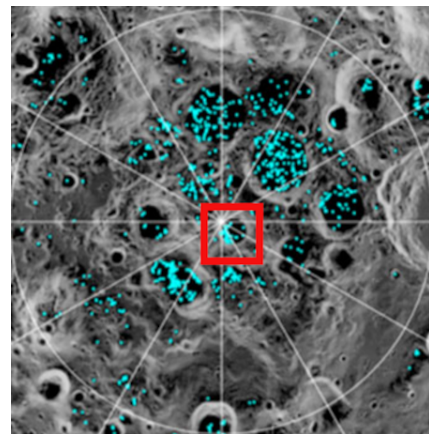


Figure 8.1. Distribution of surface ice at the Moon's south pole [12]

Appendix A

SoC tables for the Moon

Table A.1. Street-of-Coverage constellations for $n = 1$, $\varepsilon = 0$

h [km]	i [deg]	T	P	$\Delta\Omega_{co}$ [deg]	ΔM_{inter} [deg]	θ [deg]
2657.87	90	6	2	104.48	60	66.72
1507.92	90	8	2	98.42	45	57.63
1164.27	90	10	2	95.48	36	53.22
889.28	90	12	3	69.30	45	48.59
610.83	90	15	3	66.14	36	42.28
488.25	90	18	3	64.34	30	38.68
348.08	90	24	4	49.43	30	33.58
247.40	90	32	4	47.57	22.5	28.91
167.11	90	45	5	38.06	20	24.18
110.41	90	66	6	31.40	16.36	19.91

Table A.2. Street-of-Coverage constellations for $n = 2$, $\varepsilon = 0$

h [km]	i [deg]	T	P	$\Delta\Omega_{co}$ [deg]	ΔM_{inter} [deg]	θ [deg]
4211.49	90	10	2	92.09	72	73.02
2210.09	90	12	2	92.22	60	63.89
1598.52	90	14	2	91.96	51.43	58.61
1154.16	90	18	2	91.41	40	53.07
802.71	90	24	3	61.54	45	46.84
648.55	90	27	3	61.35	40	43.27
493.15	90	33	3	61.04	32.73	38.84
369.86	90	44	4	45.93	32.73	34.46
266.50	90	56	4	45.67	25.71	29.89
168.68	90	85	5	36.46	21.18	24.29
110.92	90	126	6	30.31	17.14	19.95

Table A.3. Street-of-Coverage constellations for $n = 3$, $\varepsilon = 0$

h [km]	i [deg]	T	P	$\Delta\Omega_{co}$ [deg]	ΔM_{inter} [deg]	θ [deg]
6282.84	90	14	2	90.70	77.14	77.49
3149.82	90	16	2	90.90	67.5	69.18
2172.96	90	18	2	90.92	60	63.62
1714.26	90	20	2	90.87	54	59.78
1289.55	90	24	2	90.72	45	54.97
962.93	90	33	3	60.69	49.09	49.95
683.06	90	39	3	60.60	41.54	44.13
504.76	90	48	3	60.47	33.75	39.20
378.47	90	66	3	60.29	24.55	34.80
263.99	90	84	4	45.29	25.71	29.76
171.21	90	125	5	36.20	21.6	24.45
108.46	90	192	6	30.13	16.88	19.74

Table A.4. Street-of-Coverage constellations for $n = 4$, $\varepsilon = 0$

h [km]	i [deg]	T	P	$\Delta\Omega_{co}$ [deg]	ΔM_{inter} [deg]	θ [deg]
8426.89	90	18	2	90.32	80	80.16
4160.61	90	20	2	90.46	72	72.87
2805.71	90	22	2	90.50	65.46	67.52
2161.44	90	24	2	90.51	60	63.54
1558.35	90	28	2	90.46	51.43	58.19
1281.74	90	32	2	90.40	45	54.87
911.10	90	45	3	60.37	48	49.01
704.61	90	51	3	60.34	42.35	44.65
512.34	90	63	3	60.26	34.29	39.44
380.03	90	87	3	60.16	24.83	34.86
263.18	90	112	4	45.16	25.71	29.72
179.28	90	160	5	36.12	22.5	24.98
109.99	90	252	6	30.08	17.14	19.87

Appendix B

Walker tables for the Moon

Table B.1. Walker-Delta constellations for $n = 1$, $\varepsilon = 0$

h [km]	i [deg]	T	P	F	θ [deg]
3086.59	43.57	5	5	1	68.89
2553.11	54.07	6	6	4	66.11
1721.91	56.60	7	7	5	59.85
1392.32	62.96	8	8	6	56.28
1255.96	70.35	9	9	7	54.52
1087.48	57.13	10	5	2	52.05
836.27	54.24	11	11	4	47.54
849.29	50.77	12	3	1	47.80
656.65	58.56	13	13	5	43.47
589.44	54.10	14	7	4	41.70
598.36	53.73	15	3	1	41.94
531.11	57.90	16	8	5	40.01
488.44	56.04	17	17	7	38.69
472.99	56.77	18	6	2	38.19
434.65	57.39	19	19	5	36.88
427.48	58.10	20	10	7	36.63
422.01	61.34	21	7	3	36.43
388.59	58.40	22	22	6	35.19

h [km]	i [deg]	T	P	F	θ [deg]
369.78	58.90	23	23	14	34.46
394.18	58.61	24	6	1	35.41
357.67	61.40	25	25	7	33.98
332.55	59.82	26	26	16	32.93
332.22	61.44	27	9	5	32.91
328.65	79.67	28	28	24	32.76
315.55	77.15	29	29	25	32.19
298.80	76.88	30	30	26	31.43
292.62	62.99	31	31	13	31.15
277.44	76.88	32	32	28	30.42
269.80	76.39	33	33	29	30.05
263.39	68.51	34	17	12	29.73
257.29	73.12	35	35	31	29.42
242.07	65.30	36	18	13	28.63
230.56	67.15	37	37	16	28.01
227.65	71.41	38	19	14	27.85
213.46	66.27	39	39	17	27.05
225.38	74.99	40	20	15	27.73
204.70	68.60	41	41	18	26.54
196.45	68.45	42	21	16	26.05
195.01	69.55	43	43	19	25.96
187.53	67.63	44	22	17	25.50
202.53	75.48	45	45	20	26.41
176.02	69.36	46	23	18	24.77
174.56	67.80	47	47	21	24.67
173.91	68.79	48	24	19	24.63
165.71	67.08	49	49	22	24.09
176.68	74.39	50	25	20	24.81

Table B.2. Walker-Delta constellations for $n = 2$, $\varepsilon = 0$

h [km]	i [deg]	T	P	F	θ [deg]
7076.88	61.46	7	7	2	75.79
5295.26	57.03	8	8	2	70.85
4331.39	60.77	9	3	2	66.36
3967.32	61.05	10	10	2	64.04
3664.61	53.52	11	11	9	61.71
3134.56	56.81	12	3	1	56.35
2994.92	52.85	13	13	3	54.55
2825.30	53.05	14	14	10	52.07
2773.45	55.27	15	3	1	51.23
2713.53	58.75	16	4	3	50.21
2577.85	55.03	17	17	3	47.65
2530.85	53.55	18	18	14	46.67
2477.31	54.41	19	19	11	45.49
2417.83	54.47	20	4	2	44.09
2411.50	56.81	21	21	4	43.93
2361.04	55.21	22	22	4	42.65
2345.68	54.55	23	23	18	42.24
2309.22	57.38	24	12	3	41.23
2292.75	57.03	25	25	11	40.76
2243.92	56.29	26	26	4	39.29
2234.05	57.63	27	9	3	38.98
2225.90	57.96	28	14	11	38.72
2222.13	57.78	29	29	16	38.60
2188.84	60.00	30	5	4	37.50
2164.18	60.28	31	31	25	36.64
2156.14	57.59	32	32	18	36.35

h [km]	i [deg]	T	P	F	θ [deg]
2139.73	58.88	33	33	23	35.75
2133.00	57.99	34	17	5	35.50
2125.40	58.32	35	5	3	35.21
2110.38	59.34	36	6	1	34.63
2092.38	61.23	37	37	10	33.91
2100.08	60.25	38	19	13	34.22
2073.57	61.36	39	39	22	33.13
2069.79	60.39	40	10	3	32.97
2063.24	62.41	41	41	17	32.68
2056.69	62.44	42	7	1	32.40
2035.56	61.31	43	43	36	31.45
2040.33	62.05	44	44	6	31.67
2044.30	60.71	45	15	8	31.85
2029.89	63.22	46	46	28	31.19
2028.50	62.78	47	47	29	31.12
2019.67	61.35	48	24	17	30.70
2000.91	62.83	49	49	30	29.79
1999.86	63.40	50	50	42	29.74

Table B.3. Walker-Delta constellations for $n = 3$, $\varepsilon = 0$

h [km]	i [deg]	T	P	F	θ [deg]
14097.17	59.34	9	9	3	82.92
9933.05	58.53	10	10	8	79.93
6401.79	60.21	11	11	3	74.26
5284.74	57.31	12	4	2	70.81
4549.12	50.68	13	13	4	67.55
4226.42	48.21	14	14	4	65.73
3835.54	57.27	15	15	6	63.07
3640.19	54.11	16	16	14	61.50
3460.97	56.66	17	17	15	59.88
3251.36	58.07	18	9	4	57.71
3176.81	53.85	19	19	14	56.86
2917.46	51.66	20	5	3	53.47
2802.77	55.30	21	21	5	51.71
2730.98	52.34	22	22	16	50.51
2766.80	55.38	23	23	14	51.12
2643.60	52.12	24	12	5	48.93
2670.89	53.86	25	25	9	49.44
2606.27	51.39	26	26	6	48.21
2541.23	54.98	27	3	1	46.89
2515.76	57.04	28	28	8	46.34
2482.91	56.07	29	29	13	45.62
2449.33	56.39	30	15	12	44.84
2408.25	56.19	31	31	6	43.85
2390.80	56.64	32	16	13	43.41
2370.00	56.96	33	33	15	42.88
2359.22	58.26	34	17	14	42.60

h [km]	i [deg]	T	P	F	θ [deg]
2326.68	58.33	35	35	16	41.72
2299.87	57.86	36	18	15	40.97
2288.16	58.65	37	37	17	40.63
2265.19	57.98	38	19	16	39.95
2254.47	57.91	39	39	18	39.62
2247.66	58.97	40	20	17	39.41
2236.69	59.37	41	41	19	39.07
2215.05	58.32	42	21	18	38.37
2208.74	57.05	43	43	31	38.16
2195.79	58.33	44	22	19	37.73

Table B.4. Walker-Delta constellations for $n = 4$, $\varepsilon = 0$

h [km]	i [deg]	T	P	F	θ [deg]
18972.15	66.48	11	11	4	85.19
11355.68	58.00	12	12	2	82.37
5985.35	45.51	13	13	2	77.00
5286.47	44.31	14	14	2	75.68
3530.16	55.37	15	15	2	70.74
3107.62	57.03	16	16	10	68.99
2683.30	49.15	17	17	11	66.86
2220.25	56.21	18	3	1	63.96
2079.59	57.21	19	19	5	62.92
1944.75	59.12	20	10	7	61.85
1611.19	54.38	21	3	2	58.75
1527.75	57.50	22	22	16	57.85
1417.22	56.54	23	23	17	56.58
1267.31	55.28	24	12	5	54.67
1257.53	55.90	25	25	6	54.54
1113.80	53.99	26	26	6	52.46
1107.64	54.67	27	3	2	52.36
1019.13	52.90	28	7	5	50.93
979.15	54.60	29	29	25	50.24
957.77	55.82	30	30	26	49.86
911.15	52.81	31	31	3	49.01
865.09	54.56	32	32	28	48.12
833.89	53.75	33	33	29	47.49
812.50	53.90	34	34	20	47.05
776.19	53.96	35	35	22	46.27
760.32	54.73	36	4	0	45.93

h [km]	i [deg]	T	P	F	θ [deg]
726.00	53.90	37	37	7	45.15
720.71	53.65	38	19	7	45.02
687.08	53.76	39	39	23	44.23
662.47	55.00	40	4	1	43.62
652.94	55.99	41	41	36	43.38
634.72	54.08	42	42	8	42.91
623.06	54.19	43	43	34	42.60
610.03	55.10	44	4	0	42.26
580.13	56.31	45	45	40	41.44
582.24	57.06	46	23	6	41.50
559.02	55.00	47	47	7	40.84
551.03	55.79	48	48	4	40.61
545.90	57.56	49	49	23	40.45
526.23	55.91	50	50	36	39.87

Bibliography

- [1] Hexagon and Novatel, “What are global navigation satellite systems?,” 2025.
- [2] C. Gramling, “Nasa’s lunanet lunar communications and pnt.” United Nations International Committee on GNSS (ICG) 18th Meeting, 2024.
- [3] M. Murata and K. Iiyama, “Lunar navigation satellite system (lnss) and its demonstration mission.” United Nations International Committee on GNSS (ICG) 16th Meeting, 2022.
- [4] T. J. Lang and W. S. Adams, “A comparison of satellite constellations for continuous global coverage,” in *Space Technology Proceedings*, 1998.
- [5] K. R. Lang, *The Cambridge Guide to the Solar System*. Cambridge University Press, 2011.
- [6] J. Wertz, *Orbit and Constellation Design and Management*. Microcosm, Inc, 2001.
- [7] C. (<https://math.stackexchange.com/users/86801/christoph>), “Three points on a sphere define eight spherical triangles.” Mathematics Stack Exchange. URL:<https://math.stackexchange.com/q/3043824> (version: 2018-12-17).
- [8] R. Langley, “The mathematics of GPS,” 1991.
- [9] J. G. Grimes, “GPS standard positioning service performance standard,” tech. rep., Department of Defense (USA), 2008.
- [10] CNES, *Spacecraft Techniques and Technology*. Editions Cépaduès, 2005.
- [11] E. D. Kaplan and C. J. Hegarty, *Understanding GPS/GNSS: Principles and Applications*. Artech, 2017.
- [12] S. Li, P. Lucey, R. Milliken, P. Hayne, E. Fisher, J. Williams, D. Hurley, and R. Elphic, “Direct evidence of surface exposed water ice in the lunar polar regions,” in *Proceedings of the National Academy of Sciences*, 2018.

- [13] J. Ventura, "Lunar pathfinder moonlight." United Nations International Committee on GNSS (ICG) 17th Meeting, 2023.
- [14] UNOOSA, "The interoperable global navigation satellite systems space service volume," tech. rep., United Nations Office for Outer Space Affairs (UNOOSA), 2021.
- [15] R. Roncoli, "Lunar constants and models document," tech. rep., Jet Propulsion Laboratory (JPL), 2005.
- [16] M. Cinelli, *Relazioni Compatte per il Progetto di Costellazioni Satellitari*. PhD thesis, Universitá degli Studi di Roma "La Sapienza", 2017.
- [17] O. Isik, J. Hong, I. Petrunin, and A. Tsourdos, "Integrity analysis for gps-based navigation of uavs in urban environment," *Robotics*, 2020.
- [18] J. Parker, F. Dovis, B. Anderson, L. Ansalone, B. Ashman, F. Bauer, G. D'amore, C. Facchinetti, S. Fantinato, G. Impresario, and S. McKim, "The lunar gnss receiver experiment (lugre)," in *Proceedings of the 2022 International Technical Meeting of The Institute of Navigation*, 2022.
- [19] F. Bauer, J. Parker, B. Welch, and W. Enderle, "Developing a robust, interoperable gnss space service volume (ssv) for the global space user community," in *Proceedings of the 2017 International Technical Meeting of The Institute of Navigation*, 2017.
- [20] NASA and ESA, "Lunanet interoperability specification document draft version 5," tech. rep., NASA and ESA, 2023.
- [21] C. Gramling, "Lunanet: Interoperability for lunar pnt." United Nations International Committee on GNSS (ICG) 17th Meeting, 2023.
- [22] M. Murata, M. Koga, Y. Nakajima, R. Yasumitsu, T. Araki, K. Makino, K. Akiyama, T. Yamamoto, K. Tanabe, S. Kogure, and N. Sato, "Lunar navigation satellite system: Mission, system overview, and demonstration," in *39th International Communications Satellite Systems Conference (ICSSC 2022)*, 2022.
- [23] M. Yang, J. Peng, J. Li, Y. Ni, S. Zhu, Y. Du, B. Xu, X. Huang, and Z. Zhang, "Architecture and development envision of cislunar space infrastructure," *Chinese Space Science and Technology*, 2024.
- [24] X. He, "The envision of earth-moon and deep space communication-navigation-remote sensing integrated constellation system." United Nations International Committee on GNSS (ICG) 17th Meeting, 2023.

- [25] Y. Ulybyshev, “Satellite constellation design for continuous coverage: Short historical survey, current status and new solutions,” in *5th international workshop on constellations and formation flying*, 2008.
- [26] N. Choo, D. Ahner, and B. Little, “A survey of orbit design and selection methodologies,” *The Journal of the Astronautical Sciences*, 2024.
- [27] J. Costales, “Orbital constellation design and analysis using spherical trigonometry and genetic algorithms: A mission level design tool for single point coverage on any planet,” Master’s thesis, KTH Royal Institute of Technology, 2023.
- [28] J. Walker, “Circular orbit patterns providing continuous whole earth coverage,” tech. rep., Royal Aircraft Establishment, 1970.
- [29] J. Walker, “Continuous whole-earth coverage by circular-orbit satellite patterns,” tech. rep., Royal Aircraft Establishment, 1977.
- [30] J. Walker, “Coverage predictions and selection criteria for satellite constellations,” tech. rep., Royal Aircraft Establishment, 1982.
- [31] G. Mengali and A. A. Quarta, *Fondamenti di meccanica del volo spaziale*. Pisa University Press, 2014.
- [32] NASA, “Moon fact sheet,” 2025.
- [33] M. Capderou, *Satellites: Orbits and Missions*. Springer, 2005.
- [34] Y. N. Skiba, *Mathematical Problems of the Dynamics of Incompressible Fluid on a Rotating Sphere*. Springer, 2017.
- [35] H. D. Curtis, *Orbital Mechanics for Engineering Students*. Butterworth-Heinemann, 2019.
- [36] Wikipedia, “Geopotential spherical harmonic model,” 2024.
- [37] C. Circi and E. Ortore, “Notes of traiettorie interplanetarie.”
- [38] L. Wood, “Introduction to satellite constellations orbital types, uses and related facts,” 2006.
- [39] D. Beste, “Design of satellite constellations for optimal continuous coverage,” *IEEE Transactions on Aerospace and Electronic Systems*, 1978.
- [40] R. Lüders, “Satellite networks for continuous zonal coverage,” *ARS Journal*, 1961.

- [41] Y. Ulybyshev, “Near-polar satellite constellations for continuous global coverage,” *Journal of Spacecraft and Rockets*, 1999.
- [42] S. Huang, C. Colombo, and F. Bernelli-Zazzera, “Multi-criteria design of continuous global coverage walker and street-of-coverage constellations through property assessment,” *Acta Astronautica*, 2021.
- [43] S. Janson, “Euclidean, spherical and hyperbolic trigonometry,” 2015.
- [44] achille hui ([https://math.stackexchange.com/users/59379/achille hui](https://math.stackexchange.com/users/59379/achille%20hui)), “Point in triangle with maximum distance from vertices.” Mathematics Stack Exchange. URL:<https://math.stackexchange.com/q/2397393> (version: 2023-11-14).
- [45] G. Dai, X. Chen, M. Wang, E. Fernández, T. Nguyen, and G. Reinelt, “Analysis of satellite constellations for the continuous coverage of ground regions,” *Journal of Spacecraft and Rockets*, 2017.
- [46] M. Padoan, “Methods for assessing the coverage performance of satellite constellations,” Master’s thesis, Politecnico di Milano, 2021.
- [47] J. Walker, “Satellite constellations,” *Journal of the British Interplanetary Society*, 1984.
- [48] EUSPA, “What is gnss,” 2025.
- [49] F. A. Kaya and M. Saritas, “A computer simulation of dilution of precision in the GPS using MATLAB,” *Proceedings of the 4th International Conference on Electrical and Electronic Engineering*, 2005.
- [50] A. Gabhart, M. Drosendahl, B. Robertson, and D. Mavris, “A comparative analysis of lunar pnt+ c concepts,” *AIAA SCITECH 2025 Forum*, 2025.
- [51] M. Deserno, “How to generate equidistributed points on the surface of a sphere,” *If Polymerforshung*, 2004.
- [52] A. Ballard, “Rosette constellations of earth satellites,” *IEEE Transactions on Aerospace and Electronic Systems*, 1980.
- [53] M. Barker, E. Mazarico, G. Neumann, M. Zuber, J. Haruyama, and D. Smith, “A new lunar digital elevation model from the lunar orbiter laser altimeter and SELENE terrain camera,” *Icarus*, 2016.
- [54] E. Puccinelli, “Ground location of satellite scanner data,” *Photogrammetric Engineering and Remote Sensing*, 1976.

- [55] N. Teanby, “Intersection between spacecraft viewing vectors and digital elevation models,” *Computers & Geosciences*, 2009.
- [56] S. Riazanoff, “SPOT satellite geometry handbook,” tech. rep., Spot Image, Centre national d’études spatiales (CNES), 2002.
- [57] L. Bourg, “SENTINEL 3 OLCI level 0, level 1B ATBD,” tech. rep., Thales Alenia Space, 2014.
- [58] M. Nishihama, “MODIS level 1A earth location ATBD,” tech. rep., National Aeronautics and Space Administration (NASA), 1997.
- [59] C. Armstrong, P. Swaszek, G. Johnson, and Hartnett, “Investigating the use of waas as a navigational tool for coast guard and civilian maritime use,” tech. rep., Institute of Navigation, 2005.